QUANTITATIVE CHEMICAL PROTEOMICS INVESTIGATIONS OF TARGETS OF ANDROGRAPHOLIDE AND PROTEOLYSIS OF AUTOPHAGY

WANG JIGANG
(B.Sc., South China University of Technology)

A THESIS SUBMITTED
FOR THE DEGREE OF DOCTOR OF PHILOSOPHY
DEPARTMENT OF BIOLOGICAL SCIENCES
NATIONAL UNIVERSITY OF SINGAPORE
2013

DECLARATION

I hereby declare that this thesis is my original work and it has been written by me in its entirety. I have duly acknowledged all the sources of information which have been used in the thesis.

This thesis has also not been submitted for any degree in any university previously.

Wang Jigang

05 Sep 2013

Table of Contents

Summary

The recently advanced quantitative proteomics approaches enabled the possibility of direct comparison of protein expressions for multiple samples in a high-throughput manner. Besides measuring the protein abundance changes, another important topic in proteomics is to provide direct information on protein activity and protein interaction, including protein-protein and protein-small molecule interactions. The emerging chemical proteomics offers a means to systematically analyse the protein activity and small molecule interaction other than protein abundance alone. In the first part of this thesis, we described a newly developed quantitative chemical proteomics approach which allows unbiased and specific drug target profiling. Using this method, a spectrum of specific targets of Andrographolide (Andro) was identified, revealing the mechanism of action of the drug and its potential novel application as a tumor metastasis inhibitor, which was validated through cell migration and invasion assays. Moreover, the target binding mechanism of Andro was unveiled with a combination of drug analogue synthesis, protein engineering and mass spectrometry-based approaches and the drug-binding sites of two protein targets, NF-κB and actin, were determined. In the second part of this thesis, we present a novel method to determine the autophagic protein degradation level using chemical metabolic labeling. The sensitivity and accuracy of this new methodology was validated using different autophagy induction and inhibition approaches. The two projects, though independent of each other, have both demonstrated the critical role that quantitative chemical proteomics plays in today's biomedical research.

List of Publications

(2010-2013)

1. Jigang Wang, † Chong-Jing Zhang,† Jianbin Zhang, Songbi Chen, Yingke He, Han-Ming Shen, Qingsong Lin*. Development of Quantitative Acid-cleavable Activity-based Protein Profiling (QA-ABPP) and its application for mapping sites of Aspirin induced acetylations in live cells. *(2013) Nat. Commun., submit soon*
2. Jigang Wang, Zhen Li, Caixia Li, Yew Mun Lee, Zhiyuan Gong,* Qingsong Lin.* (*co-corresponding) Quantitative Proteomics study of liver cancer using transgenic zebrafish model. *(2013), Journal of Proteome Research, submit soon*
3. Jigang Wang, Yew Mun Lee, Caixia Li, Zhen Li, Zhiyuan Gong,* Qingsong Lin.* (*co-corresponding) Effective Protein Extraction with Sodium Deoxycholate Promotes Proteomics Study of Whole Zebrafish Liver with Hepatocellular Carcinoma. *(2013), Journal of Proteomics, submit soon*
4. Jianbin Zhang*, Jigang Wang*, Shukie Ng, Qingsong Lin#, Han-Ming Shen# (* equal contribution, # co-corresponding). Development of a novel method for quantification of autophagic protein degradation by AHA labelling. *(2013), Autophagy, accepted and in press.*
5. Jigang Wang, Xing Fei Tan, Van Sang Nguyen, Peng Yang, Jing Zhou, Mingming Gao, Zhengjun Li, Teck Kwang Lim, Yingke He, Chye Sun Ong, Yifei Lay, Jianbin Zhang, Guili Zhu, Siew-Li Lai, Dipanjana Ghosh, Yu Keung Mok, Han-Ming, Qingsong Lin.* A Quantitative Chemical Proteomics Approach to Profile the Specific Cellular Targets of Andrographolide, a Promising Anticancer Agent that Suppresses Tumor Metastasis. *(2013), Molecular & Cellular Proteomics,* mcp.M113.029793. First Published on January 20, 2014, doi:10.1074/mcp.M113.029793

6. Higuchi S, Lin Q, Wang J, Lim TK, Joshi SB, Anand GS, Chung MC, Sheetz MP, Fujita H. Heart extracellular matrix supports cardiomyocyte differentiation of mouse embryonic stem cells. *J Biosci Bioeng. 2013 Mar; 115(3):320-5.*
7. Wu, H.; Ge, J.; Yang, P.-Y..; Wang, J.; Uttamchandani, M.; Yao, S.Q.* A Peptide Aldehyde Microarray for High-Throughput Detection of Cellular Events. *J. Am. Chem. Soc.* (2011), *133*, 1946-1954.
8. Kalesh, K.A.; Sim, S. B. D..; Wang, J.; Liu, K.; Lin, Q.; Yao, S.Q.* Small molecule probes that target Abl kinase. *Chem. Commun.* (2010*), 46, 1118-1120.*
9. Kalesh, K.A,; Tan, L.P.; Liu, K.; Gao, L.; Wang, J.; Yao, S.Q.* Peptide-based Activity-Based Probes (ABPs) for Target-Specific Profiling of Protein Tyrosine Phosphatases (PTPs). *Chem. Commun.* (2010), *46*, 589-591.

List of Tables

List of Figures

List of Schemes

List of Abbreviations

2-DE	Two- dimensional electrophoresis
AA	Amino acid
ABP	Activity Based Probe
Andro	andrographolide
AHA	Azidohomoalanine
BSA	Bovine serum albumin
$CaCl_2$	Calcium chloride
δ	Chemical shift in ppm
C.I	Confidence interval
CID	Collision-induced dissociation
Cu	Copper
Da	Dalton
CUAAC	Copper (I) catalyzed Azide-alkyne cycloaddition
Cy	Cyanine
DIGE	Difference in gel electrophoresis
DMSO	Dimethyl sulfoxide
DTT	Dithiothreitol
E. coli	*Escherichia coli*
EDTA	Ethylenediamine tetraacetic acid
ESI	Electrospray ionization
FACS	Fluorescence activated cell sorting
FITC	Fluorescein isothiocyanate
HEPES	4-(2-hydroxyethyl)-1-piperazineethanesulfonic acid
HGP	Human Genome Project
HPLC	High performance liquid chromatography
IC50	Half the maximal inhibitory concentration
IPG	Immobilized pH gradients
IEF	Isoelectric focusing

GO	Gene ontology
h	Hour
ICAT	Isotope-Coded Affinity Tags
IPI	International Protein Index
iTRAQ	Isobaric Tag for Relative and Absolute Quantitation
min	Minute
LC	Liquid chromatography
MALDI	Matrix-assisted laser desorption ionization
MMTS	Methylmethanethiosulphate
MudPIT	Multidimensional protein identification technology
MS	Mass spectrometry
mTOR	Mammalian Target Of Rapamycin
MOA	Mechanism of Action
NaHCO3	Sodium bicarbonate
NMR	Nuclear magnetic resonance
P.I	Propidium iodide
PAGE	PAGE polyacrylamide gel electrophoresis
PBS	Phosphate buffered saline
PBS-T	Phosphate buffered saline- Tween
PI	Isoelectric point
PTM	Post-translational modification
PVDF	Polyvinylidene fluoride
RP	Reverse-phase
ROS	Reactive oxygen species
rpm	Rotations per minute
r.t.	Room temperature
s	Second
SAR	Structure-activity relationship
S/N	Signal to noise ratio
SDS	Sodium dodecyl sulphate

SDS-PAGE	Sodium dodecyl sulphate- polyacrylamide gel electrophoresis
TBTA	Tris[(1-benzyl-1H-1,2,3-triazol-4-yl)methyl]amine
TCEP	Tris(2-carboxyethyl)
TEAB	Triethylammonium bicarbonate Buffer
TMR	tetramethylrhodamine
Tris	Trishydroxymethyl amino methane
µ	Micron
µg	Microgram
µl	Microlitre

List of Symbols

Å	angstrom
℃	degree celsius
g	gram
h	hour
k	kilo
l	litre
w	wavelength
m	milli or meter
µ	micro
M	molar
min	min
mol	mole
n	nano
p	pico
s	second

List of Twenty Natural Amino Acids

Single Letter Code	Three Letter Code	Full Name
A	Ala	Alanine
C	Cys	Cysteine
D	Asp	Aspartate
E	Glu	Glutamate
F	Phe	Phenylalanine
G	Gly	Glycine
H	His	Histidine
I	Ile	Isoleucine
K	Lys	Lysine
L	Leu	Leucine
M	Met	Methionine
N	Asn	Asparagine
P	Pro	Proline
Q	Gln	Glutamine
R	Arg	Arginine
S	Ser	Serine
T	Thr	Threonine
V	Val	Valine
W	Trp	Tryptophan
Y	Tyr	Tyrosine

Chapter 1

Introduction

1.1 Summary

Proteins are basic structural scaffolds, playing various important roles in living organisms. The large scale “omics” study, especially proteomics, is continuing to provide important insights into various biological processes. With the increasing sensitivity of modern mass spectrometry platform, thousands of proteins and numerous posttranslational modifications can be examined simultaneously in any biological system. The recently advanced quantitative proteomics approaches enabled the possibility of direct comparison of protein expressions for multiple samples in a high-throughput manner. These methods already play important roles in biomarker discovery, drug treatment perturbation and disease mechanism studies. Besides measuring the protein abundance changes, another important area in proteomics is to provide direct information on protein activity and protein interaction, including protein-protein and protein-small molecule interactions. The emerging chemical proteomics offers a means to systematically analyse the protein activity and small molecule interaction other than protein abundance alone. This chapter will give a brief overview of the currently available quantitative proteomics methods as well as the emerging chemical proteomics technology. Much attention will be focused on stable isotope-based quantitative proteomics, drug target identification and metabolic labeling of proteome with unnatural amino acids.

1.2 Proteome and proteomics

The term "proteome" is referred to as the entire proteins expressed in cells, tissue or organism at a certain time or under defined conditions. Proteomics is the large-scale study of the whole proteome, particularly their identity, expression patterns, activity and functions. Such information is extremely critical for unveiling the mechanism of disease, and designing for the diagnostic technique and therapeutic approaches (Mann et al., 2003; Abersold et al., 2001). The initial use of conventional proteomics research was mainly to identify and characterize proteins. With the advancement in chromatography and stable isotope labeling methods, Mass spectrometry (MS) and bioinformatics, proteomics has been extended to quantitative and comparative studies with wider applications (Figure 1.1), which are now playing important roles in biomarker discovery, drug treatment perturbation and disease mechanism studies (Lindsay, M.A. *et al.* 2003).

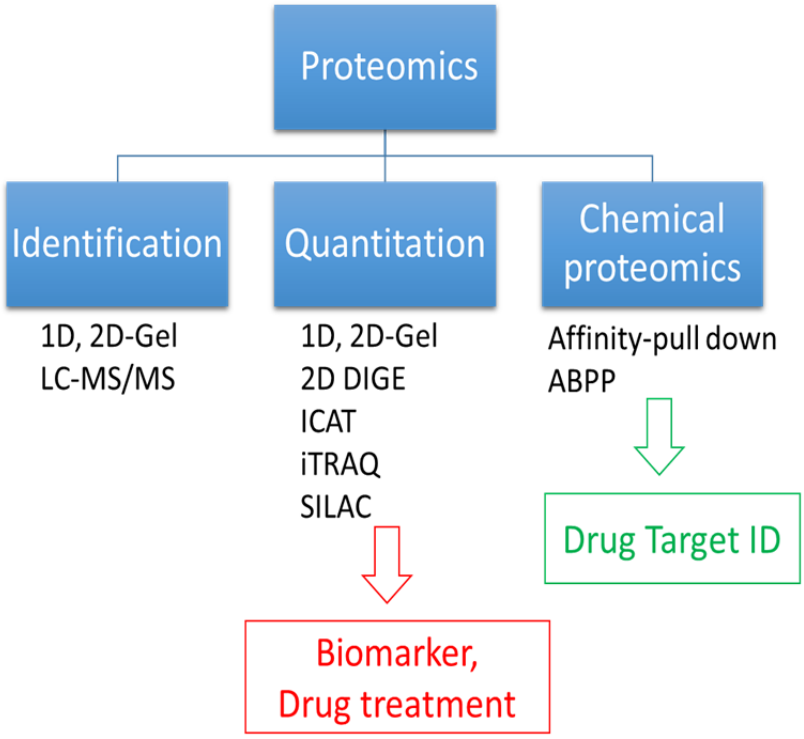

Figure 1.1 Comparison of conventional proteomics and chemical proteomics approaches.

Besides measuring the differences in protein abundance under different conditions, another important area in proteomics is to provide direct information on protein activity and protein interaction, including protein-protein and protein-small molecule interactions. However, protein activity at cellular level does not always directly correlate with its abundance, thus the traditional proteomics methods are unable to provide such activity information.

To overcome these limitations, a chemical proteomics strategy has been introduced that utilize synthetic small molecules to enrich and distinguish the interactive biding partners. This strategy offers a means to systematically analyse the protein activity and small molecule interaction other than protein abundance alone. It has been widely used in drug target identification and small molecule function study (Figure 1.1) (Harding, et al., 1989; Brown, et al., 1994).

The first key step in proteomics is the effective separation of proteins or peptides from a complex mixture (Wu, W.W., et al., 2006). This is usually achieved by either gel-based or liquid chromatography (LC)-based strategies (Figure 2). The gel-based approach (Fig. 2 left side) is the traditional one but still widely used in many studies, as it does not require very expensive equipment and can be easily set up in most laboratories. In this approach, proteins are first separated basing on two different parameters (pI & MW) and then excised, digested and identified using mass spectrometry. It allows direct visualization of the separated proteins and their isoforms after different post translational modifications. Another widely used strategy in proteomics is liquid chromatography coupled with mass spectrometry (LC-MS) (Figure 2, right side). Different from the earlier approach, the proteins are not separated before identification. The protein mixture is digested into peptides, which are subsequently separated by liquid chromatography and identified by mass spectrometry.

In the following sections, the Gel-based and LC-based quantitative

proteomics will be discussed in more details.

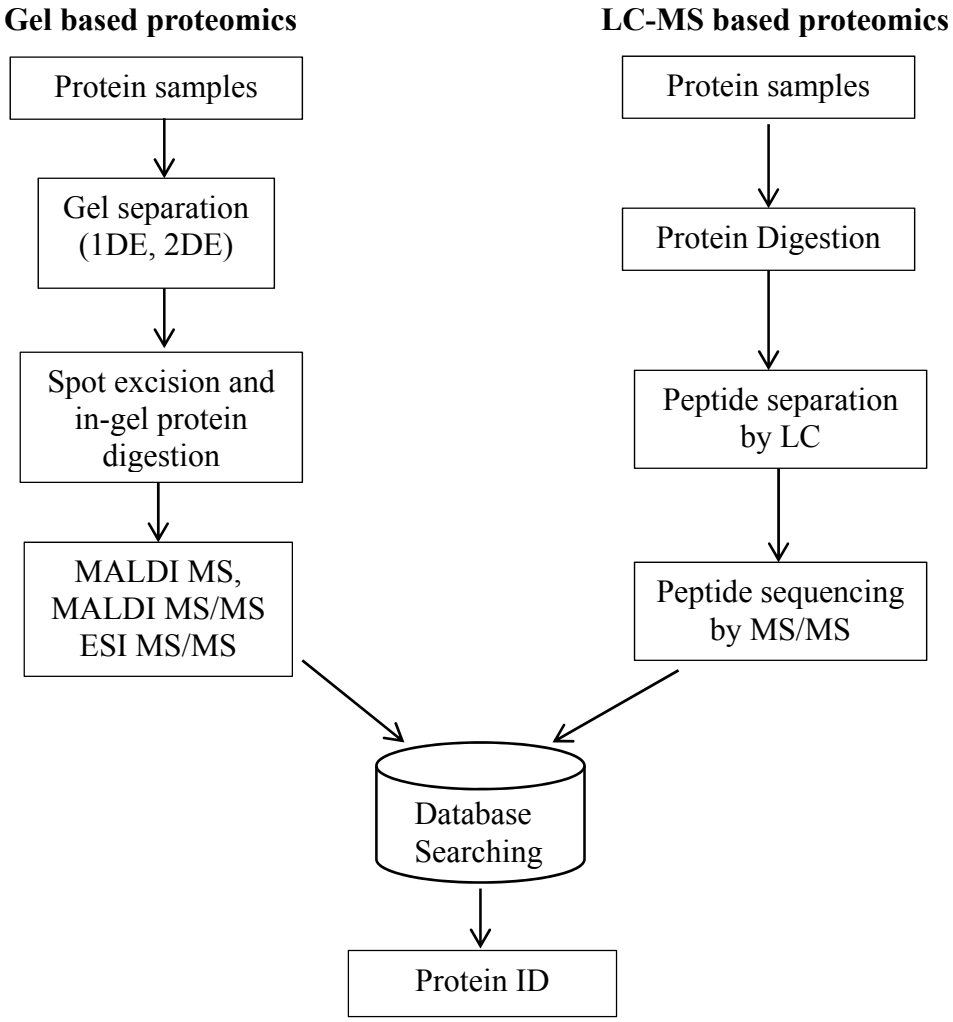

Figure 1.2 Two major strategies for protein identification.

1.3 Gel based Proteomics and Two Dimensional Gel Electrophoresis (2-DE)

Currently, the most widely used methods for profiling and quantitative proteomics include the gel-based approaches such as two-dimensional gel electrophoresis (2-DE). In 2-DE, proteins are separated by isoelectric focusing (IEF) according to their isoelectric points (pI) in the first dimension. Then, Proteins migrate on SDS-PAGE according to their molecular weights in the second dimension (Hanash, S., 2001). After 2-DE separation, the proteins can be easily visualized by staining or fluorescent scanning. Normally, we can easily separate and visualize 1000 proteins using 2-DE (Figure 1.3). When combining multiple narrow PH range gels, it even enables distinguishing up to 5000 proteins (Hoving, *et al.* 2000). The quantitation is achieved by comparing the protein expression levels (intensity of the proteins spots) of different sample pairs (normal versus diseased samples, cells at different stages or under different treatments, etc.) using a software. The differentially expressed proteins can then be excised and identified subsequently using mass spectrometry. However, the efficiency of proteins transferred from IEF to the second dimension SDS PAGE usually varies from gel to gel, and thus it is difficult to differentiate the real expression changes from the system errors. The poor reproducibility of 2-DE emphasized the need of a number of replicate gels of the same protein sample in order to avoid experimental errors (Righetti, P.G., et al.,2004). Besides the tedious process and waste of samples, the accuracy of this method still can not be guaranteed.

To overcome this issue, difference gel electrophoresis (DIGE) was developed by Unlu *et al.* (1997), where the control and treated samples are independently labeled with two structurally similar fluorescent dyes (e.g., Cy3 and Cy5, respectively) prior to 2-DE. The labeled samples are then combined

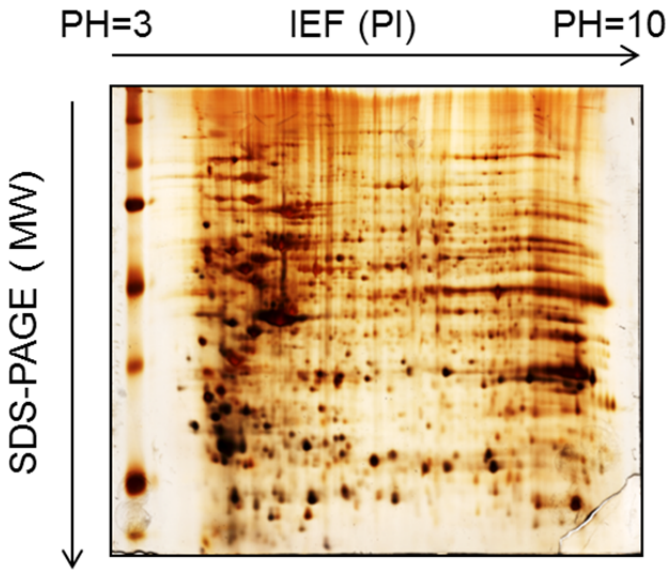

Figure 1.3 Two Dimensional Gel Electrophoresis (2-DE) separation of HCT116 whole proteome. After isoelectric focusing (IEF), the proteins are separated according to their sizes using SDS PAGE. Proteins can be visualized by staining (silver stained gel, unpublished data).

and separated in a same 2-D gel to minimize gel-to-gel variations and improve the reproducibility of the samples. 2D-DIGE technology is based on the development of the fluorescent protein labeling dye (Cy2, Cy3 and Cy5), which are identical both in mass and charge. Therefore, the same proteins labeled with different dyes from biological samples will migrate in the same pattern on 2-D gel. Consequently, this method allows two or even up to three samples directly compared in a single run. 2D-DIGE has dramatically improved the sensitivity and reproducibility of gel-based proteomics. However, the gel-based approaches still suffer from the difficulties in detecting several types of proteins, including membrane associated proteins, low-abundant proteins and proteins with extreme PI and size (Corthals, G.L. *et al.* 2000; Gygi, S.P. *et al.* 2000).

1.4 LC-MS/MS based proteomics and quantitative proteomics

Besides gel-based proteomics, LC-based proteomics has been developed and has drawn increasing attentions in the last decade. Compared with gel-based approaches, LC-based methods have several prominent advantages, such as high sensitivity and reproducibility, capability of identifying low-abundant proteins (Gygi, S.P., *et al*., 2000), highly acidic or basic proteins or proteins with extreme size or hydrophobicity. Furthermore, LC-based methods can be operated automatically to handle the high-throughput samples (Hamdan, M. and P.G. Righetti, 2002).

LC-based approaches adopt a variety of combination of stationary and mobile phases to separate complex proteomics samples at peptide level (Issaq, H.J., et al., 2005; Shi, Y., et al., 2004). Proteins are first digested into peptides using a protease (usually trypsin). In most cases, the resulting peptide mixture is extremely complex. Multi-dimensional LC is needed instead of single LC. The widely used combination is strong-cation exchange (SCX) followed by C18 reversed-phase LC coupled with mass spectrometer.

For relative quantification of proteins or peptides using LC-MS, several stable isotope tagging methods are available. Stable isotopes have the same physico-chemical properties as the natural atoms and the incorporated proteins are almost identical to their natural counterparts. In practice, isotope labeling can be achieved by metabolic incorporation or chemical tagging. The difference in peptides masses enables the determination of the relative quantities of a peptide in different samples. Other than stable-isotope labeling approach, several label-free methods have also been developed (Wu,W, et al., 2006; Liu, H., R.G. Sadygov, et al., 2004; Chelius, D., et al.,2003). For better understanding, a brief overview on LC-MS based quantitative methods, including SILAC, ICAT and iTRAQ, is provided in the following sections.

1.4.1 Stable isotope labeling by amino acids in cell culture (SILAC)

Established by Mann and co-workers in 2002 (Ong, S. et al.,2002), stable isotope labeling by amino acids in cell culture (SILAC) has now been widely used for protein abundance quantification in LC-MS/MS-based platform. SILAC is an *in vivo* metabolic labeling method for mass spectrometry (MS)-based quantitative proteomics. The principal of SILAC is that the growth of mammalian cells needs essential amino acids (e.g. arginine, methionine, lysine, leucine) from external source. Two cell populations are grown either in normal conditions ("light" - natural amino acids) or with stable isotope labeled essential amino acids ("heavy" amino acids - ^{13}C labeled L-arginine and ^{13}C, ^{15}N-labeled L-lysine, etc.) (Figure 1.4). The heavy-isotope labeled amino acids are incorporated into all newly synthesized proteins instead of the natural amino acids. After a number of cells divisions, the "light" and "heavy" amino acids can be fully incorporated into the whole proteome. Since the properties of isotopes labeled amino acid is almost the same as the natural amino acid, the cells behave exactly like the control cells grown with the natural amino acid. In MS process, there will be a mass shift of 6 Da for ^{13}C-L-arginine-labeled peptides and 8 Da for ^{13}C, ^{15}N-L-lysine-containing peptides when comparing the mass spectra of "heavy" and "light" peptides due to the use of isotope-labeled amino acids. These isotope-labeled peptide pairs behave identically during their isolation, separation, and ionization as the isotopic amino acids have the same physicochemical properties. Thus, the relative quantification of the "heavy" to the "light" peptides can be achieved by comparing the ratio of ion intensities of the SILAC peptide pairs. This ratio of peptides reflects the ratio of protein abundance in the original sample pair compared (Ong, S.E., et al., 2002; Martinović, S., et al., 2002; Ong, S.E., et al., 2003). Nevertheless, due to the inherent limitation of SILAC, such an approach takes a long time for complete incorporation of isotopic amino acids,

thus it may not be suitable for certain cells that cannot be maintained for a long time, such as platelets. Furthermore, it is also extremely difficult to apply the SILAC approach to tissue and body fluid samples, which are of particular relevance to biomedical research. In such cases, the after-mentioned chemical labeling is the alternative choice for protein quantification. Moreover, SILAC only allows the quantification of at most 3 samples at one time. Thus it is difficult to compare more than 3 different conditions like series of time points or dosages and it is impossible to include biological duplicate samples in the same LC MS/MS run. Alternatively, isobaric tags for relative and absolute quantification (iTRAQ) can be considered as iTRAQ can simultaneously quantify up to 8 different samples in a same run.

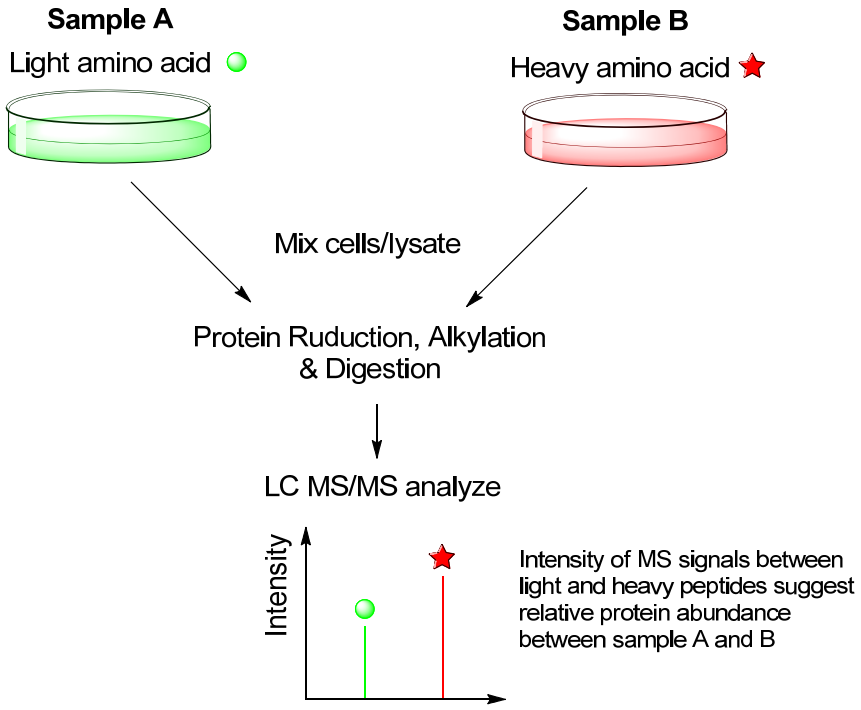

Figure 1.4 Quantitative proteomics employing the SILAC method.

1.4.2 Isotope-coded affinity tags (ICAT)

Recently developed isotope-coded affinity tags (ICAT) is another method for quantitative protein profiling (Gygi S.P. *et al.* 1999). The ICAT reagents consist of a biotin affinity tag, an isotopically labeled linker and a thiol-specific reactive group (iodoacetamide) which is specific for sulfhydryl groups (Figure 1.5A) (Brown, G., et al., 2003). By using this paired thiol-specific ICAT reagent, the side chains of cysteine residues in a reduced protein sample can be labeled with isotopically light reagent. And the equivalent cysteine group in another sample can be labeled with the eight-fold deuterated heavy ICAT label representing a second cell state. After combining the two light-and heavy-labeled samples followed by trypsin digestion, thiol-labeled cysteine containing peptides are enriched through avidin affinity chromatography to reduce the complexity. Next, isolated cysteine containing peptides are fractionated, and quantitatively analyzed by mass spectrometry (Figure 1.5B). In the LC-MS/MS analysis process, the machine can determine the quantity of the labeled peptides and analyse the sequence of the peptide thus identifying the proteins concurrently. Peaks derived from the same peptide appear as doublets in mass spectrum due to the 8 Da mass differences between light and heavy labels. The doublet peak intensities of the peptides can be compared and used to represent the relative abundance of the proteins in the two labeled samples. ICAT can significantly reduce the complexity of the mixed samples, thus allowing the determination and identification of certain low abundant proteins. Furthermore, ICAT is fully compatible with protein derived from body fluids, cells, or tissues under different conditions as well as after biochemical, immunological, or physical fractionation and treatment. However, ICAT also has several limitations including the missed identification of proteins with no or few cysteine residues (96.1% of the human proteome contains at least one cysteine), and losing information of post-translational modifications (PTM) (Tournigand, C., et al.,2004). Same as SILAC, ICAT is also limited by the small sample number (2 samples) that can

be analyzed in each run. Moreover, the modification of the peptide by ICAT reagent (around 500 Da) is relatively large, which can complicate the interpretation of tandem mass spectrometry (MS/MS) spectra due to the addition of the biotin group, especially for small peptides (Leitner, A. and W. Lindner, 2004; Goshe, M.B. and R.D. 2003). Many of these limitations have been overcome by the new cleavable ICAT (cICAT) reagent that employs ^{13}C isotopes and an acid-cleavable biotin group (Yu, L.R., et al., 2004; Hansen, K.C., et al., 2003). This new version of the reagent can make the enrichment and elution of the labeled peptide more efficient and convenient and simplify the spectra analyse process.

1.4.3 iTRAQ – Multiplexed chemical tagging for quantitation

Although powerful, aforementioned SILAC and ICAT only allow the comparisons between two or three samples at one single LC run. In order to overcome this limitation, a 4-plex followed by an 8-plex isobaric quantitative labeling technique named iTRAQ has been developed and introduced in 2004 (Ross, P.L. et al., 2004) and 2007 (Choe, L., et al., 2007) by Applied Biosystems.

8-plex iTRAQ reagents were designed as isobaric tags which consist of a reporter group (from 113-121), a mass balance group (carbonyl) and a group that reacts with peptides (NHS ester) (Figure 1.6.A). The reagents specifically label all the amine groups of the digested peptides through an amide linkage. The total mass of the reporter and the balance group are kept identical by incorporating different isotopic combinations of ^{13}C, ^{15}N, and ^{18}O atoms, thus avoiding problems with chromatographic separation seen with enrichment involving deuterium substitution (Choe, L., et al., 2007). The reporter group ranges in mass of 113-121 by incorporating the isotopic atoms, while the

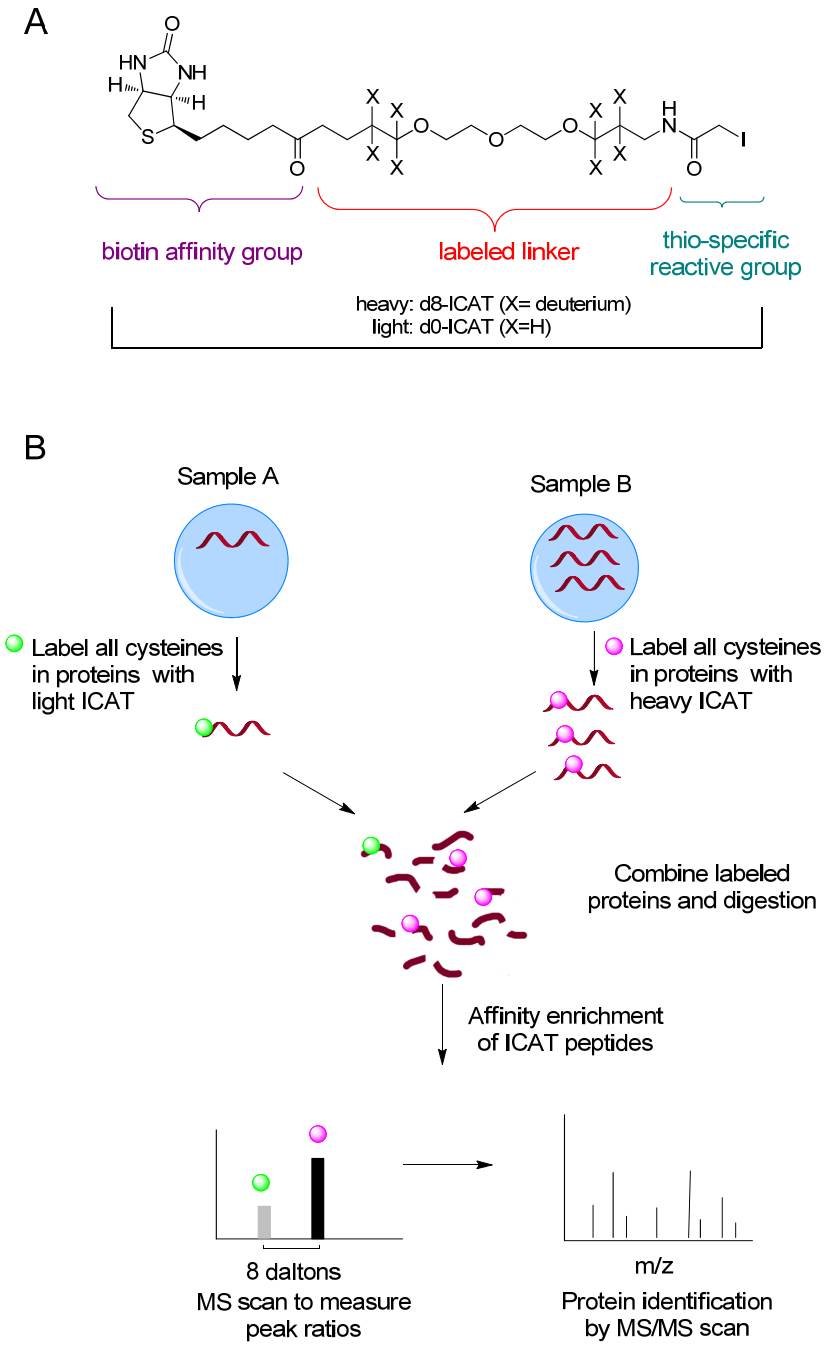

Figure 1.5 Quantitative proteomics by using isotope-coded affinity tag (ICAT). (A) The structure of ICAT reagent. (B) The work flow of ICAT labeling.

balance group has a mass of 184 to 192, thus ensuring the identical total mass is 305 for each of the four reagents. When incubating the reagent with the peptides, the amine reactive group (NHS ester) forms an amide linkage to the peptide amines (N-terminal or ε amino group of lysine). After mixing the labelled peptides, the peptides labeled with different iTRAQ tags are eluted and ionized as one single MS peak (identical *m*/*z*) as they are isobaric. The amide linkages formed by iTRAQ reagents are broken in a manner similar to backbone peptides bonds when subjected to Collision-induced dissociation (CID). Upon MS/MS fragmentation, the balance groups are lost (neutral loss) while the reporter groups generate MS/MS signature ions with m/ z 113–121. This mass range has rather clean background with almost no contamination signals (except m/z 120 for immonium ion of phenylalanine) produced due to collision induced dissociation (CID) in Tandem mass spectrometry (MS/MS). The quantification of the peptide abundance can be calculated from the relative areas of the reporter peaks in each sample (Figure 1.6C). A series of strong signature *y*- and *b*- ions were also generated to allow highly confident protein identification along with peptide quantitation during the MS/MS fragmentation process (Ross, P.L. et al., 2004; Zieske, L.R., 2006). Different from ICAT, the quantitation of iTRAQ is performed at the MS/MS process rather than in MS stage. Using iTRAQ-based quantitative proteomics, up to eight samples can be labeled and quantified simultaneously

In our study, we choose the most versatile labeling approach, iTRAQ for comparing the enriched drug interactive proteins from the non-specific binding proteins. The detailed methodology and its efficacy are described in the following chapter. iTRAQ provides precise and accurate quantitation of up to 8 samples simultaneously, allowing the inclusion of the biological replicates or drug competition of pull-down samples.

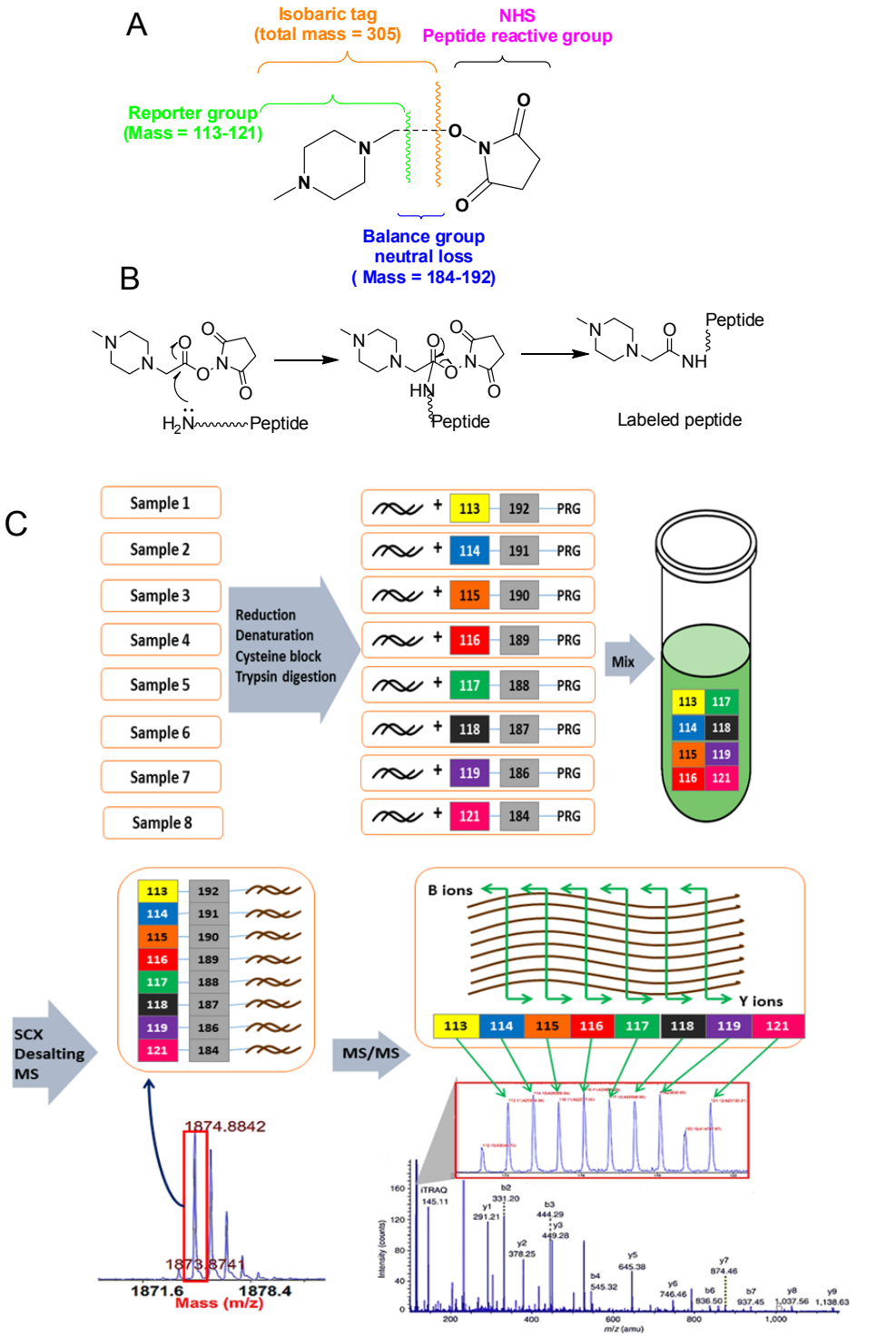

Figure 1.6 Structure of iTRAQ reagent (8-plex) and labeling work flow of iTRAQ. (A) The structure of iTRAQ reagent. (B) The reaction scheme of iTRAQ reagent reacted with amine. (C) The iTRAQ labeling work flow. After reduction, alkylation, and digestion, each sample is tagged with a different iTRAQ reagent, mixed at 1:1 ratio and analyzed by LC-MS/MS.

1.5 Emerging Chemical Proteomics

The traditional 2-DE based and gel-free proteomics enable researchers to compare the relative protein levels across multiple samples; however, these methodologies can only provide the information on protein expression level or abundance changes. As a result, these approaches are unable to disclose the direct information on protein activity and protein interaction, including protein-protein and protein-small molecule interactions, etc. Such information is extremely important for the understanding of the structures and functions of the proteins, which help people to gain more insights into the complex physiological and pathological processes.

The emerging chemical proteomics offers a means to systematically analyze the protein activity and small molecule interaction other than protein abundance alone. This multidisciplinary approach makes use of the synthetic small molecules that can covalently react with catalytic residues in an enzyme active site. The specific activity of the chemically reactive group allows specific proteins or protein complex to be tagged, purified, and identified. As a result, this technique is able to identify novel enzymatic proteins and has the potential to accelerate the discovery of new drug targets. The following sections will briefly describe the development of the chemical proteomics methods and their applications especially in drug target identification and the studies of newly synthesized proteins.

1.5.1 Drug target identification

The majority of drugs exert pharmacological effects by interacting with their target proteins. A comprehensive identification of the specific protein targets of a drug is a critical step in unravelling the mechanisms of the known drug effects and thereby enhancing our understanding of the drug pharmacodynamics to refine its clinical application in future. Besides, the

identification of molecular targets can also provide the information on so-called “off-targets” of compounds and drugs, the unexpected target proteins which may lead to unwanted biological activity and toxicity. It should be noted that the concept of “polypharmacology” has been accepted by increasing researchers recently (Ziegler et al. 2013). People found that actually most of the drugs exert their disease modulation effects by simultaneously targeting several proteins. And this rocked the concept of “one gene, one drug, one disease”(Lounkine et al. 2012).

Chemical proteomics, a multidisciplinary method which integrate organic synthesis with cell biology and mass spectrometry platform, has provided a direct and comprehensive way to profiling the targets of a drug and explaining its mechanism of action (MOA). The mostly used approaches to identify protein targets of a drug typically utilize immobilized drug affinity chromatography coupled with mass spectrometry (MS) (Harding, M.W., Galat, A., Uehling, D.E., Schreiber 1989; Brown, E.J., Albers, M.W., Tae Bum Shin, Ichikawa, K., Keith, C.T., Lane, W.S., Schreiber 1994). In this method, the bead-immobilized drugs are incubated with protein extracts followed by extensive buffer wash to remove the non-interactive proteins. Next, the targeted proteins are released by high amount of free drug or heat denaturation. Finally, the bond proteins can be identified using mass spectrometry-based proteomics methods. Using these approaches, targets of several important drugs and thief mechanisms of action have been successfully disclosed, e.g. imatinib, dasatinib, rapamicin, wortmannin, withaferin A, stauprimide, thalidomide, and etc. (Ziegler, S. et al., 2013).

Recently, several excellent studies have utilized the affinity-based drug pull down to profile the drug targets and pointed out the side effects of the drug or possible mechanism of drug resistance. Handa and his college modified thalidomide into affinity beads for enriching its functional targets(Ito et al. 2010). They identified cereblon (CRBN) as a thalidomide-targeting protein. CRBN and its downstream partner proteins are important for limb

development in zebrafish and chicks. Their result reveals the basis for thalidomide teratogenicity and may illuminate the development of new thalidomide analogues without teratogenic activity. Very recently, Zhang had used an immobilized Pyrazinamide (PZA) analogue to study its direct binding partners (W. Shi et al. 2011). Pyrazinamide (PZA) is a first-line tuberculosis (TB) drug which can shorten the duration of chemotherapy. Using the chemical proteomics approach, they identified the ribosomal protein S1 (RpsA) as one of the targets possibly through inhibition of trans-translation. They found RpsA overexpression correlated with the increased PZA resistance and three PZA-resistant clinical isolates harboured RpsA mutations. Their results also suggested inhibition of trans-translation may play an important role in the anti TB effects.

Although powerful, these methods can only be applied to cell lysates but not an *in vivo* setting, due to the requirement of a solid support. The *in vitro* target profiling may not accurately reflect the drug's actions in the physiological environment *in vivo*. To overcome this limitation, several groups have used the activity-based protein profiling (ABPP) combined with bio-orthogonal click chemistry to identify drug targets both *in vitro* and *in vivo* (Figure 1.8) (Speers et al. 2003; Ovaa et al. 2003; Evans & Cravatt 2006; Nomura et al. 2010; Paulick & Bogyo 2008; Fonović & Bogyo 2008; Böttcher et al. 2010; P.-Y. Yang et al. 2010; C.-X. Liu et al. 2012; Shi et al. 2012; Willems et al. 2011; Böttcher & Sieber 2008b; Gersch et al. 2012). ABPP probes exert their functions by a covalent reaction with the target proteins or photoaffinity-based labeling via incorporation of photoreactive groups. With the increasing sensitivity of modern MS platform, even low abundance protein targets can be successfully identified to explain the MOA of a drug. In the following section, I will briefly discuss the ABPP and clickable ABPP approach in drug target discovery process.

1.5.2 Activity-based protein profiling

Activity based protein profiling (ABPP), pioneered by Bogyo, Cravatt and others (Speers et al. 2003; Ovaa et al. 2003; Evans & Cravatt 2006; Nomura et al. 2010; Paulick & Bogyo 2008; Fonović & Bogyo 2008; Böttcher et al. 2010; P.-Y. Yang et al. 2010), is a novel functional proteomics technology to study the enzyme activities and targets of mechanism-based suicide small molecules. Activity based probes (ABPs) generally possess three basic elements: 1) a reactive group (or an electrophilic group) for targeting and covalently labeling the active sites of an enzyme; 2) a reporter tag or handle that can be used for visualization (e.g. fluorophore), enrichment and identification (e.g., biotin) of modified proteins; 3) a flexible linker connecting the reporter and reactive group and providing enough space between them. (Figure 1.7)

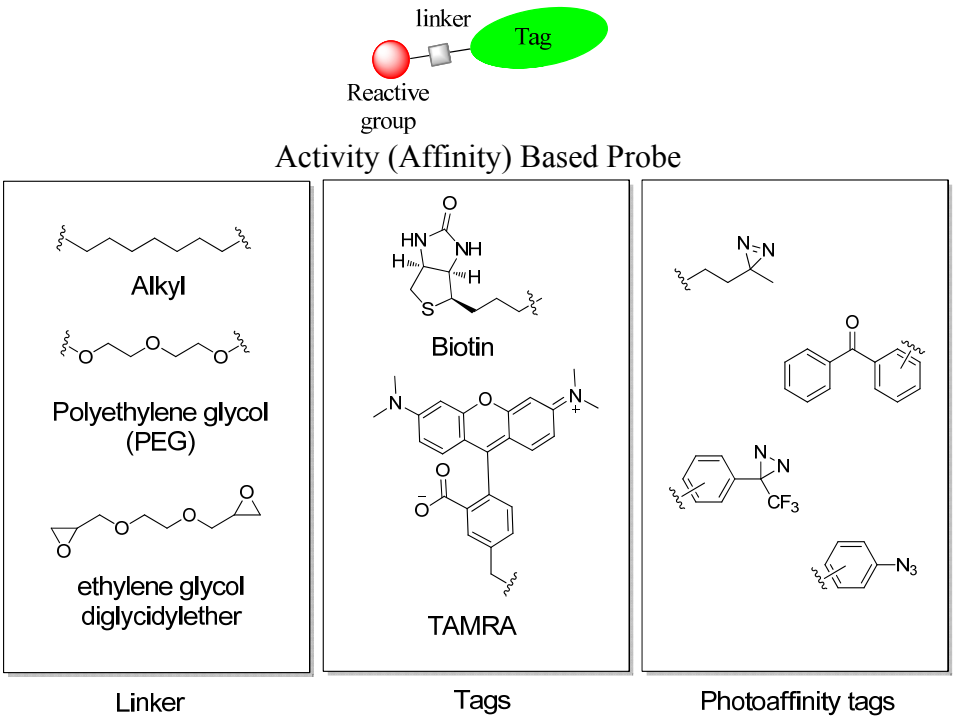

Figure 1.7 Structure of an Activity (Affinity) based probe. ABP probes usually consist of three basic components: a reactive group for covalent binding to the target proteins; a linker group to provide enough spacing and specificity; and a tag for visualization or purification, identification. For A*f*BP, it may have the photo-affinity tag to enable the covalent binding after UV irradiation.

Normally, ABPs can be categorized into mechanism-based or affinity-based probes (A*f*BP), according to whether a covalent linkage forms during the probe binding. For mechanism-based ABPs, the reactive group of the probe usually contains an electrophilic structure which can specifically and irreversibly react with catalytic residues in the enzyme's active site thus form a very stable adduct. While for the A*f*BP, the covalent interaction is lacking and the drug and targets interacted through the reversible affinity linkage. Therefore, a photo-affinity tag (Figure 1.7) can be introduced to the probe which can covalently bind to the spatially proximate target proteins upon exposure to UV light.

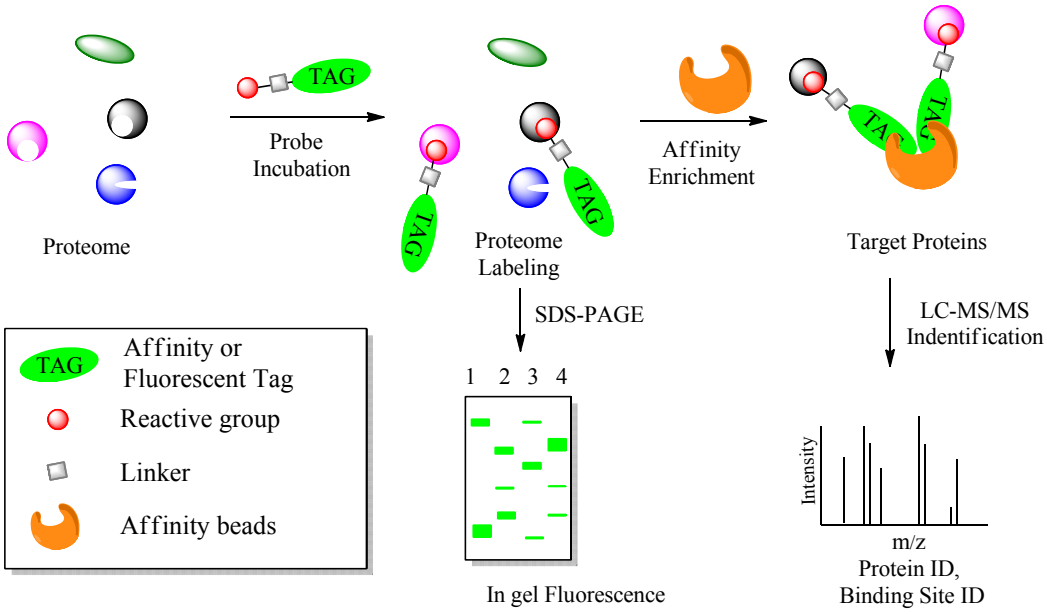

Figure 1.8 General workflow of target profiling using activity-based probe (ABP). The cell lysates are firstly incubated with ABP. Subsequently the labeled proteome can be detected by in-gel fluorescence scanning (by fluorescence -tagged probes). Alternatively, protein targets can be enriched and identified using LC- MS/MS (by biotinylated probes).

The reactive groups of ABPs usually possess an electrophile that can be covalently linked to a nucleophilic residue (mainly Ser, Cys or Lys) in the active site of an active enzyme. Notably, an enzyme that is inhibited by inhibitors or post-translationally modified will not react with an ABP since the activity of the enzyme has changed or lost.

In ABPP proteomics experiment (Figure 1.8), the ABP is incubated with the proteome (cell lysate) and the probe will bind to its active targets. Then, the probe-labeled proteins can be visualized either by in-gel fluorescence scanning (fluorescence-tagged probes) or identified through pull-down followed by LC-MS/MS (biotinylated probes).

A main advantage of ABPP is its capability of profiling the active site of the enzyme directly, not limited to only the protein relative abundance. Thus far, various ABPP probes have been developed for several enzyme classes, such as cysteine proteases, metalloproteases (Saghatelian, et.al, 2004), and serine hydrolases (Liu, Patricelli, & Cravatt, 1999). This method has a great advantage over traditional methods that depend on abundance rather than activity.

When combined with tandem mass spectrometry, ABPP allows the identification of various active enzymes or drug targets simultaneously from a single sample. This technique has been used increasingly in drug discovery and development process, which helps to explain the MOA of the compound.

1.5.3 Tandem bio-orthogonal labeling and Click chemistry for probe design

The attachment of the affinity or fluorescent tag in ABPP usually restricted the application scope of ABPP for *in vivo* study due to the low cell permeability of the commonly used tags. However, during the cell lysis process, various activators and inhibitors which influence the enzyme activity are often released due to the disruption of the cell compartments. As a result, the *in vitro* target profiling may be different and not accurately reflect the drug's actions in the physiological environment *in vivo*. In order to retain the drug activity and make the drug still cell permeable, minimal modification should be used when introducing the tags into the drug. This issue can be solved by using the bio-orthogonal chemistry methods, such as Staudinger ligation between azides and phosphines (Figure 1.9A) or copper(I)-catalyzed Huisgen-[3+2]-azide-alkyne cycloaddition (often referred to as "click" chemistry, Figure 1.9B).

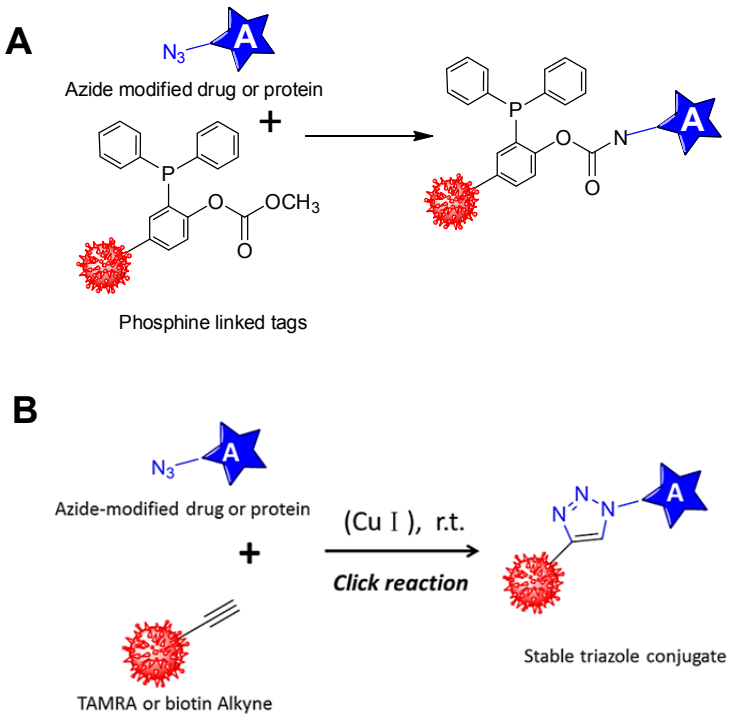

Figure 1.9 Click chemistry and Staudinger ligation. (A) Staudinger ligation. (B) Copper (I)-catalyzed "click" chemistry.

These bio-orthogonal tags (normally an azide or alkyne group) are small enough so that introducing these tags to drugs normally will not affect the cell permeability of the drug significantly. Staudinger-Bertozzi ligation was first introduced by Bertozzi in chemical biology and was initially used to profiling glycosylated proteins on cell surfaces. Although specific, however, this reaction suffers from phosphine oxidization and slow reaction kinetics (Sletten, E. M.,2009). Alternatively, "click" chemistry is a rapid reaction, through which azide can undergo Cu (I)-catalyzed [3+2] cycloaddition with terminal alkynes to yield the stable triazole conjugates. This reaction can easily proceed in aqueous environments and exhibit extremely high selectivity with its partner thus is called 'bio-orthogonal' reaction. (Prescher J.A., *et al.* 2005).

Therefore, we can first label the target proteins in living cells by using this cell-permeable clickable probe, and following cell lysis, tag them with the fluorescent or biotin tag for visualization or enrichment (Figure 1.10).

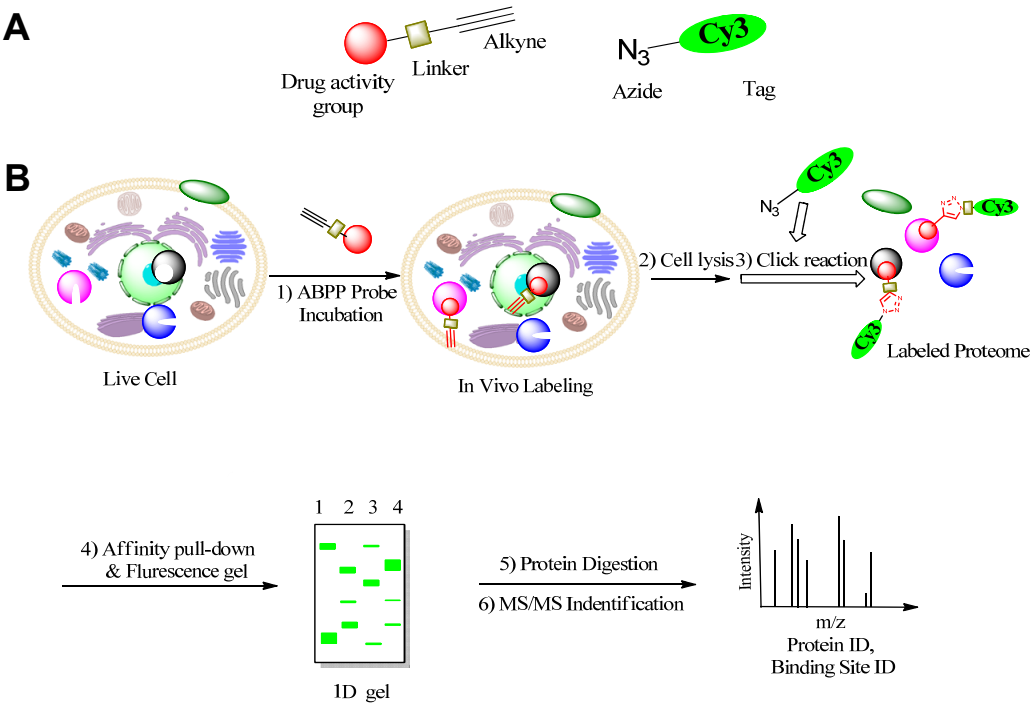

Figure 1.10 General workflow of the targets profiling using "clickable" cell-permeable probe in live cells.

1.5.4 Chemical metabolic labeling with unnatural amino acid

In chemical proteomics, besides utilizing the small molecule probes to delineate the interactive partners, another emerging field involves using chemically modified unnatural metabolites to study the dynamic protein synthesis or post-translational modification. Recently, a novel technique for labeling newly synthesized proteins has been developed by Tirrell and colleagues (Dieterich, Link et al. 2006). In this method, L-azidohomoalanine (AHA), an amino acid analog of methionine containing an azide moiety, can be incorporated into newly synthesized proteins without any manipulations and can be readily detected by a aforementioned "click chemistry" between an azide and alkyne-bearing tags (Dieterich, Link et al. 2006). Briefly, this approach involves two subsequent steps. During the first step, similar to the traditional metabolic labeling with radioactive amino acids (^{35}S-labeled methionine or cysteine), AHA is incubated with the cells or organisms and incorporated into newly synthesized proteins by cellular machinery. This azide tag allows distinguishing metabolically labeled proteins from unlabled proteins. While in the second step, the azide bearing unnatural amino acid AHA is covalently tagged with a fluorescent tag or biotin tag through bio-orthogonal click chemistry (Figure 1.11A and B). In combination with fluorescent tagging and detection, the newly synthesized proteins can be conveniently visualized by microscopic imaging or in-gel fluorescent scanning. Alternatively, the AHA labeled proteins can be "clicked" with biotin tags for affinity enrichment. After affinity purification using avidin beads and trypsin digestion, the peptides can be identified by mass spectrometry (Dieterich, Link et al. 2006; Dieterich, Lee et al. 2007). As reported, the incorporation of AHA is non-toxic to the cell. Besides, AHA will not affect the global rates of protein synthesis and degradation. Based upon this convenient technique, the metabolic labeling of AHA into newly synthesized proteins has been widely used in mammalian cells (Dieterich, Link et al. 2006), primary neuronal cells, brain slice cultures (Dieterich, Hodas et al.) and larval zebrafish (Hinz,

Dieterich et al.).

Very recently, Eichelbaum and Krijsveld utilize the AHA labeling to study the secreted proteins. They incubated the cells with a pulse of AHA, which enables the possibility to selectively enrich newly synthesized proteins secreted into the cell medium. At the same time, they also applied pulsed SILAC (pSILAC) to label two parallel cell populations with either intermediate- or heavy- arginine and lysine for a precise time window. Thus, they were able to quantify the relative abundance of the newly secreted proteins (Eichelbaum, Winter, Krijgsveld, 2012). In another recent study, Howden and Acuto demonstrated the ability to quantify stimuli-induced proteome dynamics in primary cells by combining AHA and SILAC labeling. In their study, they were able to determine the early expression level changes of >600 proteins in primary resting T cells under activation stimuli (Howden et al., 2013).

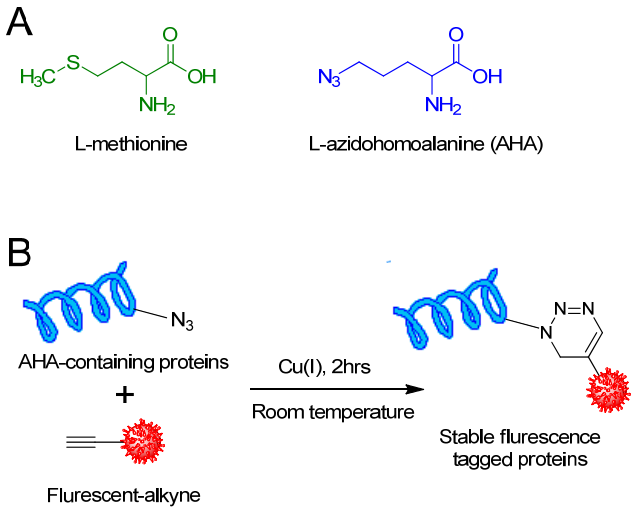

Figure 1.11 AHA labeling of newly synthesized proteins. AHA labeling of newly synthesized proteins. (A) Structure of azidohomoalanine (AHA), an analog of methionine containing an azide moiety. (B) Click azide/alkyne reaction. The azide and alkyne moieties are interchangeable, where the molecule can be labeled with an azide and react with a fluorophore- or biotin-alkyne.

1.6 Objectives

The aim of my thesis is to advance the application of quantitative and chemical proteomics in drug target identification and autophagic proteolysis research. For the first aim, the drug target identification approach we developed should be unbiased and could offer a means to specifically and comprehensively identify drug targets in live cells. It is hoped that this method can be widely applied in drug development and optimization to refine the therapeutic potentials of drugs by uncovering knowledge on their specific targets and mechanisms of action. The specific target of andrographolide will be identified using this newly developed method and validated through different bio-assays. In the second part, we developed a novel method to determine the autophagic protein degradation level using metabolic labeling. This novel method should be simple, sensitive, and specific for measuring autophagic protein degradation and could be easily adapted for high throughput screening of autophagy modulators.

Chapter 2

A Quantitative Chemical Proteomics Approach to Profile the Specific Cellular Targets of Andrographolide, a Promising Anticancer Agent that Suppresses Tumor Metastasis

2.1 Summary

Drug target identification is a critical step towards the understanding of the mechanism of action of a drug, which will help to improve the current therapeutic regime and to expand the drug's therapeutic potential. However, current *in vitro* affinity chromatography-based and *in vivo* activity-based protein profiling (ABPP) approaches generally face difficulties discriminating specific drug targets from non-specific ones. In this chapter, we describe a novel approach combining isobaric tag for relative and absolute quantitation (iTRAQ) with Clickable ABPP, named ICABPP, to specifically and comprehensively identify the protein targets of andrographolide (Andro), a natural product with known anti-inflammation and anti-cancer effects, in live cancer cells. We identified a spectrum of specific targets of Andro, which furthered our understanding of the mechanism of action of the drug. We found that Andro has a potential novel application as the tumor metastasis inhibitor, which was validated through cell migration and invasion assays. Moreover, we have unveiled the target binding mechanism of Andro with a combination of drug analogue synthesis, protein engineering and mass spectrometry-based approaches and determined the drug-binding sites of two protein targets, NF-κB and actin.

2.2 Introduction

As most drugs exert pharmacological effects by interacting with their target proteins, identification of which is a critical step in unravelling the

mechanisms of drug action. It is also imperative for our understanding of the pharmacodynamics of a known drug, suggesting the potentially unrevealed actions and thus refining its future clinical applications. Traditional approaches to identify protein targets of a drug typically utilize immobilized drug affinity chromatography coupled with mass spectrometry (MS) (Harding, M.W., Galat, A., Uehling, D.E., Schreiber 1989; Brown, E.J., Albers, M.W., Tae Bum Shin, Ichikawa, K., Keith, C.T., Lane, W.S., Schreiber 1994). These methods can only be applied to cell lysates but not an *in vivo* setting, due to the requirement of a solid support. Thus, the in vitro target profiling may not accurately reflect the drug's actions in the physiological environment *in vivo*. To overcome this limitation, several groups have used the activity-based protein profiling (ABPP) combined with bio-orthogonal click chemistry to identify drug targets both *in vitro* and *in vivo* (Figure 2.1) (Speers et al. 2003; Ovaa et al. 2003; Evans & Cravatt 2006; Nomura et al. 2010; Paulick & Bogyo 2008; Fonović & Bogyo 2008; Böttcher et al. 2010; P.-Y. Yang et al. 2010; C.-X. Liu et al. 2012; Shi et al. 2012; Willems et al. 2011; Böttcher & Sieber 2008b; Gersch et al. 2012). ABPP probes exert their functions by a covalent reaction with the target proteins or photoaffinity-based labeling via incorporation of photoreactive groups. With the increasing sensitivity of modern MS platform, low abundance protein targets can be successfully identified. Although both the conventional affinity chromatography and recent ABPP-based methods allow us to detect a set of candidate protein targets for a drug, it remains difficult to discriminate specific interactions from non-specific ones. Hence, more time and effort are needed for subsequent validation due to the presence of a large number of non-specific binders. Therefore, there is an urgent need to develop comprehensive unbiased methods for specific target identification. Quantitative proteomics has been used to profile enriched kinases using cell lysate-based kinobead pull-down. However, these types of experiments are mainly suitable for studying kinase inhibitors(Bantscheff et al. 2007). Recently, SILAC-based proteomics methods have been applied to determine the specific

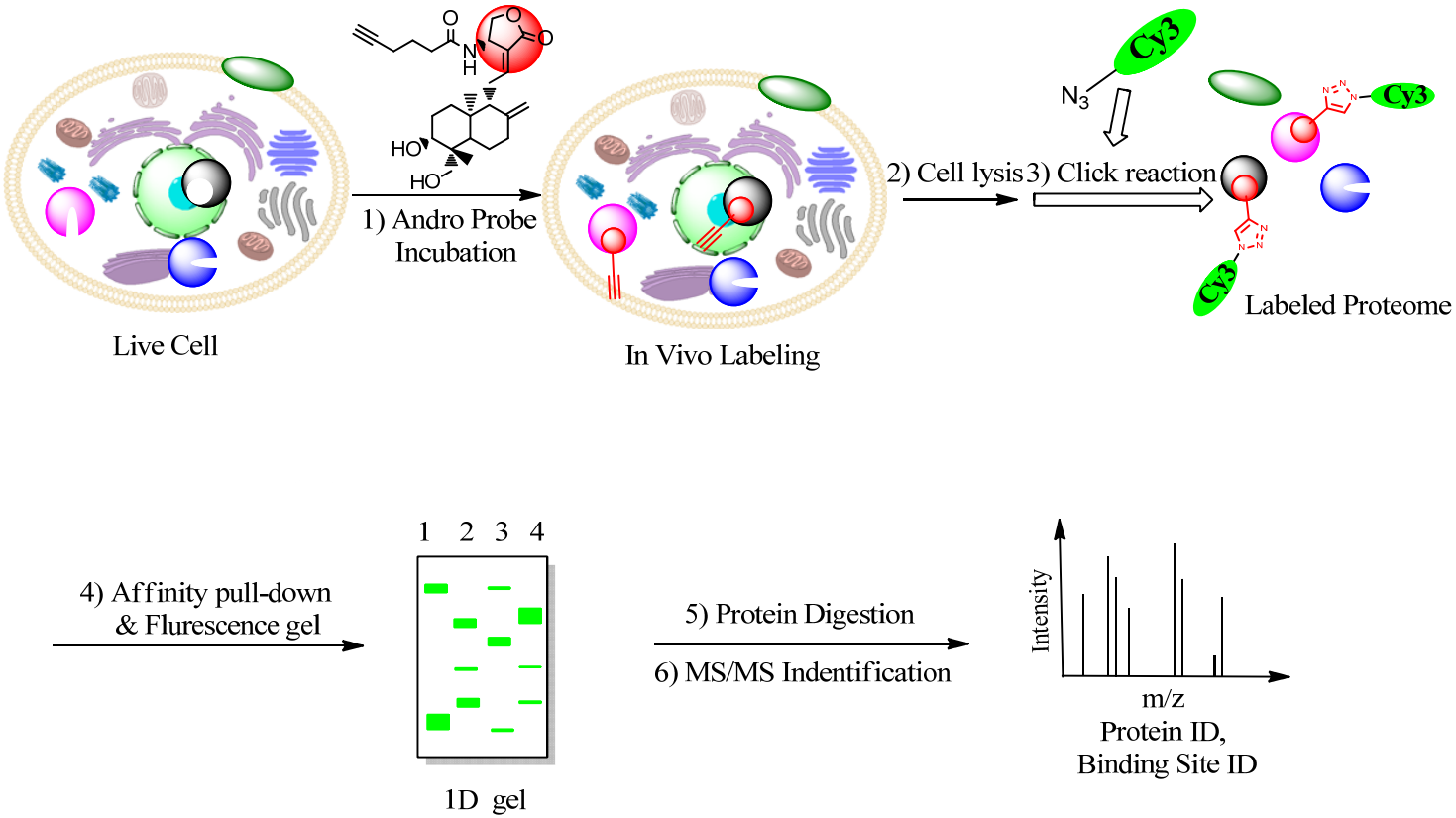

Figure 2.1 General workflow of the potential cellular targets profiling using cell-permeable, activity-based Andro probe. The live cells are firstly incubated with Andro probes followed by cell lysis. Subsequently the labeled proteome are clicked with fluorescent dye to allow visualization of target proteins by SDS-gel. Alternatively, protein targets can be fished out with biotin azide and identified using MS/MS.

binders of small molecules or proteins with certain post-translational modifications (Sharma et al. 2009; Ong et al. 2009; Li et al. 2012). These studies shed light on how quantitative proteomics can improve the specificity of the target protein identification. Nevertheless, due to the inherent limitation of SILAC, such an approach takes a long time for complete incorporation of isotopic amino acids. Furthermore, it is also extremely difficult to apply the SILAC approach to tissue and body fluid samples, which are of particular relevance to biomedical research.

Here we introduce an isobaric tag for relative and absolute quantitation (iTRAQ)-based Clickable ABPP (ICABPP) approach for unbiased, specific and comprehensive identification of target proteins in live cells. iTRAQ is a stable-isotope labeling approach for multiplexed quantitative proteome profiling (Ross et al. 2004). An overview of the technique is illustrated in Figure 2.2a. In this assay, cells are first incubated with a clickable probe or with DMSO, which serves as a negative control. After the probe permeates the cell and covalently binds to its dedicated in situ targets, the washed cells are lysed, clicked with biotin-N3 tag and enriched through avidin pull-down in parallel. The beads are washed thoroughly and the bond proteins are directly digested on beads with trypsin. The resulting peptides are labeled with respective iTRAQ reagents, and pooled together for further identification and quantification by LC-MS/MS. This technique enabled us to discriminate specific protein targets from non-specific and endogenously biotinylated proteins. Biological replicates of probe- or DMSO-treated samples are included to overcome experimental variations. As shown in Figure 2.2b, non-specific binding proteins' iTRAQ reporters have equal or similar intensities, whereas specific target proteins enriched by the probe show highly differential intensities compared to DMSO-treated control samples (as illustrated by the significantly higher reporter intensities of 116 and 117 vs. 113 and 114 shown in Figure 2.2b). The multiplexing nature of iTRAQ-based chemical proteomics method allows replicated enrichments to be compared within a single LC-MS/MS analysis, hence increasing the accuracy of identifying specific targets and minimizing experimental errors.

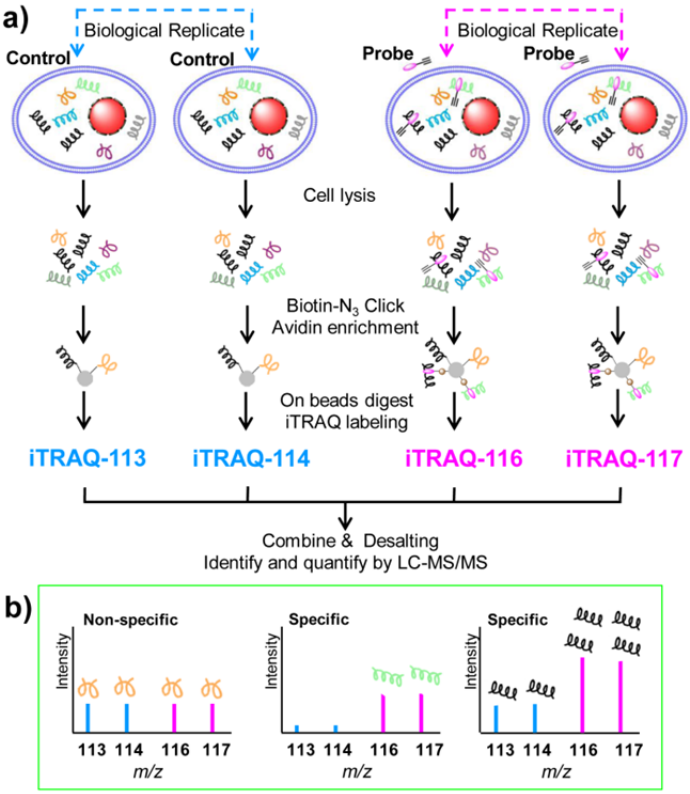

Figure 2.2 Identifying specific drug targets using ICABPP approach in live cells. a) Live cells were treated with DMSO and clickable probe in duplicates. Cells were lysed and tagged with biotin-N3 using click chemistry in parallel. The biotin bearing target proteins were enriched through avidin pull-down and directly digested on beads. The resulting peptides of the two biological replicates of control pulled-down samples were labeled with 113 and 114, respectively, and two probe pulled-down samples were labeled with 116 and 117, respectively. The labeled peptides were combined together to be identified and quantified by LC-MS/MS. b) For the non-specific targets, the iTRAQ reporters show similar intensities, while for the specific targets, the reporters show highly differential intensities.

In this context, ICABPP approach was applied to identify protein targets of andrographolide (Andro, Figure 2.3), a natural product with known anti-inflamation and anti-cancer effects, (Bao et al. 2009; Zhou et al. 2006; Zhou et al. 2010; Zhou et al. 2008; Jada et al. 2008) in live cancer cells. A spectrum of 75 potential Andro targets was identified with high confidence, which suggested that Andro may exert anti-cancer effects by acting on multiple targets to interfere with several cellular signaling pathways. Two targets, NF-κB and β-actin were validated by *in vitro* binding assay and direct

binding site mapping. Furthermore, our data revealed a novel mechanism of Andro in suppressing tumor metastasis.

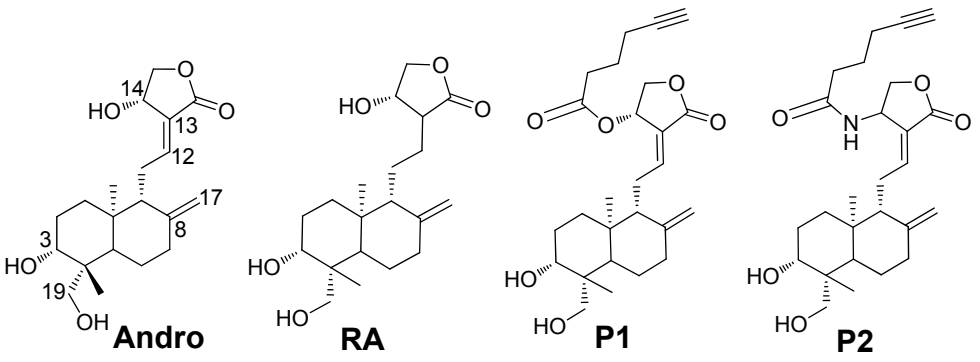

Figure 2.3 Chemical structures of Andro, reduced Andro analogue RA and Andro-based clickable ABPP probe P1 and P2.

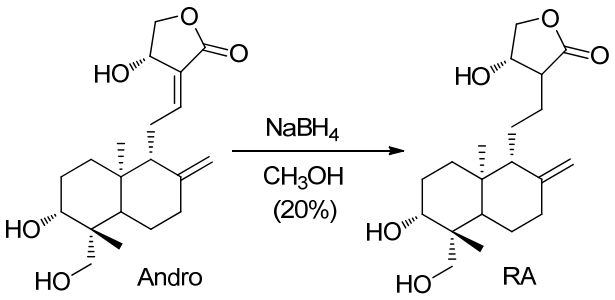

Scheme 2.1 The synthetic scheme for **RA**.

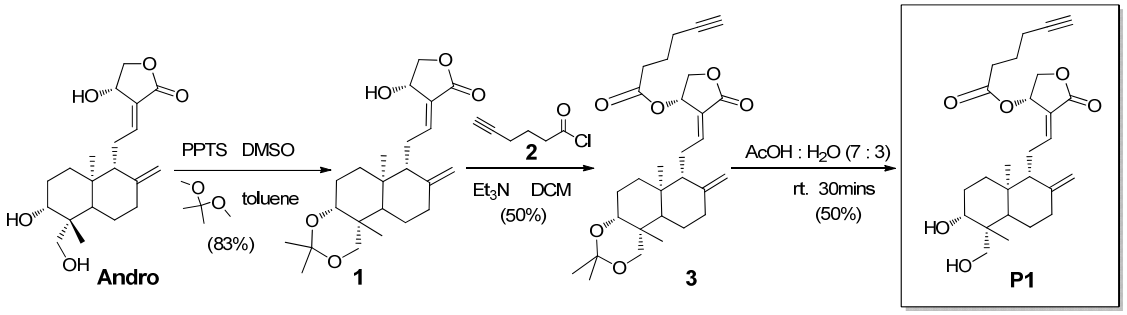

Scheme 2.2 The synthetic scheme for **P1**.

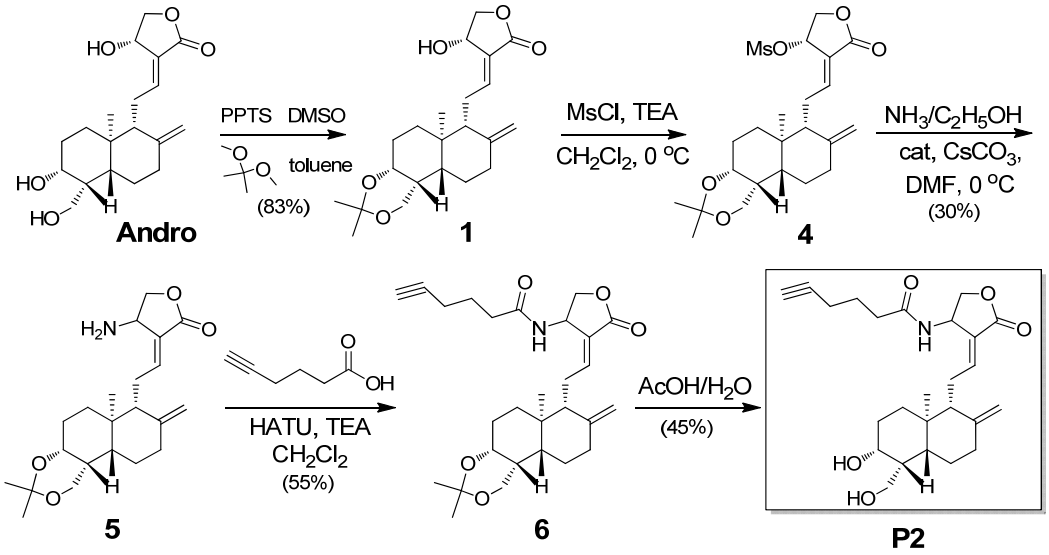

Scheme 2.3 The synthetic scheme for **P2**.

2.3 Results and Discussion

2.3.1 Design and synthesis of Andro-based probes

Ideally, the active moiety of Andro must be retained in the newly designed Andro-based ABPP probe and the attached tag should not affect its interaction with cellular targets during live cell labeling. However, the active moiety and precise mode of action of Andro remain largely elusive. Xia et al. previously reported that Andro binds covalently to Cys62 of NF-κB p50 (Bao et al. 2009; Wang et al. 2007; Xia et al. 2004). Based on this known interaction, we postulated that the α,β-unsaturated γ-lactones might be involved in the protein alkylation. The reduced form of Andro analogue RA (Figure 2.3, synthetic scheme shown in Scheme 2.1) was synthesized to test its biological activity against the colorectal cancer cell line HCT116, which is known to be sensitive to Andro treatment (Zhou et al. 2010; Jada et al. 2008). Our results suggested that Andro had potent anti-cancer effect on HCT116 cell line with IC50 of 31 μM, as well as MV4-11, HeLa and HepG2 cell lines (Table 2.1). When the C12-C13 double bond of Andro was reduced to a single bond, the analogue RA completely lost its cancer inhibitory potency even up to 100 μM

concentration (Figure 2.4), suggesting that the α,β-unsaturated γ-lactones and the covalent protein binding of Andro are critical for its anti-cancer property. Previous structure-activity relationship studies suggested that the ester derivative of Andro at C14 hydroxyl group did not affect the C12-C13 moiety and the drug's potency (Das et al. 2010; Nanduri et al. 2004; Wang et al. 2010). Therefore, we introduced an alkyne handle using the ester linkage at C14 position to synthesize the clickable probe P1 (Figure 2.3, synthetic scheme 2.2). At the same time, to overcome the limitation of the instability of the ester bond, another probe P2 with amide bond linkage was also synthesized. This probe would have better *in vitro* and *in vivo* stability, as it would be less prone to breakage or hydrolysis. (Figure 2.3, Synthetic scheme 2.3). Because the introduction of amino group partially reverted the configuration of C14 during the synthesis, P2 was a mixture of two isomers with the ration of 1:0.8. We did not separate these two isomers as we found that the anti-cancer activity was still retained (vide infra). To investigate whether the structural modifications would influence the anti-cancer potency of the probe, we conducted *in vitro* growth inhibitory assay on HCT116 using P1 and P2. Our data confirmed that P1 and P2 still possess antiproliferative activity (Figure 2.4). Therefore, both P1 and P2 meet the essential criteria for target protein identification.

Cell line	IC_{50}	Tissue of Origin
HCT116	31.2 μM	Colon
MV4-11	53.5 μM	Blood
HeLa	39.1 μM	Cervix
HepG2	42.6 μM	Liver

Table 2.1 IC_{50} values of Andro in HCT116, MV4-11, HeLa, and HepG2 cell lines. Each cell line was treated with Andro in various concentrations for 48 h. The IC_{50} values of Andro in HCT116, HeLa, and HepG2 cell lines were determined using crystal violet assay. The IC_{50} value of Andro in MV4-11 was determined using Propidium Iodide (PI) staining and flow cytometry.

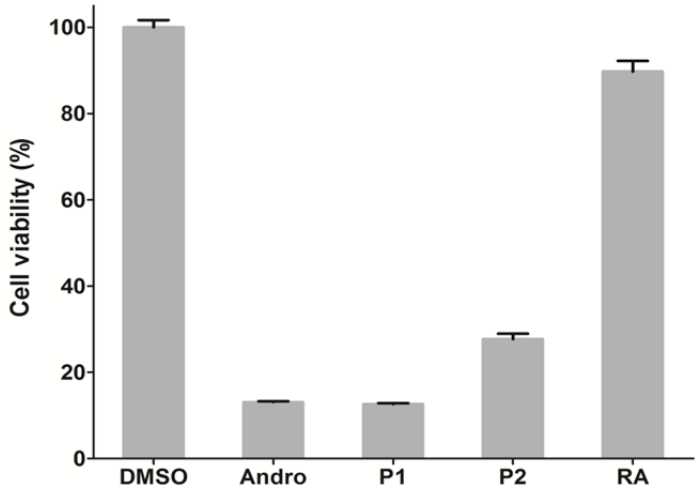

Figure 2.4 Viability of HCT116 cells after 48 hrs of treatment with Andro(100 μM), P1(100 μM), P2(100 μM) and RA (100 μM)

2.3.2 In situ proteome profiling

To visualize the native cellular targets of Andro using fluorescence gel profiling (Figure 2.1), we treated live HCT116 cells with P1 or P2. The probe-labeled proteomes were reacted with Cy3 azide via click chemistry before being resolved on SDS-PAGE for fluorescence detection. As shown in Figure 2.5, in sharp contrast to the DMSO control, P2 labeled proteome yielded high fluorescence intensity bands, signifying that there were proteins interacted with P2. As expected, P1 labeled proteome showed rather weak intensity bands, possibly due to the instability of the ester linker. These observations supported our hypothesis and were consistent with a recent review, which postulated that the elimination of the β-hydroxy group of Andro might occur during the Andro alkylation (Gersch et al. 2012). Based on our results, the stronger labeling intensity of P2 in comparison to P1 suggests that the ester bond of P1 might be broken or hydrolyzed in the reaction, while the amide bond linkage in P2 is more stable (Gersch et al. 2012). Therefore, P2 was chosen for subsequent analyses.

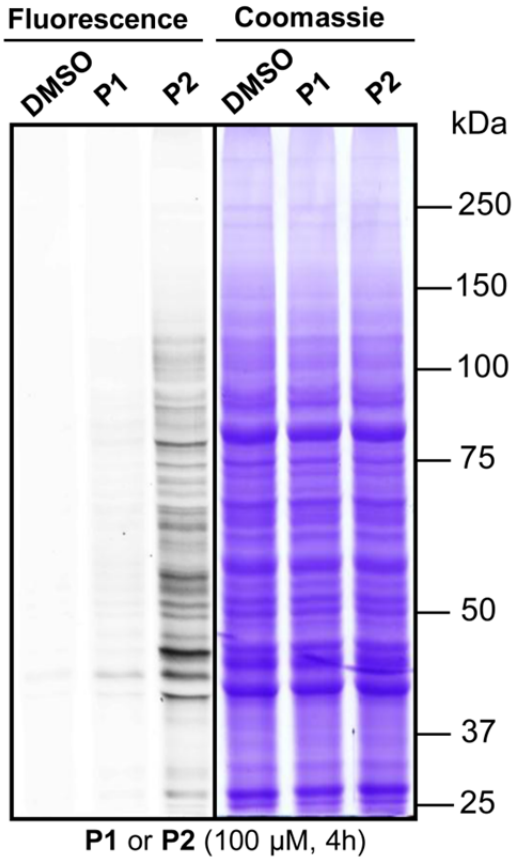

Figure 2.5 The *in situ* fluorescent labeling of HCT116 cells using P1 and P2 (100 μM) together with a DMSO-treated negative control. Probe labeled proteomes were visualized by click conjugation to the Cy3 azide tag, SDS-gel separation, and fluorescent scanning.

2.3.3 ICABPP and target identification

We next performed ICABPP using P2 to identify specific cellular protein targets of Andro (Figure 2.1), which yielded 4 sets of Andro probe vs. control pull-down ratios (116/113; 117/113; 116/114; 117/114). A total of 291 proteins was successfully identified and quantified in our experiment (Figure 2.6). Outliers were identified using p-value >0.05 and 114/113 ratio >1.3 or <0.77. This resulted in 208 proteins being considered to be statistically reliable hits (Figure 2.6). The distribution of the enrichment ratios of these proteins were further presented as a coloured heat map in Figure 2.7. To reduce false positive targets, we chose a highly stringent ratio of 2 as the cut-off to differentiate

specific (red) from non-specific (blue) binding targets. Meanwhile, proteins identified based on a single peptide are considered unreliable and were removed. Consequently, 75 proteins were regarded as the specific targets of Andro based on the above criteria (Figure 2.6). The complete list of the 75 potential targets was shown in Supplemental Table of chapter 2.

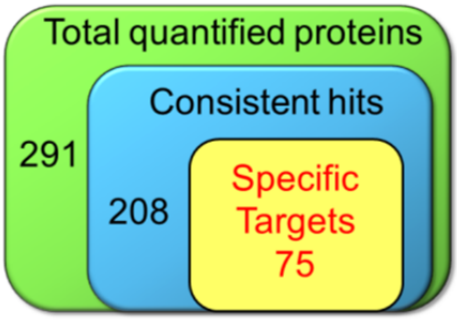

Figure 2.6 Venn diagram showing the total numbers of proteins quantified by ICABBP (green rectangle), statistically reliable proteins (blue) and specific binding targets (yellow).

NF-κB p50, a known Andro target,(Bao et al. 2009; Wang et al. 2007; Xia et al. 2004) was found to be enriched 2.8 fold in Andro pull-down when compared to DMSO control, validating our approach. The subsequent pathway analysis suggested that Andro may exert its anti-cancer effects through multiple targets and pathways: more than 30 targets were involved in cancer cell death pathways; 15 hits were involved in cell migration and metastasis (Table 2.2 and Figure 2.8); 20 hits were related to inflammation and 10 to protein synthesis pathway (the respective pathway analyses are shown in Figure 2.9 and Figure 2.10).

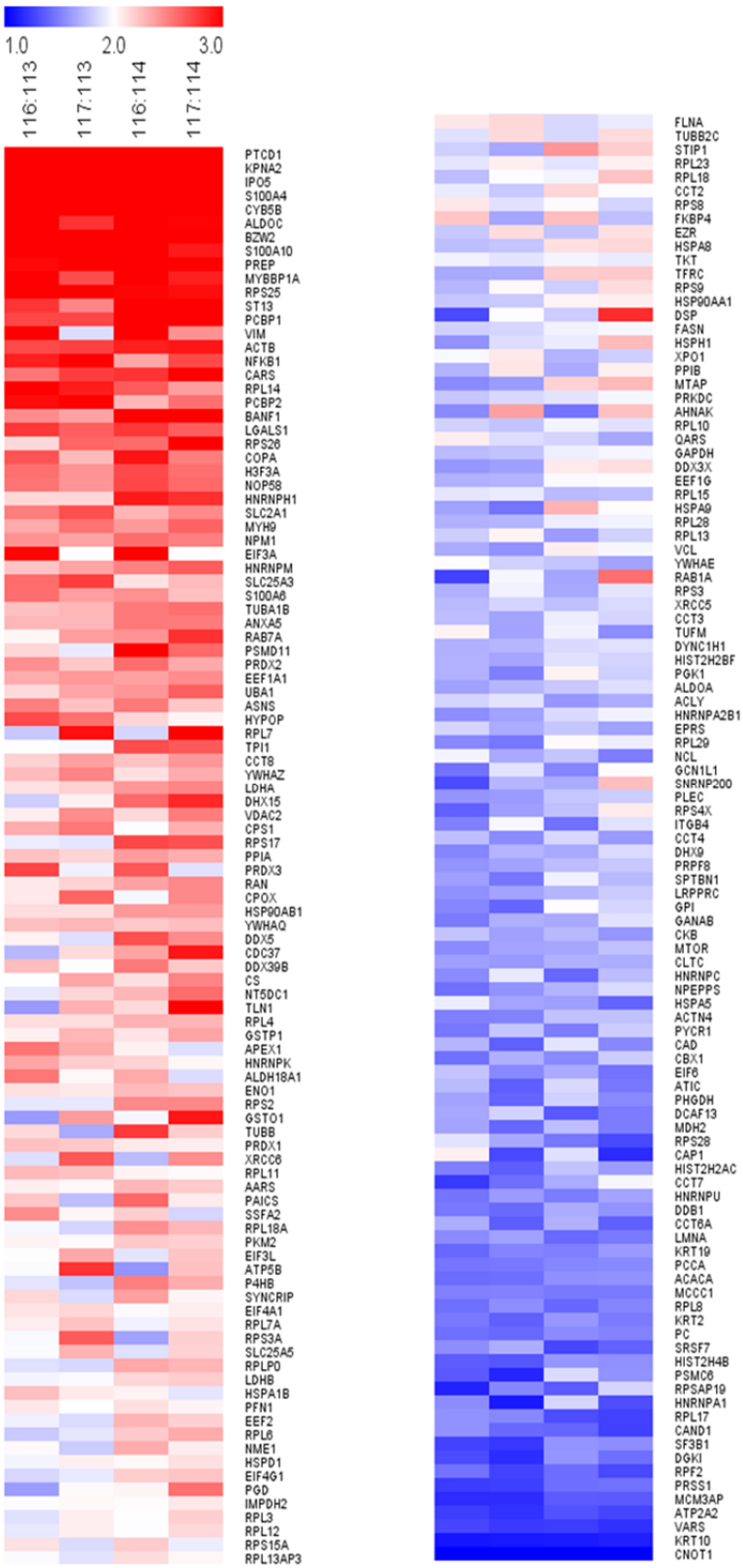

Figure 2.7 Heat map of the enrichment ratio of potential Andro targets fulfilled the statistical requirement. The most enriched proteins are displayed in red, while the least enriched proteins are shown in blue. The color scale for relative enrichment ratio is shown (top of figure).

Name	% Cov	Peptides	116:113	117:113	116:114	117:114	Ave Ratio	p-value
ACTB	60.7	27	2.71	2.75	2.88	2.92	2.81	1.1E-05
NFKB1	10.1	4	2.88	3.40	2.34	2.72	2.80	8.9E-04
HNRNPH1	17.3	4	2.16	2.16	2.90	2.82	2.48	1.5E-03
MYH9	21.6	15	2.33	2.55	2.40	2.61	2.47	5.7E-05
NPM1	26.2	6	2.43	2.36	2.57	2.50	2.46	2.0E-05
TUBA1B	39.3	10	2.25	2.28	2.52	2.56	2.40	1.2E-04
YWHAZ	42.7	8	2.26	2.48	2.12	2.32	2.29	1.3E-04
PPIA	50.3	5	2.24	2.16	2.38	2.32	2.27	3.7E-05
TUBB	46.4	17	2.15	1.67	2.78	2.19	2.16	5.1E-03
PRDX1	56.1	5	2.24	2.22	2.08	2.07	2.15	4.6E-05
HSPA1A	29	9	2.25	2.08	2.05	1.90	2.07	2.3E-04
PFN1	68.6	6	2.09	2.00	2.13	2.04	2.06	1.3E-05
NME1	34.5	4	2.02	1.80	2.32	2.07	2.04	8.4E-04
HSPD1	38.2	13	1.96	2.06	2.03	2.12	2.04	2.7E-05
FLNA	16.8	7	2.09	2.15	1.85	1.92	2.00	2.9E-04

Table 2.2 The potential protein targets related to cell migration and metastasis identified by ICABPP, sorted by average enrichment ratios.

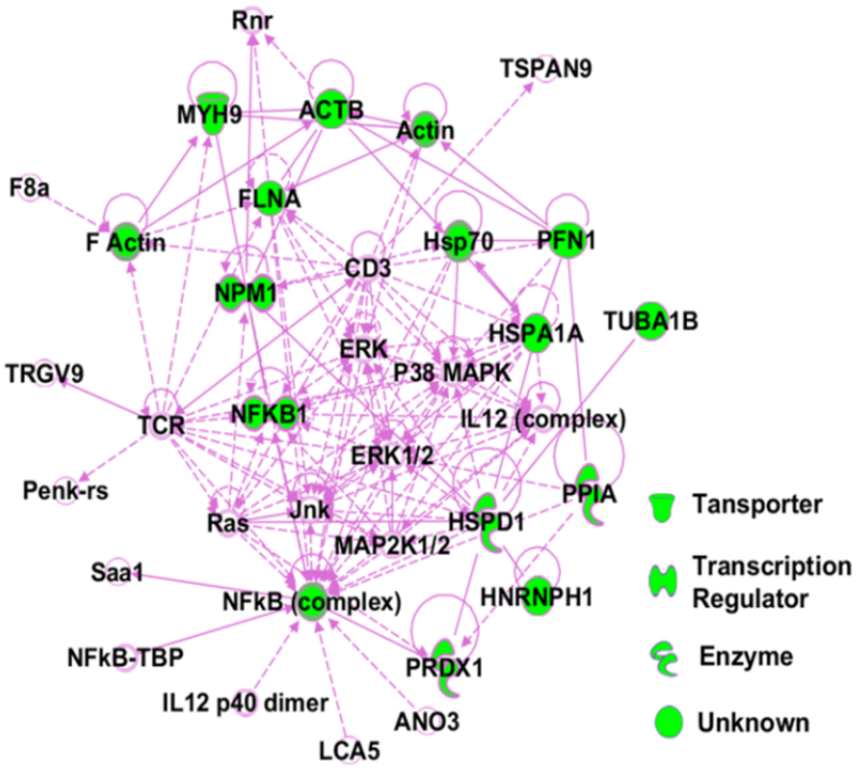

Figure 2.8 Ingenuity Pathway Analysis (IPA) revealing that Andro affects the cell migration and metastasis. All proteins shown in green nodes were identified as the specific targets of Andro.

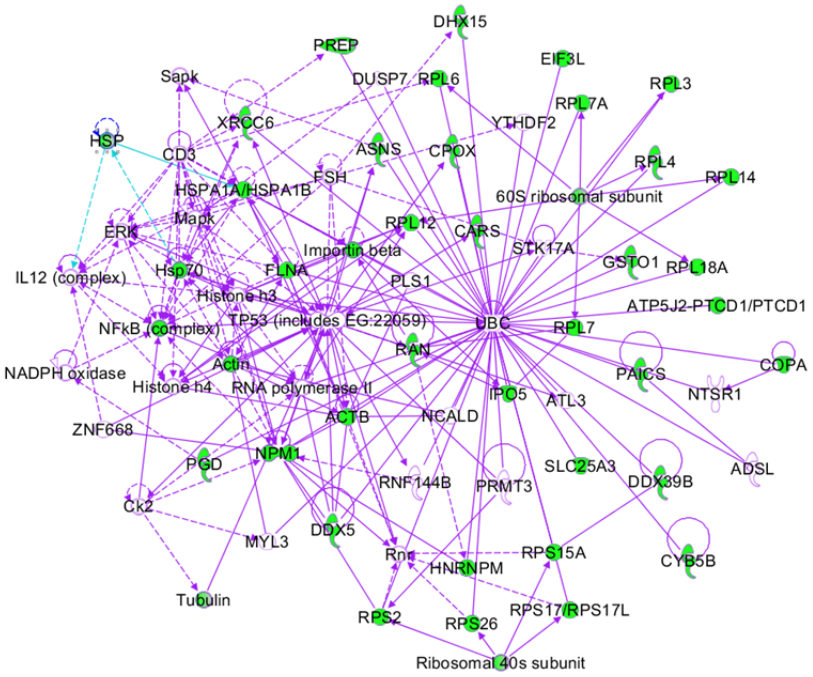

Figure 2.9 Ingenuity Pathway Analysis (IPA) reveals Andro affecting cancer cell death and survival. All proteins shown in green nodes were identified as specific targets of Andro.

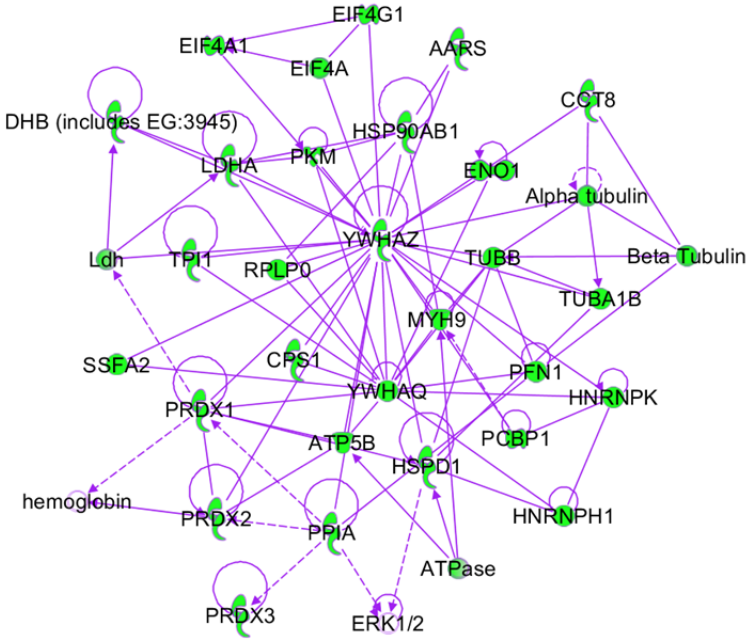

Figure 2.10 Ingenuity Pathway Analysis (IPA) reveals Andro affecting inflammatory and immunological pathways. All proteins shown in green nodes were identified as the specific targets of Andro.

Previously, many studies have been carried out to investigate the effect of Andro in inducing cancer cell death and anti-inflammatory effects(Zhou et al. 2006; Zhou et al. 2010; Zhou et al. 2008; Jada et al. 2008). Interestingly, our targets and pathway analysis revealed the anti-metastatic effects of Andro, which has not been extensively studied thus far (Shi et al. 2009). Among these target proteins (Table 2.2) MYH9 and NPM1 have been reported to be associated with regional lymph nodes tumor metastasis (Liang et al. 2011; Y. Liu et al. 2012). YWHAZ has been reported to promote epithelial-mesenchymal transition in lung cancer (Chen et al. 2012). FLNA may promote metastasis by enhancing cell migration in melanoma (Gawecka et al. 2010). PFN1 is an actin-binding protein which was reported to be highly related to tumor cell metastasis (Hu et al. 2001). α/β-tubulin, known to be expressed at elevated levels in tumor cells, plays essential roles in maintenance of cellular shape and process of metastasis. HSPA1A and HSPD1 have been reported to play an important role in tumorigenesis and metastasis of breast cancer (Barazi et al. 2002). Previous studies reported NF-κB p50 as a critical player in cancer metastasis by up-regulating MMP-9 and down-regulating anti-metastatic TIMPs and PAI 2 (Andela et al. 2000). Actin, one of the most abundant cytoskeleton proteins, participates in cancer metastasis by regulating cell motility (Yamaguchi & Condeelis 2007). The anti-metastatic effects of a variety of actin-binding agents have been extensively studied due to their therapeutic potential (Statsuk et al. 2005; Tannert et al. 2010; Kita et al. 2011; Quideau et al. 2011). In particular, we found NF-κB and β-actin were the top two target proteins with the highest differential ratios among all the other targets involved in the metastatic pathway. Thus, these two proteins were chosen for further validation of Andro's anti-metastatic effect in view of their critical roles in tumor metastasis.

2.3.4 Targets validation and functional analysis

Direct interaction of Andro with both NF-κB and Actin were first validated by pull-down followed by Western blot (Figure 2.11). Recombinant NF-κB p50 protein was used for subsequent *in vitro* labeling experiments. The protein was incubated with different concentrations of P2 for 4 hrs with DMSO-treated p50 as the negative control (Figure 2.12). The labeling only occurred to the native p50 in the presence of P2. Heat denatured p50 could not be labeled, suggesting the interaction is specific and physiologically relevant. Competition assay by pre-treating p50 with 10-fold excess of Andro resulted in drastically diminished fluorescent signal, further confirming the specific binding between p50 and the drug. The presence of reducing agents DTT and BME dramatically reduced the labeling, indicating that the reaction site might be cysteine residues. Previous research has suggested Cys62 of p50 as the binding site of Andro (Xia et al. 2004). Our *in vitro* labeling result confirmed the important role of Cys62 of p50 in Andro binding, which upon mutation to Ala significantly diminished the labeling efficacy (Figure 2.12, lane 11).

We further explored the exact modification site of Andro on p50 using MS/MS sequencing. The Andro-treated p50 protein, together with the untreated control, were digested with trypsin and analysed by MS/MS. The peptide YVCA*EGPSHGG-LPGASEK (Figure 2.13) was identified, in which Andro bound to the cysteine residue with the loss of one molecule of H2O (Figure 2.14) (Xia et al. 2004; Gersch et al. 2012). Based on above results, we were able to confirm Andro's binding site on p50 protein with great confidence.

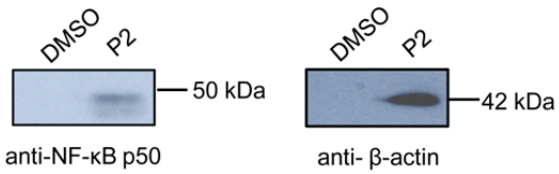

Figure 2.11 Western-blot validation of pulled-down fractions of HCT116 by P2 (or DMSO as negative control) with NF-κB p50 and β-actin antibodies.

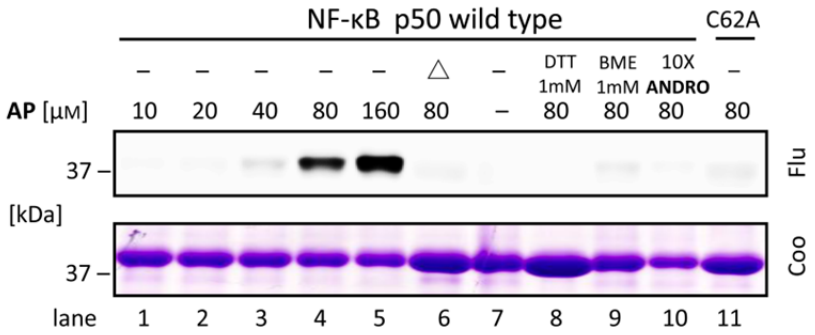

Figure 2.12 *In vitro* labeling of recombinant NF-κB p50 protein with P2: P50 is concentration-dependently labeled by P2 only in its native form, Δ=heat denaturation control; DTT and β-mercaptoethanol (BME) co-treatment, 10-fold excess Andro pre-treatment reduce the labeling; Drastically reduced labeling of p50 mutant shows Cys62 is the critical amino acid for Andro labeling. Coo=Coomassie staining; Flu=fluorescence scanning image.

To gain insight on how Andro alkylation inhibits DNA-binding activity of p50, a docking model was constructed. The thiol group of Cys62, which is located in the DNA-binding motif, is critical in DNA recognition of the p50 subunit. As shown in Figure 2.15, the docking simulations presented a comprehensive model, in which Andro binds p50 at the active DNA-binding site through interaction with Cys62, the critical amino acid, thereby inhibiting transcription by blocking DNA binding of NF-κB. Our docking model thus provided further hint that the anti-cancer effects of Andro is at least in part through inhibiting the DNA binding of NF-κB protein.

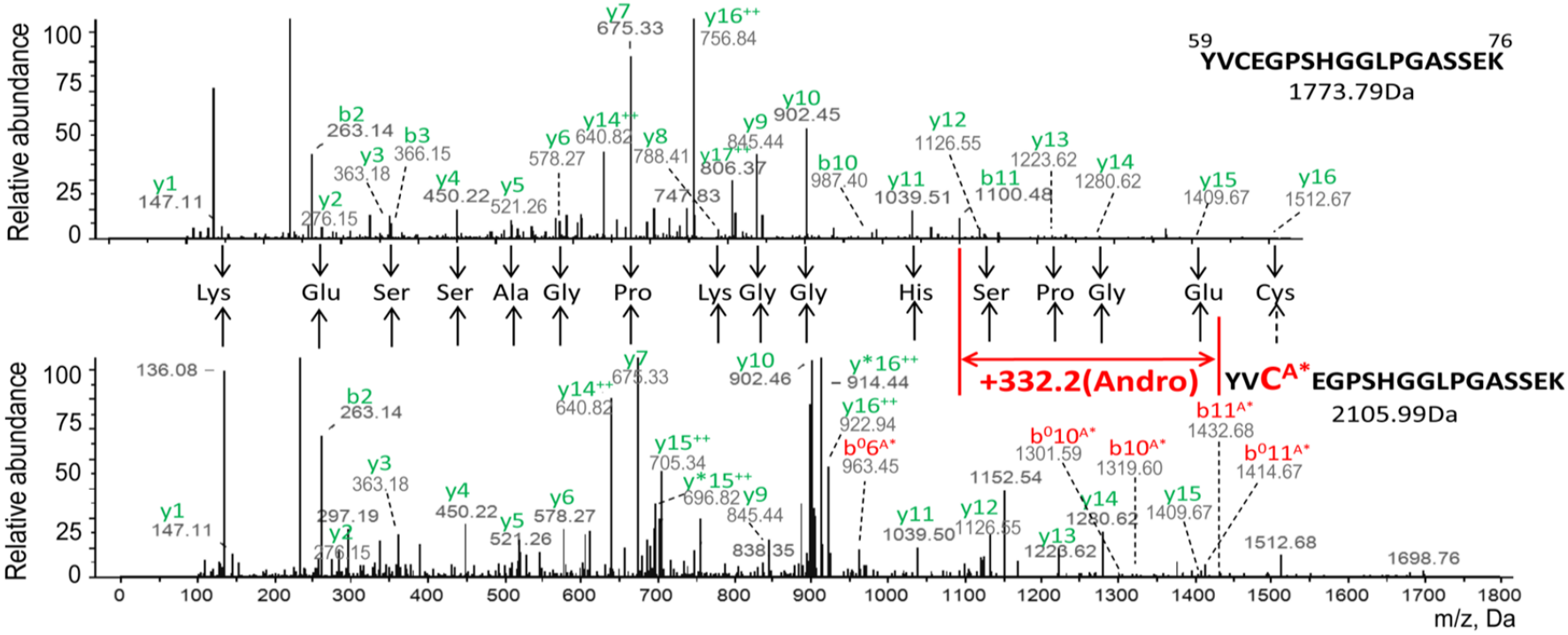

Figure 2.13 The MS/MS spectra of the NF-κB p50 peptide containing Cys62. P50 was incubated without (top) and with (bottom) Andro for 4hrs, and digested by trypsin. C^{A*} represents the Andro modified Cys. Fragment ions containing modified Cys are indicated with ^{A*} in red**.**

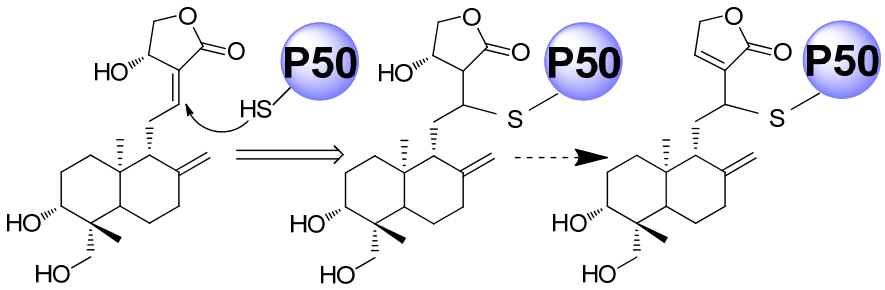

Figure 2.14 The schematic of the reaction of Cys with Andro.

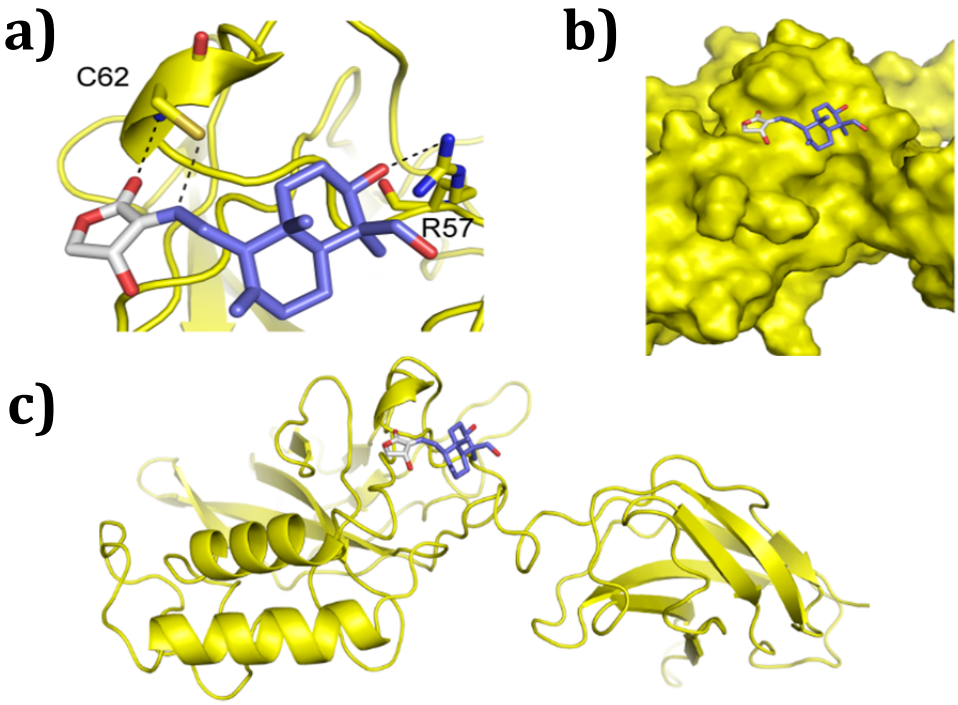

Figure 2.15 Docking simulation model showing Andro binding to the NF-κB p50 subunit through the critical amino acid Cys62 and Arg57. a, c) Ribbon diagram, b) Molecular surface diagram.

Previous studies showed that several small molecules can bind to actin by forming a covalent bond with Cys via similar Michael addition reactions (Statsuk et al. 2005; Aldini et al. 2007; Gayarre et al. 2006). To validate the interaction between actin and Andro, β-actin in G-buffer and F-buffer were incubated with Andro, respectively. The results demonstrated that Andro selectively bound to polymerized F-actin (Figure 2.16). The binding site of Andro on actin was subsequently confirmed to be Cys272 by MS/MS, which was reported as a highly reactive cysteine due to its full solvent accessibility (Figure 2.17)(Lassing et al. 2007; Landino 2008; Rozycki et al. 1995)

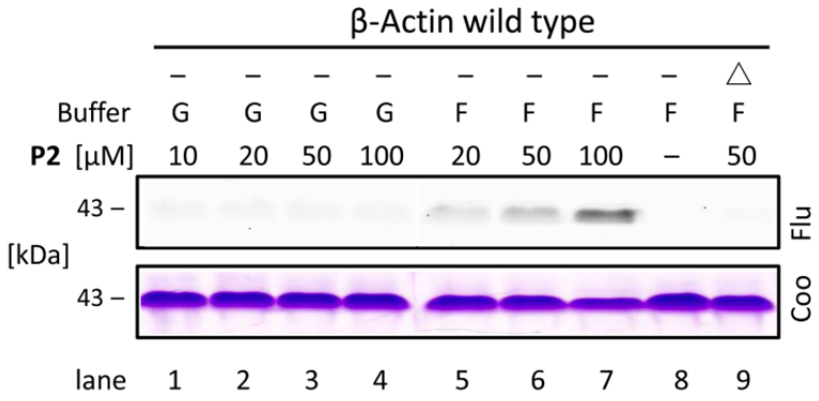

Figure 2.16 *In vitro* labeling of purified β-actin protein using P2. G: actin in G-buffer; F: actin in F-buffer; Δ=heat denaturation prior to labeling. Coo=Coomassie staining, Flu=fluorescence scanning.

Finally we verified the anti-metastatic potential of Andro using cell migration and invasion assays. HCT 116 cells were treated with RA and Andro at a non-cytotoxic concentration of 5μM for 30 hrs. The results showed that Andro can effectively suppress the migration and invasion of HCT116 cells (Figure 2.18). These results further supported our novel finding on the role of Andro in inhibiting tumor metastasis, thus broadening its therapeutic applications as an anti-cancer agent.

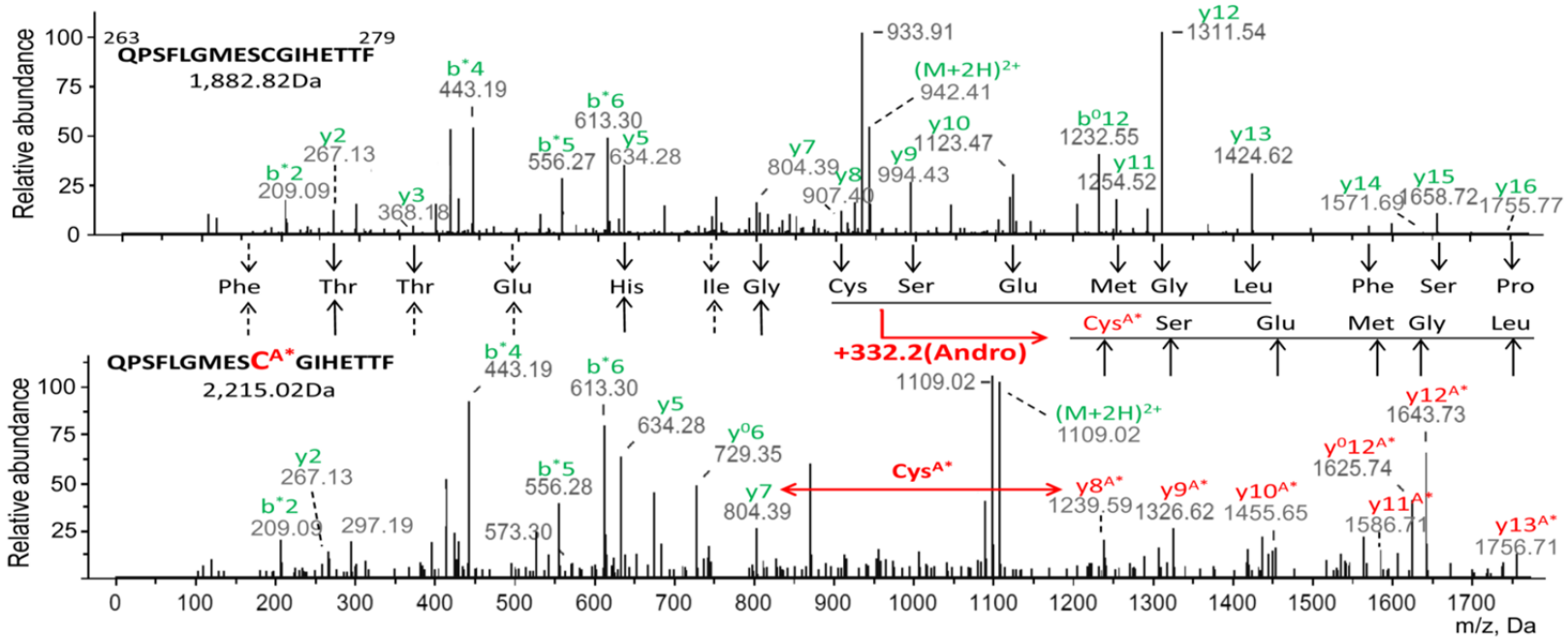

Figure 2.17 The MS/MS spectra of β-actin peptide containing Cys272. Polymerized actin in F-buffer was incubated without (top) and with (bottom) Andro for 4hrs, and digested by chymotrypsin. C^{A*} represents the Andro modified Cys. Fragment ions containing modified Cys are indicated with ^{A*} in red.

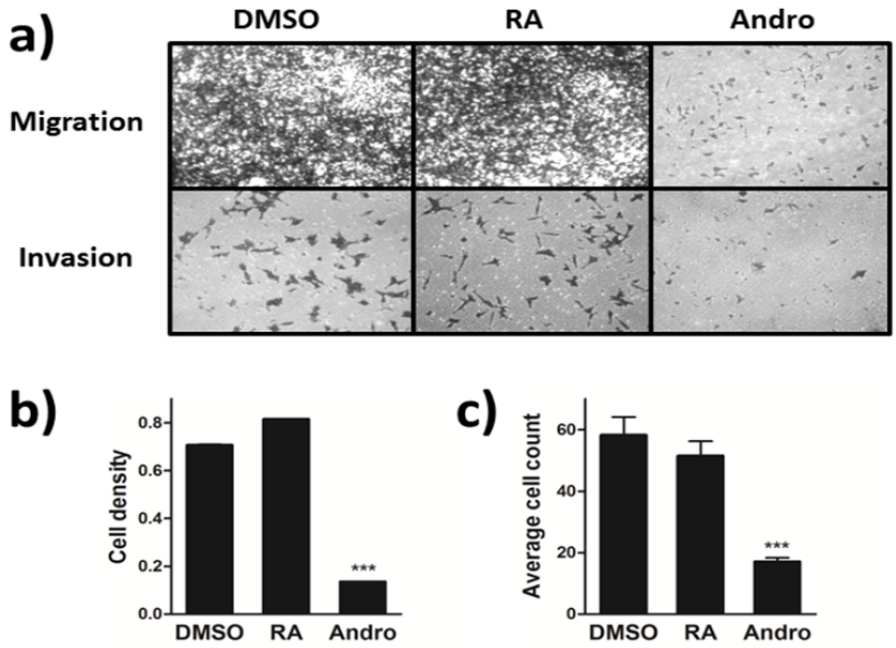

Figure 2.18 Inhibition of cancer cell migration and invasion by Andro. a) Cell migration and invasion assays of HCT116 cells treated with DMSO, RA (5 μM) and Andro (5 μM), respectively. Cells were seeded in inserts coated with either fibronectin or matrigel and allowed to migrate and invade towards FBS containing medium for 30 hrs before imaging and quantification. b) & c) Histogram showing significant differences in cell migration and cell invasion, respectively. (*** p-value<0.001)

As actin plays an important role in cytokinesis, we further examined Andro's effect on cell cycle using flow cytometry. Our data showed that HCT116 cells were arrested at G2/M phase upon Andro treatment in a time-dependent manner (Figure 2.19). We also analyzed the cell cycle using other cell lines including HeLa and HepG2. Significant cell cycle arrest was also observed at G2/M phase upon Andro treatment (Figure 2.20).

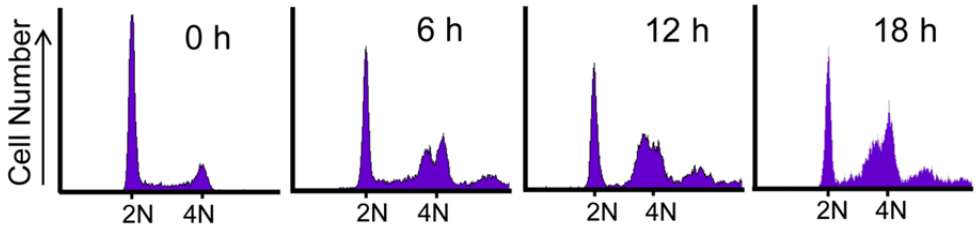

Figure 2.19 Flow cytometry cell cycle analysis of HCT116 cells treated with Andro (31 μM).

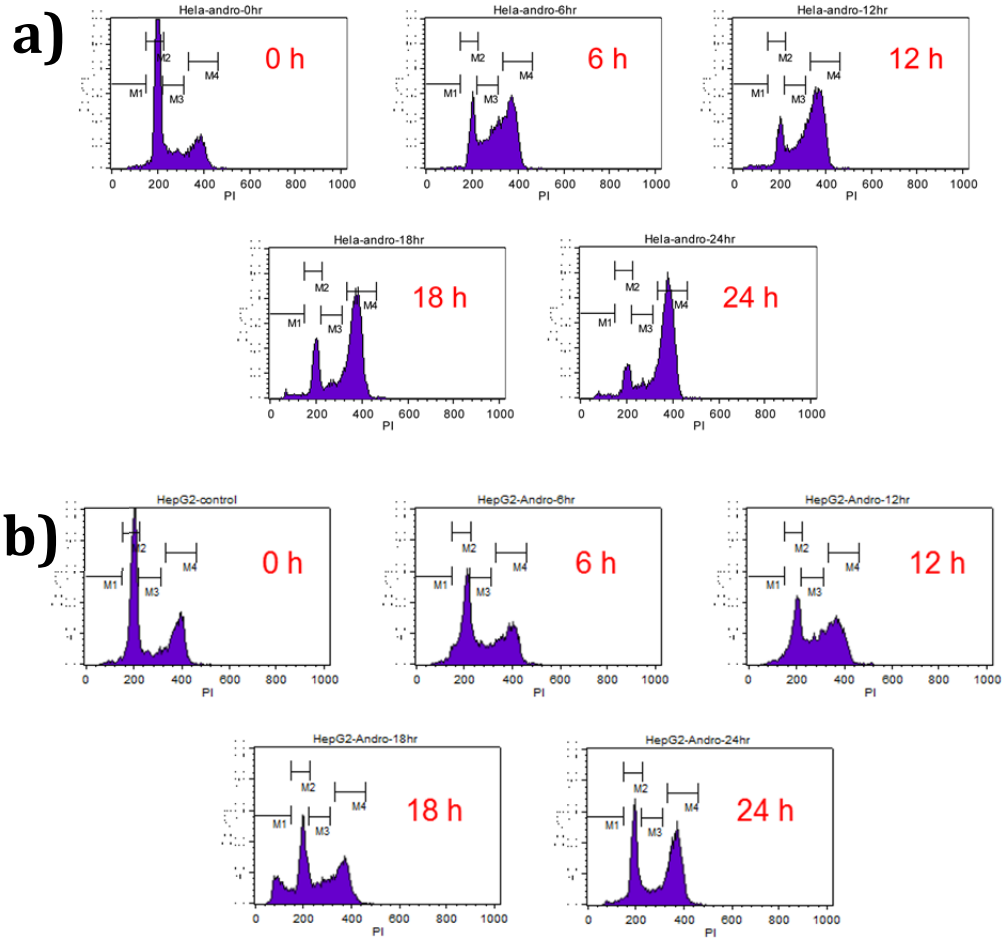

Figure 2.20 Cell cycle analysis of Andro-treated HeLa cells (a) and HepG2 cells (b) by flow cytometry.

2.4 Conclusion

In conclusion, our results demonstrated that the ICABPP method, which combines clickable ABPP and iTRAQ, is a powerful approach to identify specific drug targets in live cells. In this study, a spectrum of specific targets of Andro was identified using this new method. In particular, we have identified the novel anti-metastasis potential of Andro through targets and pathway analysis, which have been validated through subsequent migration and invasion assays. To the best of our knowledge, this is the first report that systematically combines the iTRAQ-based quantitative proteomics with the clickable activity-based probe to profile specific drug targets in live cells.

In practice, ICABPP method can be easily optimized and used in all kinds of affinity chromatography or ABPP-based target identification. The multiplexing property of the iTRAQ enables the precise and accurate quantitation of up to 8 samples simultaneously, allowing the inclusion of the biological replicates or drug competition of pull-down samples. Moreover, it can be used to study drug targets using tissue or body fluid samples in clinical research. We anticipate this ICABPP approach to be widely applied in drug development and optimization to refine the therapeutic potentials of drugs by uncovering knowledge on their specific targets and mechanisms of action.

Chapter 3

Development of a novel method for quantification of autophagic protein degradation by AHA labeling

3.1 Summary

Autophagy is a cellular catabolic process that cellular components including protein aggregates and organelles are degraded via a lysosome-dependent pattern to sustain cellular metabolic homeostasis during nutrient or energy deprivation. Measuring the rate of proteolysis of long-lived proteins is a classical assay for measurement of autophagic flux. However, the traditional methods, like the radioisotope labeling assay, are technically tedious and with low sensitivity. In this chapter, we report a novel method for quantification of long-lived protein degradation based on L-azidohomoalanine (AHA) labeling in mouse embryonic fibroblasts (MEFs) and in human cancer cells. AHA is a surrogate for L-methionine, containing a bioorthogonal azide moiety. When added to cultured cells, AHA is incorporated into proteins during active protein synthesis. After a click reaction between an azide and an alkyne, the azide-containing proteins can be detected with an alkyne-tagged fluorescent dye, coupled with flow cytometry. Induction of autophagy by starvation or mTOR inhibitors was able to induce a significant reduction of the fluorescence intensity, consistent with other autophagic markers. Coincidently, inhibition of autophagy by pharmacological agents or by Atg deletion abolished the reduction of the fluorescence intensity. Comparing to the classical radio-isotopic pulse labeling method, we believe that our method is a sensitive, quantitative, no-radioactive and easy to perform, and can be applied to both human and animal cell culture systems.

3.2 Introduction

Autophagy is an evolutionarily conserved self-digestive process in response to starvation or other stress conditions to sustain cellular homeostasis (Nakatogawa, Suzuki et al. 2009; Yang, Zhao et al. 2009). Autophagy plays crucial roles in development, innate immune defense, tumor suppression, and cell survival (Mizushima and Levine ; Levine and Kroemer 2008). During the induction of autophagy, portions of cytoplasmic materials, including macromolecules (such as stable, long-lived proteins) are engulfed into specialized double-membrane structures to form autophagosomes, which then fuse with lysosomes to degrade their cargos and regenerate nutrients (Mizushima 2007). Under normal growth conditions, autophagy is kept at a basal level to maintain turn-over of long-lived proteins and damaged organelles. Under starvation conditions, autophagy is induced to enhance the catabolic process to provide cells with additional internal nutrient supplies. This induction is largely due to inhibition of the mechanistic target of rapamycin (MTOR), the key negative regulator of autophagy through suppression of the ULK1 complex consisting of ULK1, FIP200 and Atg13 (Mizushima ; Hosokawa, Hara et al. 2009).

Among various assays developed to measure the autophagic flux, the classical method is determination of long-lived protein degradation by radioisotope labeling assay. This method firstly pulse-labeled the cellular proteins by incorporation of radioactive amino acids [^{14}C]-leucine or [^{14}C]-valine (Ogier-Denis, Houri et al. 1996; Roberts and Deretic 2008), and then followed by a long cold-chase to chase out short-lived proteins. Next, the time-dependent release of acid-soluble radioactivity from the degraded proteins in intact cells is measured. Although the radioisotope-based autophagic proteolysis of long-lived proteins assay is considered to be a gold standard in measuring autophagic proteolysis, this method is technically tedious, insensitive, and inconvenient (with requirement of radioactive containment). Though Doherty et al. (Doherty, Hammond et al. 2009) updated this method by using dynamic stable isotope labeling with amino acids in cell

culture (SILAC), coupled with quantitative mass spectrometry, the lengthy and laborious process would limit its wide application. Thus, a radioactive-free method which can quickly and specifically quantify the long-lived protein degradation is highly demanded.

Recently, new techniques for labeling a variety of molecules based on the principle of bio-orthogonal metabolic labeling have been developed (Best 2009), such as bio-orthogonal noncanonical amino acid tagging (BONCAT) and fluorescent noncanonical amino acid tagging (FUNCAT) which have been used to tag and identify or visualize newly synthesized proteins (Dieterich, Link et al. 2006). Such methods are particularly useful when direct labeling or the use of antibodies is not applicable or efficient. L-azidohomoalanine (AHA), an amino acid analog of methionine containing an azide moiety, can be incorporated into *de novo* protein synthesis and can be readily detected by a chemoselective ligation between an azide and alkyne-bearing tags (Dieterich, Link et al. 2006). AHA has been successfully used for detection of nascent protein synthesis, in combination with proteomic techniques, including gels, blots, and mass spectrometry (Dieterich, Link et al. 2006; Dieterich, Lee et al. 2007).

Here we report a novel method which combines the pulse-AHA labeling, click-chemistry tagging and flow cytometry detection to quantitatively measure the long-lived protein degradation during autophagy. We tested this method in both normal and cancer cells, under various autophagy induction and inhibition conditions. This assay provides a fast, sensitive, and non-radioactive method for quantification of autophagic proteolysis, applicable to *in vitro* cell culture systems. This method could also be adapted for high-throughput screening of novel pharmacological agents that enhance or inhibit autophagy, and also of genes that modulate autophagy.

3.3 Results

3.3.1 AHA labeling and detection of AHA by click reaction

As shown in Figure 3.1A, AHA is an effective surrogate for methionine, an essential amino acid, which does not require any further manipulations to be incorporated as a substrate by the methionyl-tRNA synthetase into the proteins during *de novo* protein synthesis.

The amount of AHA incorporated into the protein can be detected using the "click" reaction between azide and alkyne, and a broad range of functionally and biochemically diverse proteins that incorporated with AHA can be specifically tagged with a corresponding alkyne-containing dye or hapten, and subject to subsequent analysis by flow cytometry, imaging or standard biochemistry techniques such as gel electrophoresis (Figure 3.1B).

Based on the AHA labeling and click reaction as described above, we here developed a protocol for quantification the long-lived protein degradation in autophagy, as shown in Figure 3.2. Firstly, cells are incubated with AHA to allow incorporation of AHA into proteins, followed by a period of cold-chase to get rid of the short-lived proteins. Subsequently cells were subject to modulation of autophagy (induction and/or suppression). Finally, cells were harvested, fixed and permeabilized followed by a click reaction with TAMRA alkyne. Using flow cytometry, the AHA signal intensity will be measured which is inversely correlated to the amount of long-lived proteins left after autophagy.

3.3.2 Optimization of AHA labeling

Growth medium, cell density, cell type variations and other factors may influence the AHA labeling capacity. For initial experiments, we optimized the labeling and reaction conditions in terms of AHA concentration and incubation time. Mouse embryonic fibroblasts (MEFs) were plated at desired density (70~80%) overnight in full culture medium with 10% FBS. After the full

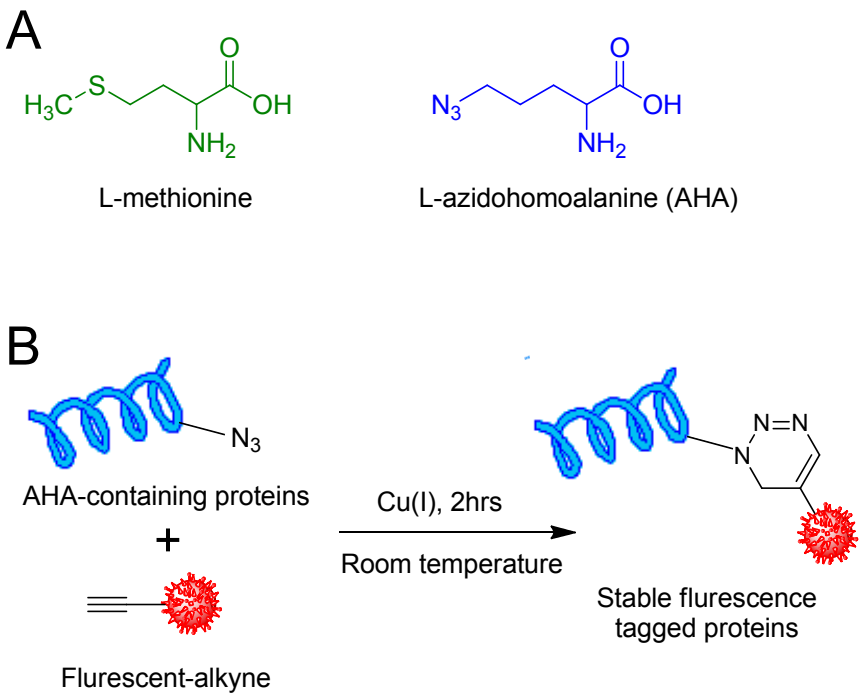

Figure 3.1 AHA labeling of newly synthesized proteins. AHA labeling of newly synthesized proteins. (A) Structure of azidohomoalanine (AHA), an analog of methionine containing an azide moiety. (B) Click azide/alkyne reaction. The azide and alkyne moieties are interchangeable, where the molecule can be labeled with an alkyne and react with a fluorophore- or hapten-azide.

medium was removed and washed with PBS twice, cells were then cultured in L-methionine-free DMEM with different dosages of AHA (Note that cells should be labeled in methionine-free medium, as methionine is the preferred substrate for methionyl tRNA transferase (Kiick, Saxon et al. 2002)).

Firstly, we tested a range of AHA concentrations to determine the optimal concentration for our cell type and experimental conditions. As shown in Figure 3.3A, we observed a dose-dependent increase of the AHA signal intensity up to 100 μM, while the signal reached the plateau by the concentration of 25 μM. Next, we tested the time-course of AHA labeling by incubating MEFs with 25 μM AHA for up to 24 h, resulting in a time-dependent

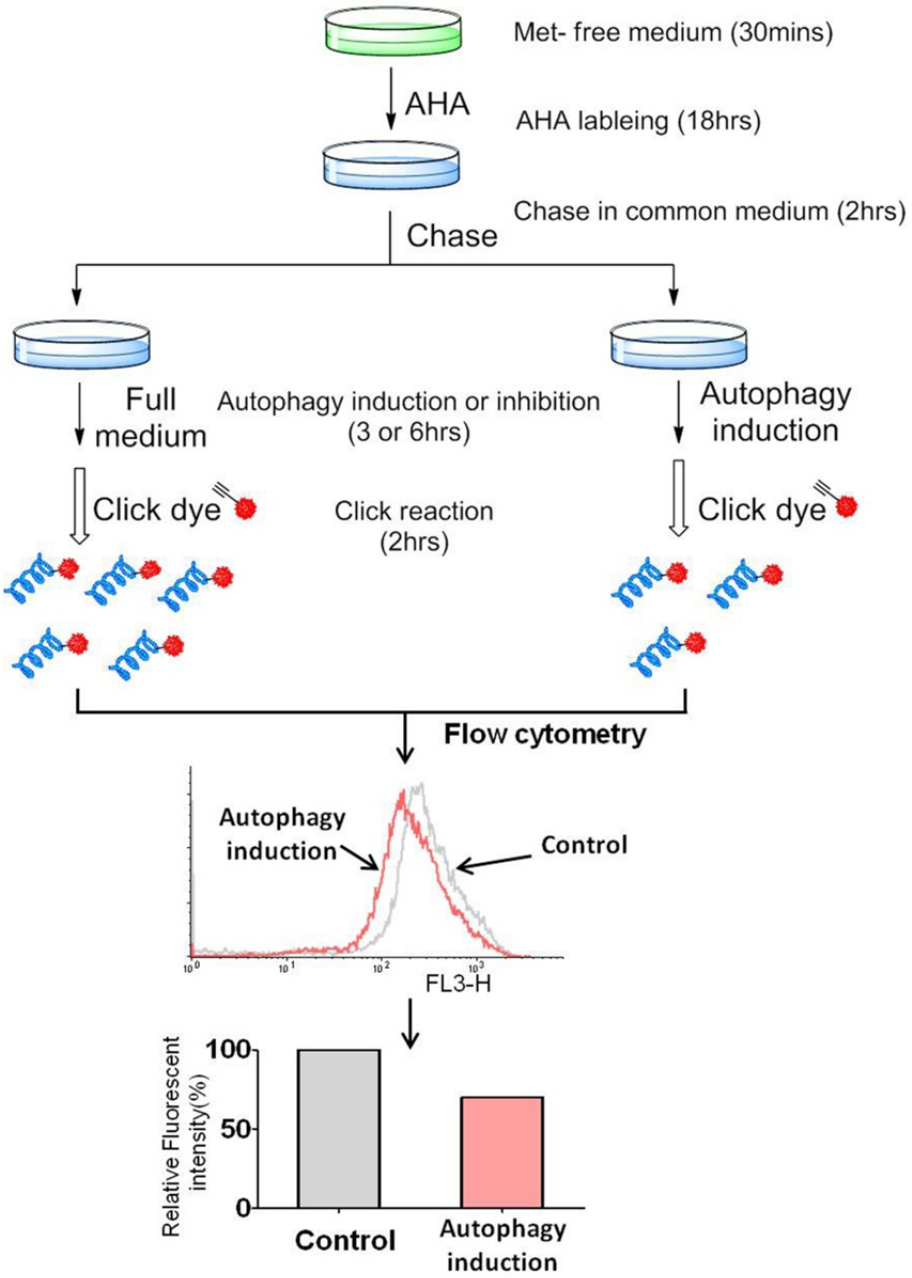

Figure 3.2 Workflow for AHA labeling-based quantitative analysis of protein degradation. The bioorthogonal noncanonical amino acid tagging (BONCAT) strategy for labeling, detection and identification of newly synthesized proteins. Cells are incubated with AHA to allow protein synthesis. After incubation, cells were harvested, fixed and permeabilized. Nascent protein synthesis was detected following a click reaction with TAMRA alkyne and analysis was performed using flow cytometry

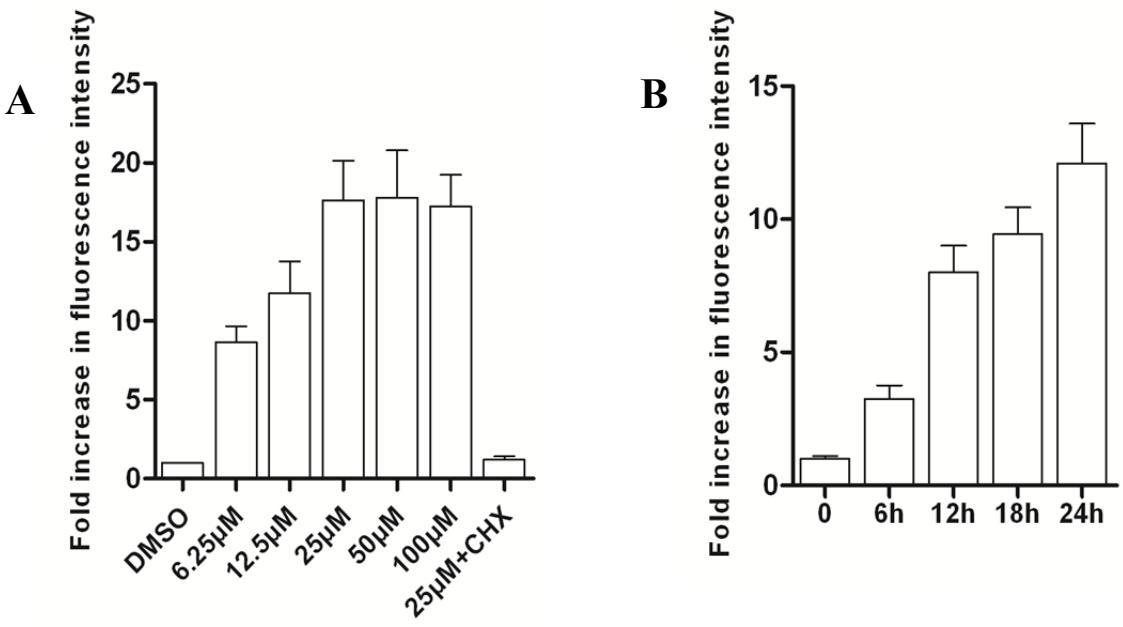

Figure 3.3 Dose- and time-dependent metabolic labeling of AHA in MEFs. (A) MEFs were treated in L-methionine-free meidum with different dosages of AHA for 18 h. Cell were then transferred into common medium with 10x L-methionine (2 mM) for 2 h. Finally, the cells were harvested, fixed and permeabilized for the click reaction, as described in Materials and Methods. (B) as in (A), MEFs were labeled with 25 μM AHA at different time points (6, 12, 18 and 24 h) and cellular fluorescence intensity was analysed as described.

increase of the AHA signal intensity (Figure 3.3B). We further confirmed the AHA label by examining the fluorescence intensity in SDS-PAGE. As shown in Figure 3.4, only the cells labeled with AHA were detected with fluorescence. The Coomassie staining was used to show the equal loading of the protein samples.

To determine the specificity of AHA incorporation into newly synthesized proteins, we added a protein synthesis inhibitors cycloheximide (CHX) into the labeling medium along with AHA. As shown in Figure 3.4, the presence of CHX completely abolished the fluorescence signal in cells with AHA labeling, confirming that this procedure labels newly synthesized proteins with high specificity.

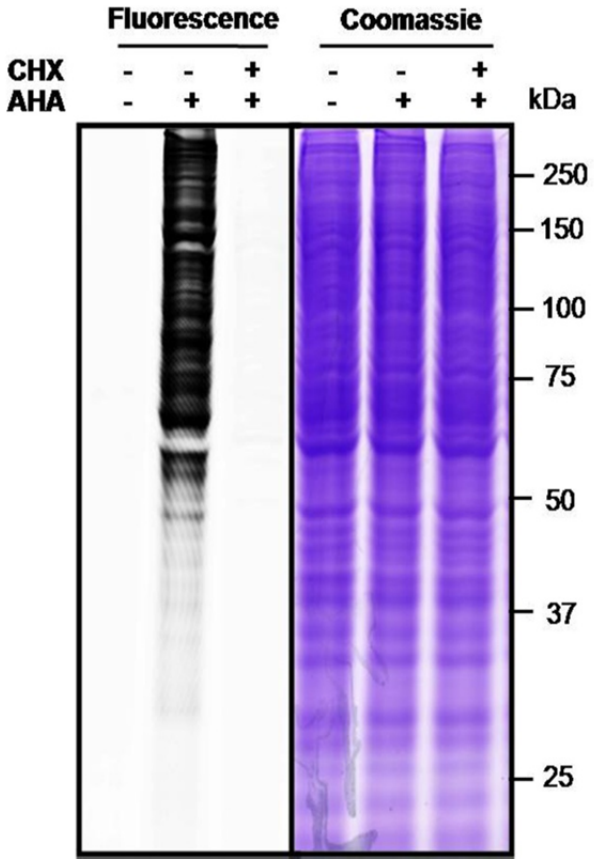

Figure 3.4 Visualization of AHA-labeled proteins. MEFs were labeled with AHA (25 μM x 18 h) and then the cells were harvested for click tagging and in-gel fluorescence scanning. Coomassie staining was used to show the equal protein loading. Cycloheximide (CHX, 10 μg/ml) was added to inhibit *de novo* protein synthesis and the cells cultured in common medium were used as the negative control.

It has been reported that the metabolic labeling of mammalian cell with AHA did not alter global protein synthesis rates or protein degradation (Dieterich, Link et al. 2006). As shown in Figure 3.5, labeling with different concentrations of AHA for 18 hours did not change the cell morphology, indicates that AHA is not toxic to MEFs.

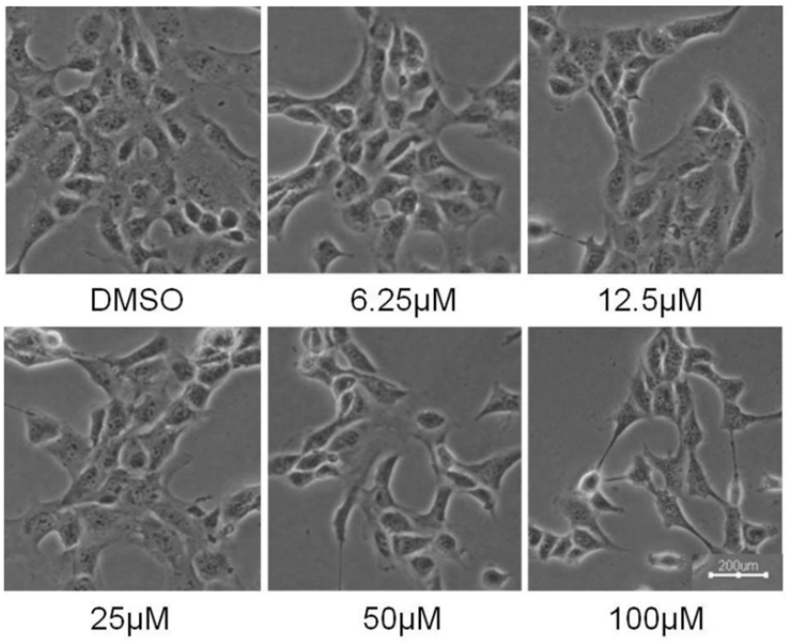

Figure 3.5 Morphological changes of MEFs with different dosages of AHA labeling were examined and photographed with an inverted microscope (Scale bar 200 μM).

3.3.3 Autophagy-mediated protein degradation detection by AHA fluorescence

We next tested the changes of AHA fluorescence intensity in MEFs undergoing autophagy induced by a well-established autophagy inducer starvation (culturing cells in amino acid-free medium) (Munafo and Colombo 2002). As shown in the left panel of Figure 3.6A, starvation for 3 h caused a 20% reduction in the AHA signal intensity, and the magnitude of reduction is agreeable to a previous report detected by the degradation of mitochondrial (Kawai, Takano et al. 2006). Starvation for a longer period of time (6 h) induced a further reduction in cell fluorescence intensity, with about 70% of signal intensity remaining (Figure 3.6B).

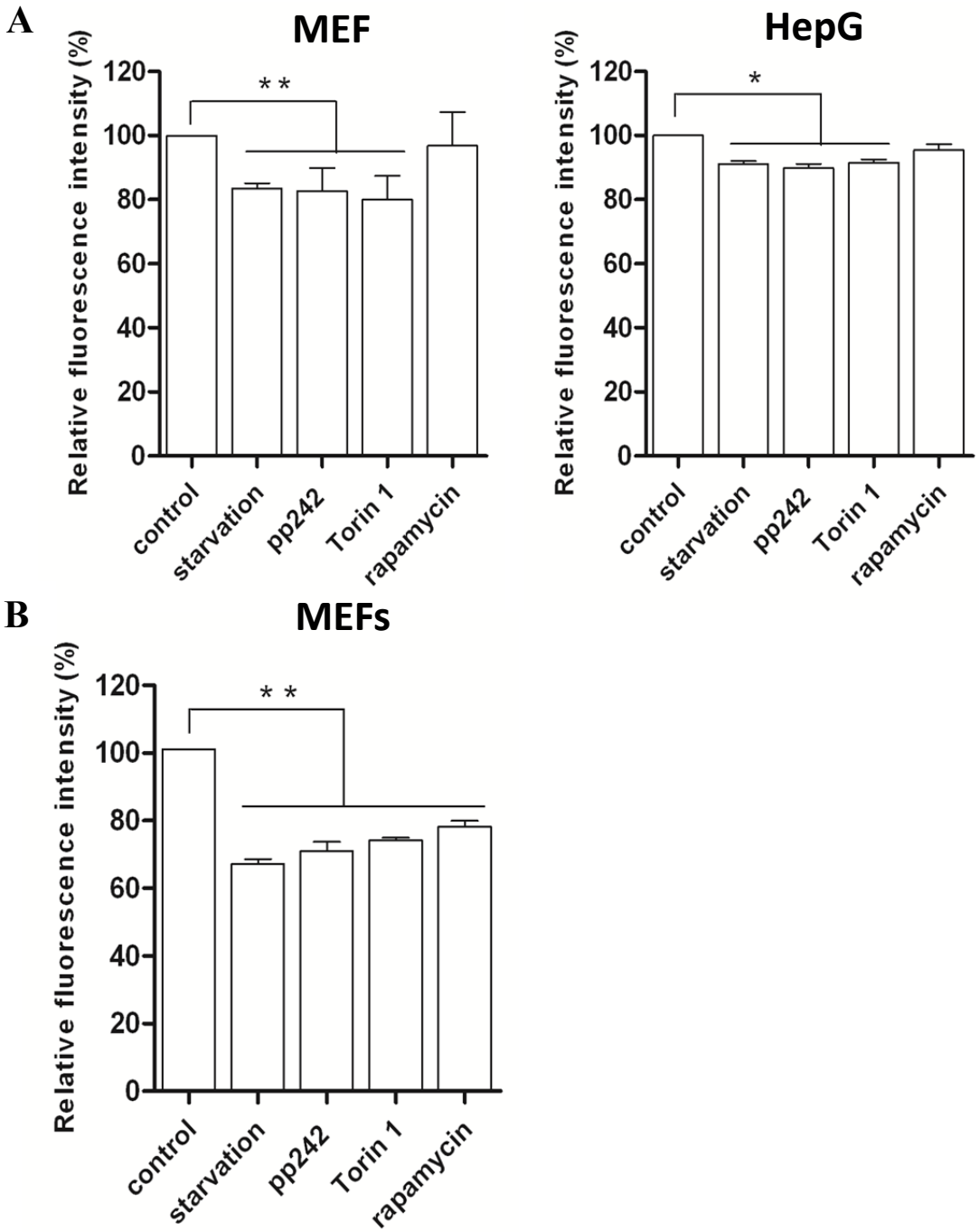

Figure 3.6 Autophagy induction increased long-lived protein degradation. Cells were first labeled with AHA as described above, and then the cells were cultured in starvation or treated with mTOR inhibitors (rapamycin×1 μM, pp242×1 μM or Torin1×1 μM) for 3 h (A). Left panel for MEFs; right panel for HepG2 cells. Data for the relative signal intensity were expressed as the ratio of treated cells to control cells, as mean ± SD from three independent experiments, * $p < 0.05$, ** $p < 0.01$, Student's *t*-test. (B) MEFs were treated with starvation or mTOR inhibitors for 6 h and cellular fluorescence intensity was measured.

In addition to starvation, we also measured autophagic protein degradation induced by different mTOR inhibitors, including rapamycin (an allosteric mTOR inhibitor), and pp242 and Torin 1 (two catalytic mTOR inhibitors) (Huo, Iadevaia et al.). As shown in the left panel of Figure 3.6A, both pp242 and Torin 1 were found to be as effective as starvation in causing protein degradation, and also in a similar time-dependent manner. Interestingly, rapamycin failed to induce a significant decrease of AHA fluorescence intensity with a shorter treatment duration (3 h) and the degree of autophagic proteolysis by rapamycin was weaker compared to other treatments, which is consistent with the previous study that rapamycin was found to be a relatively weaker autophagy inducer (Kawai, Takano et al. 2006).

Similar results were also obtained in HepG2 cells (Figure 3.6A, right panel), although the average AHA fluorescence intensity reduction was about 10% in cells under starvation and mTOR inhibitors (pp242 and Torin 1) for 3 h, which is relatively weaker when compared to MEFs, suggesting that cell type variations may influence autophagic proteolysis rate measured by this assay.

To further evaluate the efficiency of autophagy induction, we also performed western blotting to determine changes of mTOR activity and autophagy markers. As shown in Figure 3.7, starvation and mTOR inhibitors, such as rapamycin, pp242 and Torin 1, increase LC3-II level and decrease p62 level, indicating a higher autophagy level. Meanwhile, the effectiveness of starvation and mTOR inhibitors were verified with the phosphorylation blockage of S6 (S235/236) seen in MEFs and HepG2 cells. Different from other treatments, rapamycin was largely ineffective on phospho-4E-BP1 (Thr37/46). Such observations are consistent with the current understanding that rapamycin is an allosteric inhibitor of mTOR and only suppresses part of mTOR function, while both pp242 and torin1 are catalytic inhibitors that are able to fully suppress mTOR (Thoreen, Kang et al. 2009).

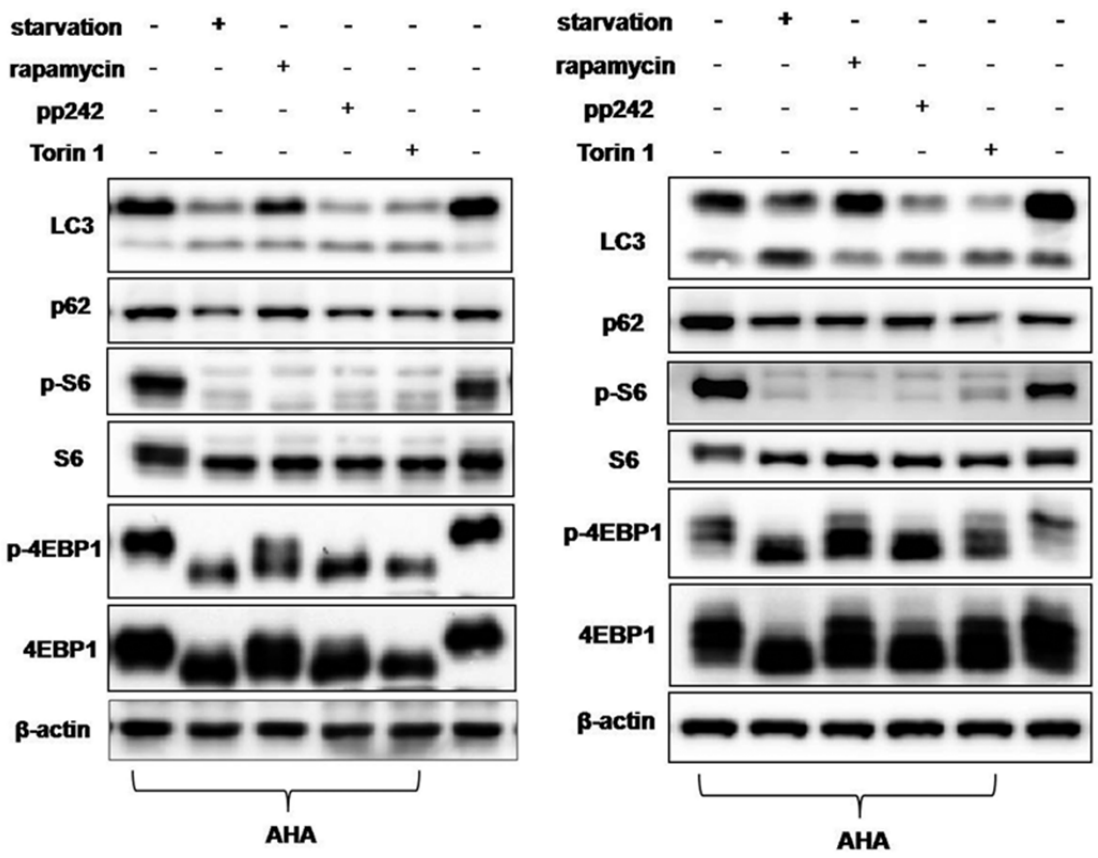

Figure 3.7 Western confirmations of Starvation and chemical induced Autophagy in MEFs. MEFs were treated as in Figure 3.6A and cell lysates were prepared for western blotting. β-actin was used as the loading control. (left panel: 3 hrs treatment; right panel: 6 hrs treatment)

3.3.4 Autophagy inhibitors reversed the reduction of AHA fluorescence

To verify this method of autophagic proteolysis, we utilized pharmacological inhibitors of autophagy to observe the changes of AHA fluorescence. Wortmannin, a phosphatidylinositol-3-kinase (PI3K) inhibitor, can specifically inhibit macroautophagy (Kovacs, Rez et al. 2000). Bafilomycin A1, a selective inhibitor of the lysosomal V-ATPase, is able to block the fusion between autophagosome and lysosome (Yoshimori, Yamamoto et al. 1991). In cells under starvation for 3 h (Figure 3.8A, left

panel for MEFs and right panel for HepG2 cells), both inhibitors were able to significantly reverse the reduction of AHA fluorescence intensity, although wortmannin appeared to be more effective than bafilomycin A1.

We also tested the effects of these two autophagy inhibitors on autophagy induction by pp242. As shown in Figure 3.8B (left panel for MEFs and right panel for HepG2 cells), both inhibitors were also able to abolish the reduction of AHA fluorescence.

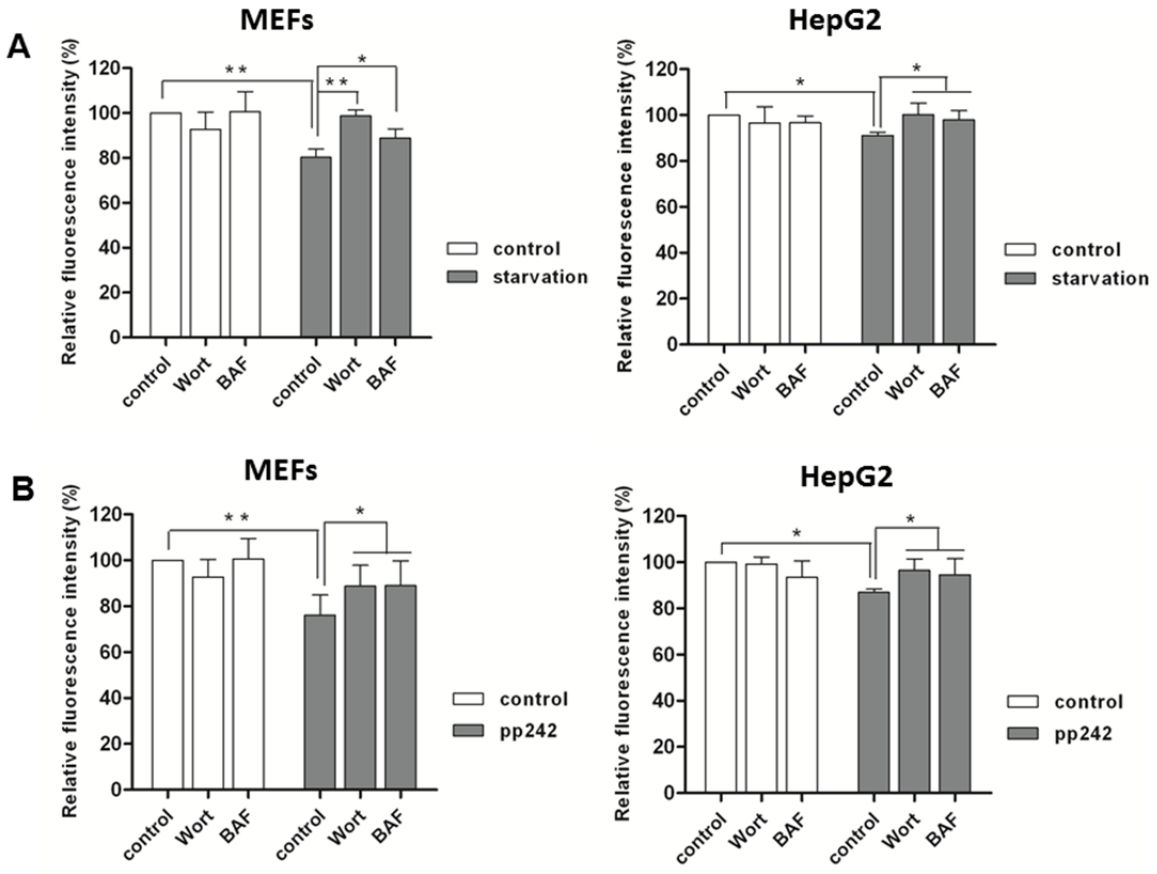

Figure 3.8 Autophagy inhibition blocked long-lived protein degradation. Cells were labeled with AHA as described earlier and then cultured in common medium with 10× L-methionine (2 mM) for 2 h in the presence or absence of autophagy inhibitors (Wort×100 nM or BAF×50 nM), followed by either starvation (A) or pp242×1 μM (B) for 3 h, in the presence or absence of autophagy inhibitors. Left panel for MEFs; right panel for HepG2 cells. Data for the relative signal intensity were expressed as the ratio of treated cells to control cells, as mean ± SD from three independent experiments, * $p < 0.05$, ** $p < 0.01$, Student's *t*-test.

Meanwhile, we performed western blotting to confirm the effectiveness of wortmannin and bafilomycin A1 to block autophagy induced by starvation and pp242. In MEFs (Figure 3.9) and HepG2 cells (Figure 3.10), starvation and pp242 increased the autophagic flux, accompanied with a further increase in LC3-II level and decrease in p62 level when bafilomycin A1 was added; whereas wortmannin led to a further decrease in LC3-II level and increase in p62 level. In addition, the effectiveness of starvation and pp242 were verified with the phosphorylation blockage of S6 (S235/236) and 4E-BP1 (Thr37/46). Thus it further supported that the degradation of protein by autophagy can be effectively measured by our proposed AHA-labeling system.

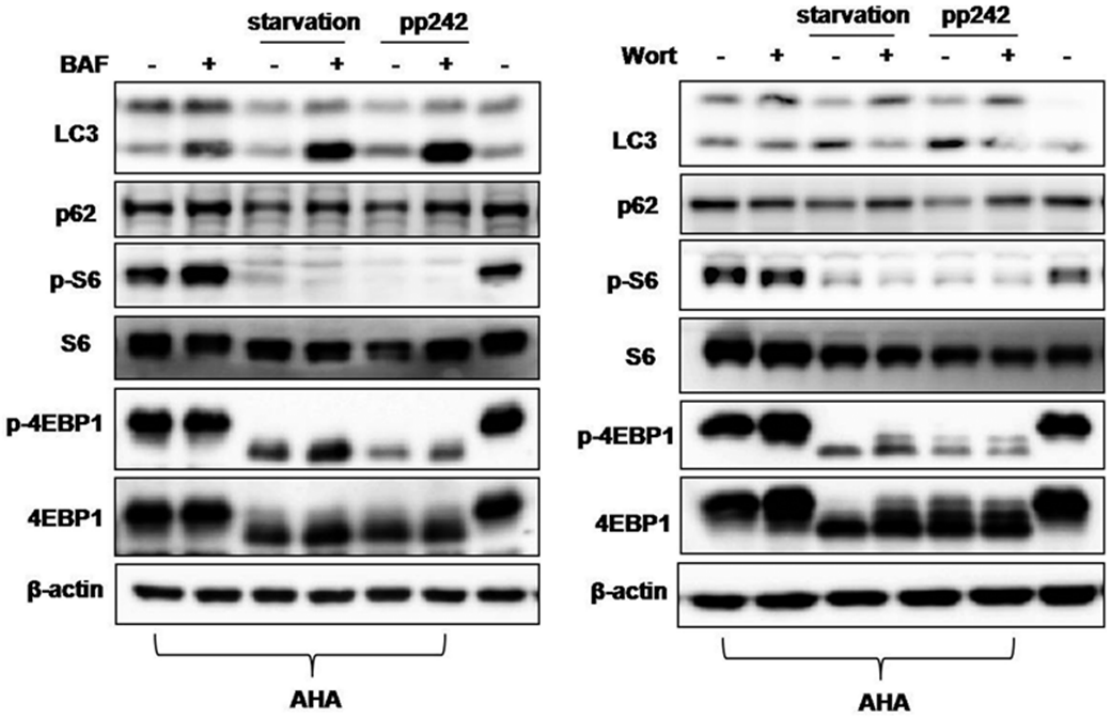

Figure 3.9 Western confirmations of Autophagy inhibition by Bafilomycin and Wortmannin in MEFs. MEFs were treated as described in Figure 3.8A and Figure 3.8B. Cells were then harvested and protein from cell lysates was analyzed with western blotting. β-actin served as a loading control.

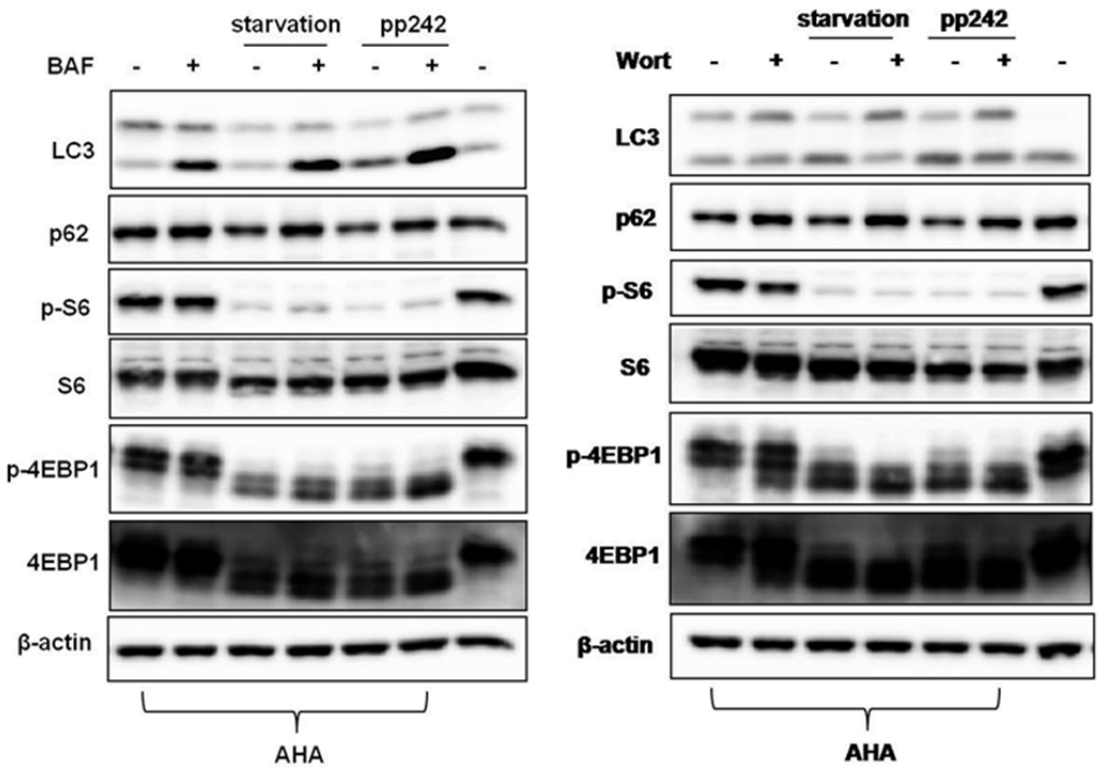

Figure 3.10 Western confirmations of Autophagy inhibition by Bafilomycin and Wortmannin in HepG2. HepG2 cells were treated as described in Figure 3.8A and Figure 3.8B. Cells were then harvested and protein from cell lysates was analyzed with western blotting. β-actin served as a loading control.

3.3.5 Autophagy deficiency prevented protein degradation measured by AHA labeling

To further examine the usefulness of this assay in measuring autophagic proteolysis, here we measured the changes of AHA fluorescence in cells deficiency of key autophagy-related genes including Atg5 and Atg7. We observed only minor degree of protein degradation in both Atg5 KO MEFs and Atg7 KO MEFs under various autophagy inducers, in comparison to their respective wild-type counterparts (Figure 3.11A and 5B, respectively). Interestingly, we also observed some reduction of AHA fluorescence intensity

in the Atg5 or Atg7 KO MEFs, especially in Atg7 KO MEFs under starvation, suggesting the possibility of autophagy-independent protein degradation in the treated cells, such as proteasome-mediated protein degradation (Vabulas and Hartl 2005). Meanwhile, western blotting analysis was performed to determine the identity of the cells and autophagy markers induced by starvation or mTOR inhibitors (Figure 3.12A and B). Autophagy inducers increased LC3-II level and decreased p62 level in wild type MEFs, but not in autophagy deficiency cells, although their suppressive effects on mTORC1 activity were found to be similar.

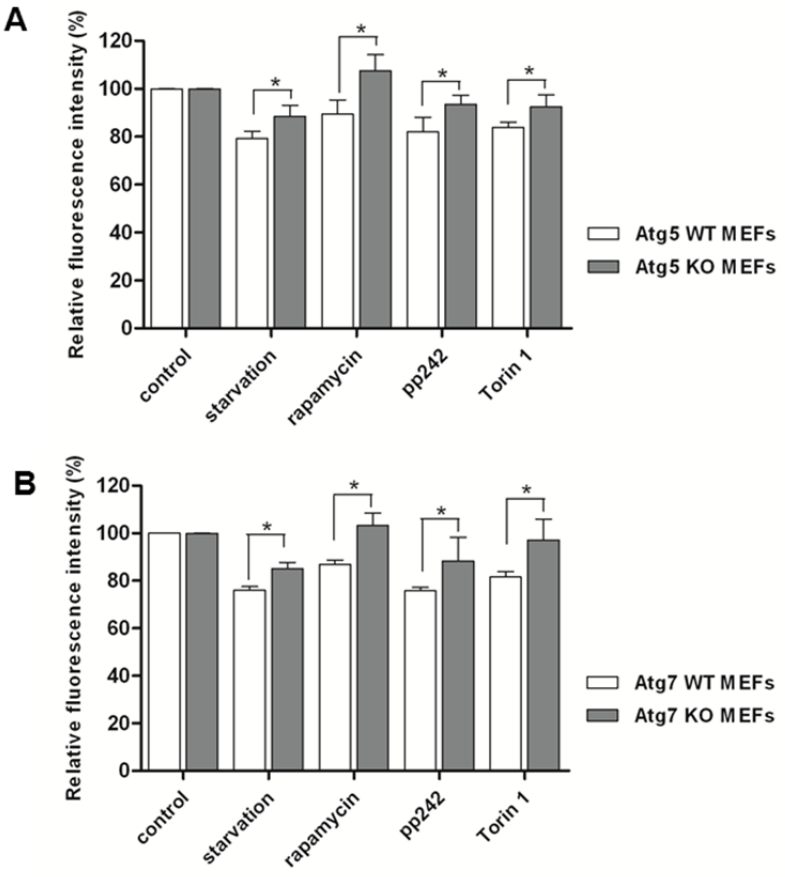

Figure 3.11 Defective autophagy impaired long-lived protein degradation. Atg5 WT and KO MEFs (A) and Atg7 WT and KO MEFs (B) were labeled with AHA and then treated with starvation or mTOR inhibitors for 3 h, as described in Figure 3.6A. Data for the relative signal intensity were expressed as the ratio of treated cells to control cells, as mean ± SD from three independent experiments, * $p < 0.05$, Student's *t*-test.

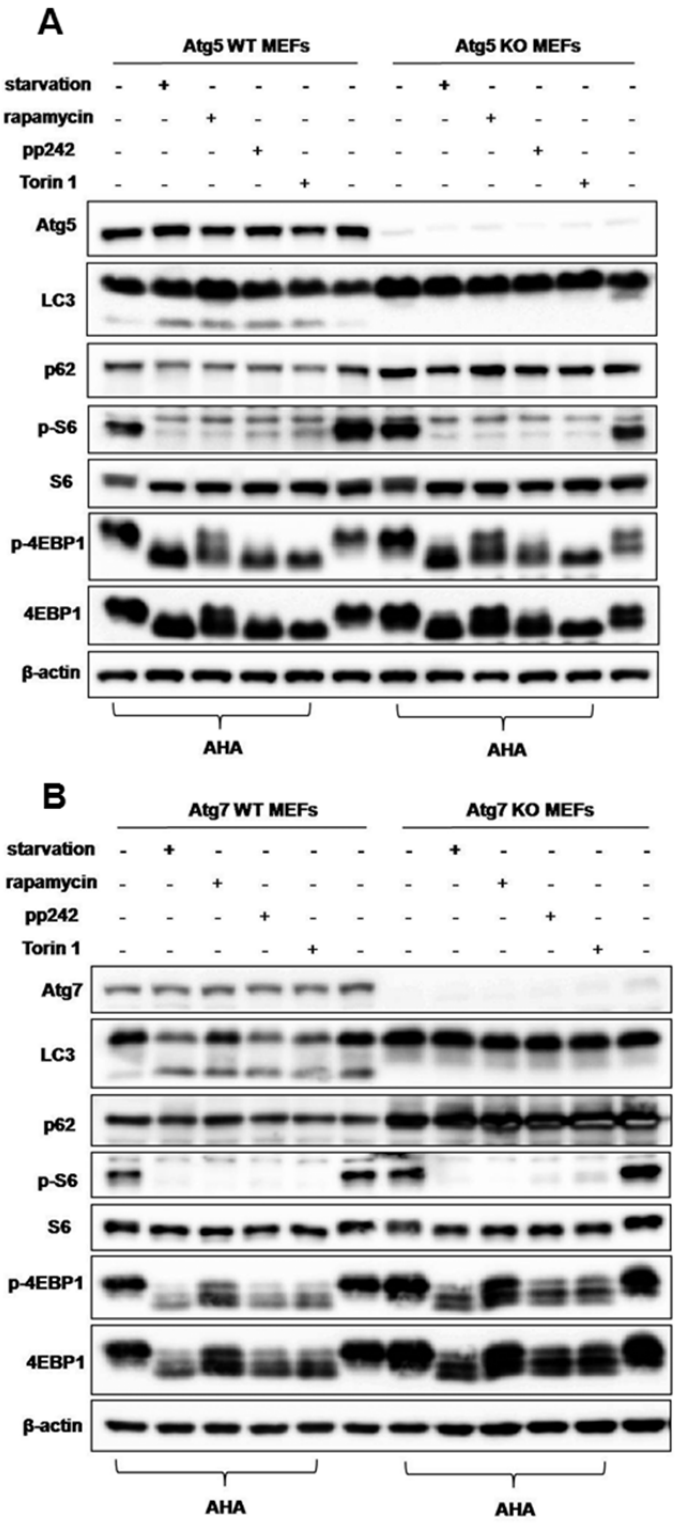

Figure 3.12 Western confirmations of Autophagy inhibition and deficiency in Atg WT and KO MEFs. Atg5 WT and KO MEFs (A) and Atg7 WT and KO MEFs (B) were treated as described in panel A and B, and then harvested and proteins from cell lysates were analyzed with western blotting. β-actin served as the loading control.

3.4 Discussion

At present, measurement of “autophagic flux” in the autophagy study is still technically challenging (Klionsky, Abdalla et al.). Several assays have been described and commonly used, including (i) turnover of autophagy markers such as LC3-II and GFP-LC3 puncta in the presence of lysosomal inhibitors such as chloroquine (CQ); (ii) changes of p62/sequestosome protein level, and (iii) use of the GFP and RFP tandemly tagged LC3 (tfLC3), and (iv) quantification of autophagic proteolysis by radioisotope labeling. In the present study, we described a novel assay to quantify long-lived protein degradation in autophagy using AHA labeling coupled with flow cytometry. Comparing to the classical radioisotope labeling method, this assay is non-radioactive, sensitive, specific, quantitative, relatively easy to perform and versatile in the mammalian cell culture systems, and thus offers a good tool to many laboratories in the field of autophagy research.

Recently, the BONCAT technique has been used to identify newly synthesized proteins in mammalian cells through the co-translational introduction of azide groups into proteins and the chemoselective tagging of azide-labeled proteins with an alkyne affinity tag (Dieterich, Link et al. 2006). Based upon this technique, the metabolic labeling of AHA into newly synthesized proteins has been widely used in mammalian cells (Dieterich, Link et al. 2006), primary neuronal cells and organotypic brain slice cultures (Dieterich, Hodas et al.) and larval zebrafish (Hinz, Dieterich et al.). Labeling with AHA is similar to the traditional metabolic labeling with radioactive amino acids (^{35}S-labeled methionine or cysteine). Unlike other labels, the azide is small enough to be tagged with biomolecules (such as sugars and amino acids) that are acceptable as substrates for the enzymes to incorporate them into proteins. However, the application of AHA labeling in measuring protein degradation has not yet been explored at present. In this study, we established a novel technique for the study of autophagic proteolysis. In cells induced by starvation or mTOR inhibitors to activate autophagy, there was a significant reduction of the AHA signal intensity (Figure 3.6A and 3B).

Consistently, suppression of autophagy by pharmacological inhibitors effectively prevented the reduction of AHA signal intensity (Figure 3.8A and 4B). More importantly, no obvious reduction of AHA signal was found in MEFs with deletion of Atg5 or Atg7 (Figure 3.11A and 4B). Therefore, it is thus believed that the reduction of the AHA signal intensity specifically measures the protein degradation due to autophagy.

When compared to radioisotope labeling in the measurement of autophagic proteolysis, there are a few advantages of AHA labeling. Firstly, AHA labeling is much simpler and easier to perform, non-toxic, and does not affect global rates of protein synthesis or degradation (Dieterich, Link et al. 2006). In contrast, radioisotope labeling is more laborious and requires a high level of technical expertise to operate the instruments and conduct experiments. Moreover, radioisotope labeling diminishes half-lives of proteins and alters metabolic stability (Yewdell, Lacsina et al.). For example, commercially available radioisotope-labeled amino acids from bacteria contain bacterial components which may influence protein stabilities through triggering cellular innate immune receptors (Lelouard, Gatti et al. 2002).

Secondly, in AHA-labeled cells, the cellular fluorescence intensity reflects the amount of remaining proteins (Dieterich, Link et al. 2006), including both cytosolic and membrane proteins, and thus exclude factors related to free AHA release, implicating that this is a more accurate and reliable method. In contrast, in radioisotope-labeled cells, only the acid-soluble radioactivity released into the medium from the labeled proteins in intact cells is measured (Yewdell, Lacsina et al. ; Ogier-Denis, Houri et al. 1996; Roberts and Deretic 2008). Therefore, the latter method seems less accurate and sensitive compared to our methodology.

There are several important technical issues in establishing this assay. Firstly, AHA labeling has to be performed in methionine-free medium with dialysed fetal bovine serum (FBS, elimination of L-methionine from other sources), because the incorporation efficiency of AHA is much lower than natural methionine (Kiick, Saxon et al. 2002). Therefore, theoretically the presence of endogenous methionine inside the cells may adversely affect AHA

labeling. Secondly, AHA labeling is unable to pick up proteins without methionine. Based on the estimation that such proteins only constitute 1.02% of all entries in a human protein database and that 5.08% of the human proteome possess only a single, N-terminal methionine that may be removed by post-translational modification (Dieterich, Link et al. 2006), AHA labeling is applicable to about 94% of the mammalian proteomes. Lastly, we acknowledge that this assay is unable to measure the basal proteolysis rate in the control cells, as it only determines the extent of protein degradation in the treated cells in comparison to the control cells. However, we believe that this limitation should not impair the value of this assay as a tool in autophagy study.

3.5 Conclusion and future directions

In summary, we have successfully developed a novel method by using AHA labeling as a simple, sensitive, specific and quantitative tool to measure autophagic protein degradation. This assay is mainly applicable to cell culture systems *in vitro* and it could be easily adapted for high throughput screening of autophagy modulators.

In future, we will focus on individual protein degradation rate and reveal inherent protein intracellular stability. Following AHA labeling, subcellular fractionation and immunopurification of protein complexes can be prepared and mass spectrometry will be performed to assess the temporal and spatial dynamics of certain subcellular compartments, organelles and protein-protein interaction networks. According to the previous studies, Mary K. Doherty et al performed dynamic SILAC, stable isotope labeling by amino acids in cell culture for mass spectrometry (MS)-based quantitative proteomics, and profiled the intracellular degradation rate of almost 600 proteins from human A549 adenocarcinoma cells(Mary K. Doherty et al, 2009). In contrast to SILAC, Hsueh-Chi Sherry Yen developed a highly parallel multiplexing strategy, called global protein stability profiling (GPSP) by coupling flow cytometry with microarray technology, to monitor global protein turnover and

examine the stability of individual proteins. In HEK293T cells, they measured the stability of ~8000 human proteins and identified proteosome substrates (Hsueh-Chi Sherry Yen, 2008). However, cross-correlating the SILAC and GPSP data sets showed a plotted 339 shared gene products against each other (Yewdell JW, et.al. 2011). Surprisingly, no significant correlation between the common members of the two data sets was observed. Therefore, in our next step, we will conduct AHA labeling in combination with mass spectrometry to investigate global protein turnover profiles in autophagy and may reveal the discrepancy between the above two reports.

Chapter 4

Experimental Procedures

4.1 General

All chemicals and solvent used in this dissertation were purchased from commercial suppliers and used without further purification unless otherwise stated. The andro probes were designed by the dissertation author and synthesised by commercial company.

4.2 Materials and methods of Chapter 2

4.2.1 General Information (Synthesis)

All chemicals and solvents were obtained from commercial sources and used without purification. Andrographolide (Andro), PPTS, 2,2-Dimethoxy-propane, hex-5-ynoic acid, Pd/C and $NaBH_4$ used in synthesis were purchased from Alfa (China). All reactions requiring anhydrous conditions were carried out under an argon or nitrogen atmosphere in flame dried glassware. HPLC grade solvents were used. Experiments were monitored by thin layer chromatography (TLC) or liquid chromatography mass spectrometry (LC-MS).

^{1}HNMR and ^{13}C NMR spectra were recorded on a Bruker AVANCE III 300 and 500 MHz spectrometer. Chemical shifts are reported in δ ppm, and *J* values are reported in Hz. Liquid chromatography mass spectra were obtained using a Shimadzu LC-IT-TOF spectrometer or a Shimadzu LC-ESI spectrometer. 0.1% TFA/H_2O and 0.1% TFA/acetonitrile were used as eluents for all HPLC experiments.

4.2.2 Synthesis of Reduced Andro Analogue RA

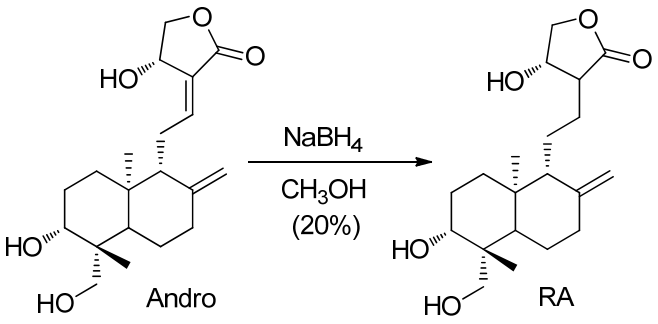

Scheme 4.1 The synthetic scheme for **RA**.

Andro (50 mg, 0.14 mmol) was dissolved in methanol (20 mL). Then $NaBH_4$ (6 mg, 0.14 mmol) was added under Argon. After addition, the reaction mixture was stirred at 0 °C for 30 min. The reaction mixture was quenched by addition of water (10 mL) and EA. (100 mL). The organic phase was separated from the aqueous phase, washed with brine (20 mL), dried with Na_2SO_4, and then concentrated to obtain the crude product, which was purified with Prep-TLC (silica gel, eluent : dichloromethane/methanol=15 : 1) to obtain **RA (**10 mg) as white solid. Yield: (20%). ^{1}H NMR (500 MHz, DMSO-d_6), δ 5.39 (d, J = 4.0 Hz, 1H), 5.05 (d, J = 4.5 Hz, 1H), 4.78 (s, 1H), 4.74 (s, 1H), 4.36 (m, 1H), 4.24 (dd, J_1 = 3.0 Hz, J_2 = 10.0 Hz, 1H), 4.12 (d, J = 5.0 Hz, 1H), 4.05 (d, J = 10.0 Hz, 1H), 3.84 (d, J = 9.0 Hz, 1H), 3.24 (m, 2H), 2.32 (m, 1H), 1.91 (m, 1H), 1.58-1.73 (m, 6H), 1.42-1.50 (m, 2H), 1.32 (m, 2H), 1.07 (s, 3H), 0.60 (s, 3H); ^{13}C NMR (500 MHz, DMSO-d_6), δ 178.8, 148.0, 107.4, 79.0, 75.1, 68.0, 63.1, 56.1, 56.0, 45.0, 42.7, 40.9, 39.2, 38.4, 37.0, 28.4, 24.5, 23.5, 22.7, 21.5, 15.3. LC-MS (IT-TOF) calcd for $[M+H]^+$: 353.47, Found: 353.50.

4.2.3 Synthesis of the clickable probe P1

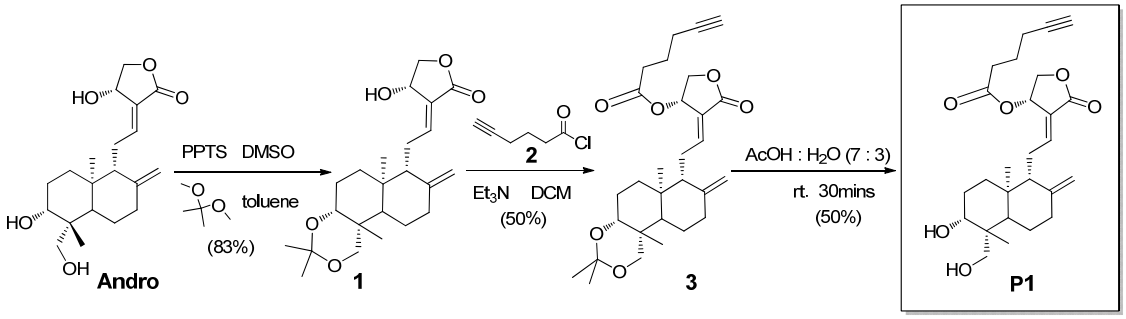

Scheme 4.2 The synthetic scheme for **P1**.

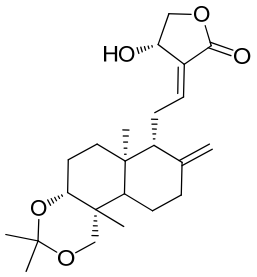

1

To a suspension of **Andro** (1.4 g, 4.0 mmol) and 2, 2-Dimethoxy-propane (2.08 g, 20.0 mmol) in toluene (50 mL), PPTS (0.1 g, cat.) and DMSO (2 mL) were added. The mixture was heated to reflux for 2 hrs. After the reaction mixture was cooled down, water (100 mL) and EA (150 mL) were added. The organic phase was separated, washed with brine (50 mL), dried with $NaSO_4$, and then concentrated and purified by column chromatography (EtOAc: PE=1:10-50% EtOAc) to yield 1.3 g (83%) of the product **1** as a white solid. LC-MS (IT-TOF) calcd for $[2M+H]^+$: 781.49, Found: 781.10; $[2M+Na]^+$: 803.47, Found: 803.10,

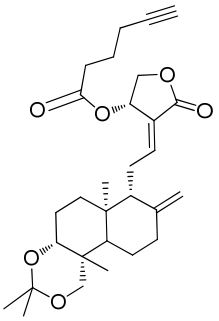

3

To a solution of compound **1** (200 mg, 0.51 mmol) in DCM (50 mL), Et_3N (103 mg, 1.02 mmol) was added at 0 °C under N_2. Then compound **2** (100 mg, 0.77 mmol) was added dropwise at 0 °C, The mixture was stirred at ambient temperature overnight by mechanical agitation. Then water (50 mL) was added, and the organic phase was separated and washed with brine (50 mL), dried with $NaSO_4$, and then concentrated and purified by column chromatography (EtOAc: PE=1:20-40% EtOAc) to yield 100mg (40%) of the product **3** as a white solid. LC-MS (IT-TOF) calcd for $[M+H]^+$: 485.29, Found: 485.10.

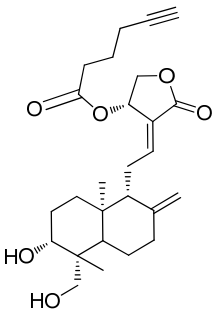

P1

Compound **3** (50mg, 0.10 mmol) was dissolved in AcOH: H_2O = 7:3 (5 mL) at ambient temperature. The mixture was stirred for 30 min. Then pH was adjusted to 6 by $NaHCO_3$. The desired aqueous solution was extracted with EA (50 mL × 3), the organic phase was washed with brine (50 mL), dried with Na_2SO_4, and then concentrated and purified by column chromatography (EtOAc: PE=1:10-100% EtOAc) to yield 20 mg (45%) of the product **P1** as colorless oil. ^1H NMR (300 MHz, $CDCl_3$), δ 7.01 (dd, *J*= 6.9, 5.3 Hz, 1H),

5.92-5.94(d, *J*= 6.0 Hz, 1H), 4.88 (s, 1H), 4.53-4.59 (dd, *J*= 11.2, 6.1Hz, 1H), 4.49 (s, 1H), 4.16-4.26 (m, 2H), 3.49 (m, 1H), 3.33 (d, *J*= 11.3 Hz, 1H). 2.53 (t, *J*= 7.4 Hz, 2H), 2.26-2.44 (m, 7H), 1.99 (t, *J*= 2.6 Hz, 2H), 1.71-1.91 (m, 6H), 1.26 (s, 6H), 0.67 (s, 3H); ^{13}C NMR (500 MHz, DMSO-d_6) δ 173.7, 171.1, 151.3, 148.8, 125.5, 108.9, 80.7, 73.1, 70.5, 69.2, 64.9, 57.1, 56.2, 43.6, 39.9, 38.9, 38.1, 33.4, 29.0, 26.4, 25.2, 24.8, 23.4, 18.4, 15.6; LC-MS (IT-TOF) calcd for $[M+Na]^+$: 467.24, Found: 467.00.

4.2.4 Synthesis of P2

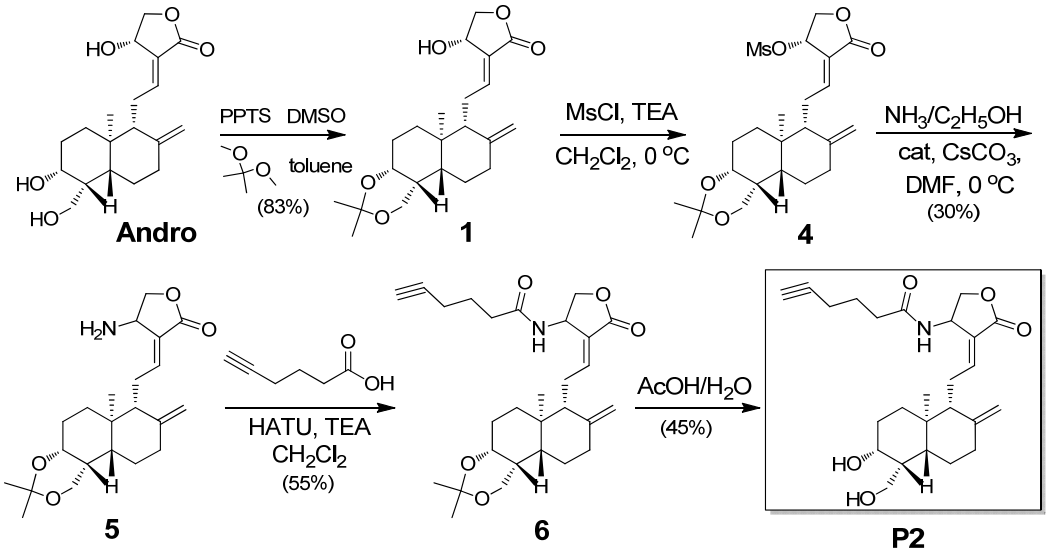

Scheme 4.3 The synthetic scheme for **P2**.

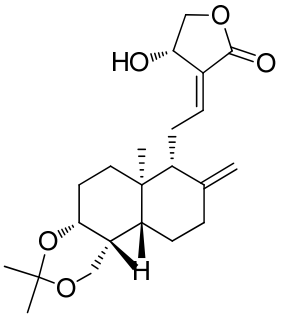

To a suspension of **Andro** (1.4 g, 4.0 mmol) and 2, 2-Dimethoxy-propane (2.08 g, 20.0 mmol) in toluene (50 mL), PPTS (0.1 g, cat.) and DMSO (2 mL) were added. The mixture was heated to reflux for 2 hrs. After the reaction mixture was cooled down, water (100 mL) and EA (150 mL) were added, and the organic phase was separated, washed with brine (50 mL), dried with $NaSO_4$. And then concentrated and purified by column chromatography (EtOAc: PE=1:10-50% EtOAc) to yield 1.3 g (83%) of the product **1** as a white solid. LC-MS (IT-TOF) calcd for $[2M+H]^+$: 781.49, Found: 781.10; $[2M+Na]^+$: 803.47, Found: 803.10,

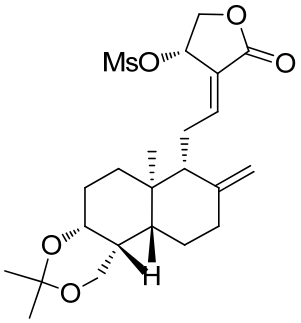

4

Compound **1** (100 mg, 0.26 mmol, 1 equiv) was dissolved in dry CH_2Cl_2 (5 mL), and the mixture was cooled to 0 °C. TEA (31 mg, 0.31 mmol, 1.2 equiv) was added. MsCl (35 mg, 0.31 mmol, 1.2 equiv) was added dropwise, and the mixture was warmed to room temperature and allowed to stir for 30 min. Upon consumption of starting material, the solvent was evaporated and the residue (crude compound 4) was used in next step without further purification.

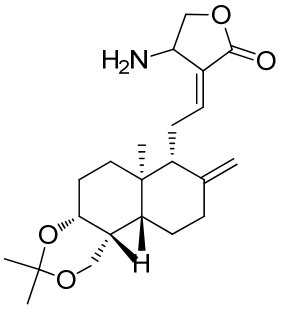

5

To a solution of crude **4** in DMF (5 mL), NH_3/C_2H_5OH (2 mL) was added at 0 °C, followed by a catalytic amount of cesium carbonate (10 mg), and the reaction was stirred at 0 °C for 0.5 h. Then the reaction was quenched with water (10 mL), and the aqueous phase was extracted with EA (10 mL), dried and concentrated. The residue was purified by silica gel column chromatography with EA to DCM: CH_3OH=10:1 to obtain the compound **5** as white solid (30%). The configuration at C14 was partially reverted during this step, which made compound 5 a mixture of two isomers. The ratio of the two isomers was 1:0.8 as calculated in the NMR spectrum of P2. LC-MS (IT-TOF) calcd for $[M+H]^+$: 390.26, Found: 390.00.

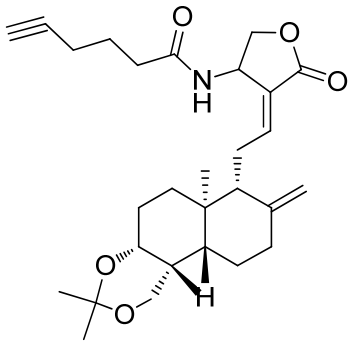

6

To a solution of compound **5** (100 mg, 0.26 mmol) in DCM (10 mL), HATU (148 mg, 0.39 mmol), TEA (79 mg, 0.78 mmol) and hex-5-ynoic acid (30 mg, 0.39 mmol) were added. The mixture was stirred at RT for 2 hrs, and subsequently washed with water followed by brine, dried and concentrated, and the residue was purified by column chromatography with CH_2Cl_2:CH_3OH=30:1 to obtain the compound **6** (55%) as a light yellow solid. LC-MS (IT-TOF) calcd for $[M+H]^+$: 484.31, Found: 484.30.

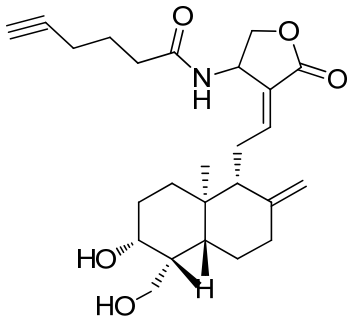

P2

Compound 6 (50mg, 0.10 mmol) was dissolved in AcOH: H_2O = 7:3 (5 mL) at ambient temperature. The mixture was stirred for 30 min. Then pH was adjusted to 6 by $NaHCO_3$. The desired aqueous solution was extracted with EA (50 mL × 3), and the organic phase was washed with brine (50 mL) and dried with Na_2SO_4. The organic phase was then concentrated and purified by column chromatography (CH_3OH: DCM=1 : 30) to obtain 20 mg (45%) of the product P2 as white solid. ^1H NMR (300 MHz, CD_3OD), δ 7.46 (m, 0.44H), 7.40 (m, 0.55H), 4.74-4.99 (m, 8H), 4.06-4.11 (m, 1H), 3.33-3.43 (m, 1H), 2.14-2.46 (m,6H), 1.93-2.00 (m, 1H), 1.75-1.89 (m, 7H), 1.52-1.65 (m, 1H),

1.18-1.21 (m, 3H), 0.69 (s, 3H); ^{13}C NMR (300 MHz, CD_3OD) δ 174.7, 174.6, 174.5, 174.3, 150.1, 148.6, 148.0, 147.6, 136.0, 133.8, 108.3, 107.9, 84.1, 80.8, 80.7, 72.0, 70.5, 70.2, 64.9, 56.7, 56.4, 54.0, 53.8, 46.6, 45.9, 43.7, 43.6, 40.2, 39.7, 39.5, 39.3, 38.1, 37.9, 35.6, 35.5, 29.2, 29.1, 29.0, 28.9, 25.9, 25.8, 25.4, 23.4, 18.7, 18.6, 16.0, 15.7; LC-MS (IT-TOF) calcd for $[M+H]^+$: 444.27, Found: 444.30.

4.2.5 Materials and Reagents (Biology experiments)

Andrographolide (98%), Tris [(1-benzyl-1H-1,2,3-triazol-4-yl) methyl]amine(TBTA), Tris (2-carboxyethyl) phosphine (TCEP), streptavidin beads, acetonitrile (ACN), Trifluoroacetic acid (TFA), urea, dithiothreitol (DTT), phosphoric acid, and iodoacetamide (IAA) were purchased from Sigma-Aldrich. Antibody against NF-κB p50 (SC-7178) was from Santa Cruz Biotechnology, Inc. Antibody against actin (1:4000) was from BD Transduction Laboratories. Migration assay and matrigel invasion assay chamber were purchased from BD Biosciences, San Jose, CA. Cy3-Azide (CLK-CCA-9294-1) and biotin-Azide were from Jena Bioscience, Inc. β-actin from human platelet (>99% pure) was obtained from Cytoskeleton, Inc. Sequencing grade trypsin was obtained from Promega. Chymotrypsin, protease and phosphatase inhibitors cocktail were purchased from Roche. Ultrapure water used for all experiments was purified with an ELGA water system. Unless otherwise indicated, all the other reagents used for the biochemical methods were purchased from Sigma-Aldrich.

4.2.6 Cell Culture

HCT116, HepG2, HeLa and MV4-11 were purchased from ATCC (Manassas, VA**).** HCT116 was maintained in modified McCoy's 5A medium with L-glutamine (Sigma, St. Louis, MO), supplemented with 10% fetal bovine serum (Invitrogen, Carlsbad, CA) and 1x antibiotic/antimycotic (Invitrogen, Carlsbad, CA) at 37^oC in 5% (v/v) CO_2. HepG2 and HeLa cell lines were cultured in Dulbecco's Modified Eagle Medium (Sigma, St. Louis, MO) supplemented with 10% fetal bovine serum (Invitrogen, Carlsbad, CA)

and 1x antibiotic/antimycotic (Invitrogen, Carlsbad, CA). MV4-11 cell line was cultured in RPMI 1640 (Invitrogen, Carlsbad, CA) supplemented with 10% fetal bovine serum and 1x antibiotic/antimycotic. Cells were maintained at 37 ℃ in a humidified incubator supplemented with 5% CO_2.

4.2.7 Inhibition of Cancer Cell Proliferation

HCT116, HeLa and HepG2 Cell Lines: 20,000 cells was seeded into 96 well plate and allowed to attach for 24 hrs. Cells were then treated with Andro at various concentrations for 48hrs. At the end of the treatment, media was removed and the wells were washed once with PBS. The cells were then stained with 0.5% crystal violet in 20% methanol for 10 min. Excess crystal violet was washed off with PBS and the wells were allowed to dry. Solubilization was done using 1% SDS for 30 min and the absorbance measured at 550nm.

MV4-11 Cell Lines: Cells were treated with increasing concentration of Andro for 48 hrs. Following the intended treatment, the cells were centrifuged and resuspended in 2 mL medium. A volume of cell suspension containing $1x10^5$ cells was centrifuged into a pellet. After dislodging the pellet, the samples were added with 10 μL of 50 μg/mL propidium iodide (PI) and subjected to flow cytometric analysis using the Beckman Counter (EPICS-Xl MCL).

4.2.8 *In situ* Fluorescence Labeling Experiments

HCT116 cells were grown to 80-90% confluence in 6-well plates. After the media was removed, cells were washed twice with PBS. P1 or P2 (100 μM) in 2 ml medium with a final DMSO concentration of 1% was added and cells were incubated for 4 hrs at 37 °C and 5% CO_2. Equal volume of DMSO was used as a negative control. For concentration optimization experiment, increasing concentrations (20-200 μM) of P2 were used to culture the cells for 4 hrs. Subsequently, the medium was removed and cells were washed with PBS and detached with trypsin. The cell pellet was resuspended in PBS, washed, followed by sonication in 150 μl of PBS to lyse cells. The resultant

cell lysate was cleared by centrifuging at 13,000 rpm for 30 min. Protein concentrations of the cell lysates were determined using the Bradford assay. Equal amounts (100 μg) of different treatment samples were used for subsequent fluorescent labeling. For each reaction, Cy3-azide (20 μM), Tris(2-carboxyethyl) phosphine (TCEP) (1mM, 100×fresh stock in water), Tris[(1-benzyl-1H-1,2,3-triazol-4-yl)methyl] amine (TBTA ligand) (100 μM, 100×stock in DMSO), and $CuSO_4$ (1mM,100×stock in water) were added to the lysate. The samples were incubated at room temperature for 2 hrs. Next, clicked proteins were precipitated by acetone and air dried. 100 μL 1× SDS loading buffer was added to dissolve the sample and 50 μL of sample was separated by SDS gel electrophoresis on 10% polyacrylamide gel. After SDS-PAGE, gels were visualized using a Typhoon 9410 laser scanner (GE, health care) and images were analyzed by TotalLab software.

4.2.9 Cells Labeling using andro probe

In the subsequent ICABPP study, two biological duplicate of P2 treated and two DMSO treated samples were pulled down and digested in parallel. The two DMSO control samples were labeled with iTRAQ reagent and quantified by iTRAQ ratios. Briefly, HCT116 cells were grown to 80-90% confluence in T175 flasks. Spent medium was then aspirated and the cells washed twice with PBS. P2 (100 μM) in 20 ml medium with a final DMSO concentration of 1% was added to the cells in the flasks and incubated for 4 hrs in the CO_2 incubator.. Culture medium containing 1% DMSO was used as negative control. Subsequently, P2- and DMSO- containing media were removed, and then the cells were washed with PBS and detached with trypsin. The cell pellet was resuspended in PBS, washed and lysed by sonication in PBS. The cell lysates were clarified by centrifugation at 13,000 rpm for 30 min followed by Bradford protein assay. Equal amount (5 mg) of cell lysates (2 Andro probe treated and 2 DMSO treated samples) were used for subsequent click chemistry to conjugate proteins with the biotin tags separately. For each reaction, Biotin-azide (20 μM), Tris(2-carboxyethyl) phosphine(TCEP) (1mM, 100× fresh stock in water), Tris[(1-benzyl-1H-1,2,3-triazol-4-yl)methyl] amine

(TBTA ligand) (100 μM, 100×stock in DMSO), and $CuSO_4$ (1mM,100×stock in water) were added to the cell lysates and incubated at room temperature for 4 hrs. Next, clicked proteins subjected to precipitation with acetone and air dried. Subsequently, the pellet was dissolved in 1 mL PBS and incubated with 50 μL of Streptavidin beads (Sigma-Aldrich) under gentle mixing for 2 hrs at room temperature.

4.2.10 On-beads Digestion

The beads were washed a total of 9 times; thrice with 1% SDS, followed by 3 times with 6M urea and thrice with PBS. The extensively washed beads were resuspended in 25mM ammonium bicarbonate (NH_4HCO_3) and 2 μL tris-(2-carboxyethyl) phosphine (TCEP, 100 mM stock solution) added. The beads were placed in a 65°C heat block for 60 min. Next, 1μL methyl methane-thiosulfonate (MMTS, 200mM stock solution) was added and the samples left in the dark and allowed to react for 15 min at room temperature. Following reduction and alkylation, trypsin (12.5 ng/ μL, Promega) was added and incubated at 37°C overnight. The digested peptides were separated from the beads using a filter-spin column (GE, healthcare). These digested peptides could be stored at -20 °C for several months pending iTRAQ labeling and mass spectrometry analysis.

4.2.11 iTRAQ Labeling of the Digested Pull-Down Samples

iTRAQ labeling was performed out using iTRAQ Reagent kit (AB SCIEX, Foster City, CA, USA) based on the vender's instruction manual with minor modifications. The two biological replicates of the negative control pull-down samples were labeled with iTRAQ reagent 113 and 114, respectively. Similarly, two biological replicate of digested Andro pull-down samples were labeled with reagent 116 and 117, respectively. Briefly, the on-beads digested peptides were dried and reconstituted with equal volume of dissolving buffer (0.5M TEAB). The peptides were then labeled with the respective iTRAQ reagents and incubated at room temperature for 2 hrs before all the samples were pooled together. The iTRAQ workflow is shown in Figure 2.2 in chapter 2.

4.2.12 Strong Cation Exchange (SCX) Chromatography, C18 Desalting of Labeled Samples

To remove interfering substances like SDS, isopropanol, dissolution buffer (TEAB), reducing agent (TCEP), alkylating agent (MMTS), calcium chloride and excess iTRAQ reagents etc., the pooled iTRAQ-labeled peptides sample was subjected to strong cation exchange chromatography (SCX) using the iTRAQ Method Development Kit (AB SCIEX, Foster City, CA, USA). The bound peptides were eluted with 5 % ammonium hydroxide (NH_4OH) in 30 % methanol. The eluate was desalted using a Sep-Pak C_{18} cartridge (Waters, Milford, MA), dried and then reconstituted with 100 μL of diluent (98% water, 2% acetonitrile, 0.05% formic acid).

4.2.13 Proteins Identification and Quantification

Nano LC−ESI-MS: The detailed methods for LC-MS/MS was described previously (Tang et al. 2012). Briefly, separation of the iTRAQ labeled peptides was carried out on an Eksigent nanoLC Ultra and ChiPLC-nanoflex (Eksigent, Dublin, CA) in Trap Elute configuration. A volume of 5 μL of the sample was loaded to the LC system. Peptides were separated by a gradient formed by 2% ACN, 0.1% FA (mobile phase A) and 98% ACN, 0.1% FA (mobile phase B): 5−12% of mobile phase B (20 min), 12−30% of mobile phase B (90 min), 30−90% of mobile phase B (2 min), 90% of mobile phase B (5 min), 90−2% of mobile phase B in 3 min, and 50−5% of mobile phase B in 13 min, at a flow rate of 300 nL/min. The MS analysis was performed on a TripleTOF 5600 system (AB SCIEX, Foster City, CA) in information dependent mode.

ProteinPilot Analysis: The detailed method of ProteinPilot analysis was described previously.[2] Briefly, the protein identification and iTRAQ quantification were performed with ProteinPilot™ 4.5 (AB SCIEX, Foster City, CA) which uses the Paragon™ algorithm to perform database searches. The database used includes the International Protein Index (IPI) v3.87 human protein sequences (total 91 468 entries). The search parameters used were as

follows: Cysteine alkylation of MMTS; Trypsin Digestion; TripleTOF 5600; Biological modifications. Redundancy was eliminated by the grouping of identified proteins using the ProGroup algorithm in the software. A decoy database search strategy was used to determine the false discovery rate (FDR) for peptide identification. A corresponding randomized database was generated using the Proteomics System Performance Evaluation Pipeline (PSPEP) feature in the ProteinPilot™ Software 4.5. In this study, a strict total score cut-off >1.3 was adopted as the qualification criterion, which corresponded to a peptide confidence level of 95%. The identification and quantification results were then exported into Microsoft Excel for manual data analysis.

4.2.14 Data Analysis

To determine the cut-off threshold for the fold change of proteins identified from the iTRAQ study to be considered as significantly regulated, two equal amounts of six-protein mixtures (Applied Biosystems) were trypsin-digested and labeled with the iTRAQ reagents.[3] The standard deviation (S.D) of all the ratios of the labeled peptides was computed to be 0.15. Thus by using a 1 + 2 S.D formula the fold-change cut-off thresholds were set as 1.3 for up-regulated proteins and reciprocally 0.77 for down-regulated proteins. This strategy was adopted for our quantitative study. This cut-off was used to eliminate protein targets where the two biological replicate samples showed significant change (ratio >1.3 or <0.77). Basing on this strategy, 208 proteins were considered to be the statistically reliable hits (Figure 2.6), and the distribution of the enrichment ratios of these proteins were further presented as the colored heat map as illustrated in Figure 2.7. The 4 set ratios of Andro pull-down vs. DMSO pull-down were presented as colored heatmap, using the MultiExperiment Viewer (MeV) (Saeed et al. 2006; Saeed et al. 2003). Proteins with enrichment ratio closed to 1 are denoted in blue and likely to exhibit non-specific binding. In contrast, proteins labeled in red showed enrichment ratio above 2 or close to 3, suggesting that they are likely the specific binding targets.

To reduce the likelihood of selecting the false positive drug targets, we

chose a stringent ratio equivalent to 2 as the cut-off to identify specific protein targets for subsequent experiments. Meanwhile, proteins identified based on a single peptide are considered unreliable and were removed. Using these criteria, 75 proteins were identified and selected (Figure 2.6). The full list of the 75 potential targets is shown in Supplemental Table of chapter 2.

4.2.15 Pathway Analysis of Andro Targets

The specific Andro targets identified using the ICABPP approach were analyzed using the Ingenuity Pathway Analysis software (Ingenuity® Systems, Redwood city, CA, USA). A spreadsheet containing the list of Andro targets was uploaded into IPA. The software mapped each of the proteins to the repository of information in the Ingenuity Pathways Knowledge base. Molecular networks and canonical pathways regulated by these drugs targets were obtained using IPA core analysis.

4.2.16 Validation of Drug Target using Western Blot

Andro probe affinity pull-down sample was separated by 1D-SDS PAGE together with DMSO pull-down sample. After SDS-PAGE, the proteins were transferred onto PVDF membranes (Bio-Rad). The blots were blocked with 5% (w/v) BSA in PBS with 0.1% Tween 20 (PBS-T) for 4hrs at room temperature. The membranes were incubated with rabbit anti- NF-κB p50 (1:1500), from Santa Cruz Biotechnology, Inc. as well as mouse anti- β-actin (1:4000) from BD Transduction Laboratories. HRP-conjugated from Pierce Biotechnology, or HRP-conjugated anti-mouse IgG (1:5000) from GE Healthcare were used as secondary antibodies and incubated for 2 hrs at room temperature. The membrane was washed 3 times in PBS-T between each antibody incubation step. Subsequent visualization was performed using ECL substrate (Pierce Biotechnology).

4.2.17 Expression of Wild Type and Mutated NF-κB p50

DNA insert of P50 Rel homology domain (aa 39-364), a gift from Prof. G. Ghosh of UCSD, was subcloned into pET-M expression vector. P50-C62A mutant was generated by PCR-based site-directed mutagenesis method. The plasmids were transformed into *E. coli* BL21 (DE3) cells for protein expression. A single colony of *E.coli* BL21 (DE3) cells containing the desired plasmid was cultured overnight in 10 ml LB medium containing 100 μg/ml ampicillin. Two milliliters of overnight cultures were inoculated into 1L LB broth culture medium containing 100 μg/ml ampicillin. The culture was grown at 37°C until OD_{600} of 0.6 was reached. Protein expression was induced with 0.35 mM of IPTG at 37 °C for overnight. The cell suspension was harvested and resuspended in Ni binding buffer containing 20 mM Tris-Cl pH 8.0, 0.5 M NaCl, 5 mM Immidazole. The cell suspension was lysed by sonication on ice and subsequently centrifuged at 18,000x g for 30 min. The supernatant of the cell lysate was loaded on the Ni column and the column was washed 10 times with a total volume of 500 ml Ni washing buffer containing 20 mM Tris-Cl pH8.0, 0.5 M NaCl, 30 mM immidazole to remove unbound proteins. Recombinant p50 with Histidine tag was eluted with 20 mM Tris-Cl pH8.0, 0.5 M NaCl, 500 mM Immidazole. The eluted p50 was dialyzed overnight against 1xPBS pH 7.3 to remove imidazole. This protein was subsequently further purified using gel filtration column Superdex 200 (Amersham).

4.2.18 *In vitro* Labeling of Human Recombinant NF-κB p50

Recombinant NF-κB p50 was reconstituted with PBS as 1 mg/ml. 1 μL protein solution was diluted with 42 μL PBS and incubated with 1 μL P2 at a final concentration of 0, 10, 20, 40, 80, 160 μM for 4 hrs, followed by Click reaction, SDS-PAGE and fluorescence scanning. For heat denatured sample, 1 μL protein solution was diluted with 40 μL PBS and 2 μL of 25% SDS and the sample was heated at 96 °C for 10 min. Then the heated sample was cooled to room temperature and reacted with 80 μM P2 at. Competition assay was carried out with the pre-treatment of 10× excess free Andro for 4 hrs, and then labeled with P2. 1mM DTT or 5mM BME co-treatment together with Andro

were also included in our experiment. Mutated C62A p50 was labeled with 80 μM to test this critical amino acid in Andro reaction.

4.2.19 Andro Binding Site Mapping of NF-κB p50

To map out the exact binding site of Andro in NF-κB p50, the recombinant p50 was treated with Andro or DMSO. After trypsin digestion, the resulting peptides were analyzed by MS/MS. Briefly, 1 μL of 10 mM Andro or 1 μL DMSO was incubated with 50 μg NF-κB in 100 μL PBS for 4 hrs at room temperature. The labeled samples were buffer exchanged against 50 mM NH_4HCO_3 to remove unbound drug using a filter spin column (10 kDa cut-off). The final solution volume was adjusted to 50 μL using 50 mM NH_4HCO_3. This was followed by the addition of 1 μg trypsin to the NF-κB samples and incubated for 16 hrs at 37°C. The digested samples were analyzed by high resolution LC-MS/MS. The MS/MS spectra of the native NF-κB peptide containing Cys62 are shown in Figure 2.13 (top). The MS/MS spectra of the Andro labeled NF-κB peptide containing Cys62 are shown in Figure 2.13 (bottom). C^{A*} represents the Andro modified Cys. Peptide ions containing modified Cys are indicated ^{A*} in red.

4.2.20 Molecular Docking

Autodock is an automated procedure for predicting optical conformations and orientations for the ligand, protein or DNA with the target proteins at the binding site (Morris et al. 1998)(Morris et al. 2009). NF-κB-Andro docking simulations were performed using Autodock version 4.2 (**http://autodock.scripps.edu/**) with the Lamarckian Genetic algorithm (LGA) method. Polar hydrogen atoms were added to the target protein p50 and its nonpolar hydrogens were merged. The molecule Andro was treated as flexible ligand and only torsions of freedom were explored, keeping both bond angles and lengths constant. The grid box was centered on p50 (PDB: 2V2T) with a dimension of 100×100×100 points. Each docking simulation was repeated 20 times using different random generator seeds. The interactions of complex p50-Andro conformations were analyzed using Pymol.

4.2.21 *In vitro* Labeling of Human Recombinant β-actin

β-actin from human platelet ((>99% pure), Cytoskeleton, Inc.) were reconstituted as 1mg/ml in G-buffer (2 mM Tris-HCl, 0.2 mM ATP, 0.2 mM $CaCl_2$, 0.2 mM DTT, 0.005% NaN_3, pH 8.0) or F-buffer (2 mM Tris-HCl, 2 mM $MgCl_2$, 100 mM KCl, 0.2 mM DTT, 0.2 mM $CaCl_2$, 0.5 mM ATP, pH 7.5), incubated for 18 hrs at room temperature. 1 µL protein in G-buffer or F-buffer was diluted with respective buffers and incubated with 1 µL P2 at a final concentration of 0, 10, 20, 50 or100 µM for 4hrs, followed by Click reaction, SDS-PAGE and fluorescence scanning. For heat-denatured sample, 1 µL protein in F-buffer was diluted with 40 µL F-buffer and 2 µL of 25% SDS and the samples were heated at 96 °C for 10 min. The heat-denatured control was subsequently cooled to room temperature and reacted with P2 at 100µM.

4.2.22 Andro Binding Site Mapping of β-actin

To indentify the exact binding site of Andro in β-actin, the polymerized actin was treated with Andro or DMSO. After chymotrypsin digestion, the resulting peptides were analyzed by MS/MS. Briefly, 1 µL of 10 mM Andro or 1 µL DMSO was incubated with 50 µg polymerized actin in F-buffer (2 mM Tris-HCl, 2 mM $MgCl_2$, 100 mM KCl, 0.2 mM DTT, 0.2 mM $CaCl_2$, 0.5 mM ATP, pH 7.5) for 4 hrs in room temperature. The labeled samples were buffer exchanged against 50 mM NH_4HCO_3 to remove unbound drug using a filter spin column (10 kDa cut-off). The final solution volume was adjusted to 50 µL using 50 mM NH_4HCO_3. 1 µg chymotrypsin was added to the β-actin samples and incubated for 16 hrs at 37°C. The digested samples were analyzed by high resolution LC-MS/MS. The MS/MS spectra of the native β-actin peptide containing Cys272 are shown in Figure 2.17 (top). The MS/MS spectra of the Andro labeled β-actin peptide containing Cys272 are shown in Figure 2.17 (bottom). C^{A*} represents the Andro modified Cys. Peptide ions containing modified Cys are indicated ^{A*} in red.

4.2.23 Cell Cycle Determination by Flow Cytometry

Andro's effect on cell cycle was evaluated by flow cytometry. Briefly, after the designated treatments, cells were detached using trpsin-EDTA. The cells were collected and washed 2× with PBS, then fixed and permeabilized in 70% pre-chilled ethanol for at least 2 hrs. Fixed cells were stained with PI staining solution (0.1% Triton X-100, 200 mg/ml RNaseA and 20 mg/ml PI in PBS) for 15 min at 37°C. Subsequently, the PI stained sample were detected by flow cytometry analysis.

4.2.24 Transwell Migration Assay

Migration assay was carried out using 8.0 μm cell culture insert for 24 well (BD Biosciences, San Jose, CA) according to manufacturer's protocol. Briefly, the inserts were coated with 10 μg/ml fibronectin (Sigma, St. Louis, MO) in PBS overnight at 4 ^{o}C. The coated inserts were washed once with PBS before using. HCT116 were seeded at a density of 50,000 cells into the top chamber of each insert with 5 μM of Andro or RA in media without FBS. Media containing 5 μM of respective drugs were supplemented with FBS and added to the bottom chamber. 1% DMSO was used as negative control. After incubation for 30 hrs, cells from the top layer of the inserts were removed by scrubbing. Subsequently, the inserts were fixed in 3% paraformaldehyde (Sigma, St. Louis, MO) in PBS for 20 min before staining with crystal violet for 30 min. Excess stain was washed off and the inserts were allowed to dry. Solubilization was done using 1% SDS for 2 hrs and the absorbance were measured at 550nm.

4.2.25 Matrigel Invasion Assay

Matrigel invasion assay was carried out using matrigel coated inserts for 24 -well plate (BD Biosciences, San Jose, CA) according to manufacturer's protocol. 150,000 cells were seeded into the top chamber of each insert with Andro or RA in media without FBS. Media containing 5μM of respective drugs were supplemented with FBS and added to the bottom chamber. After

30 hrs incubation, cells from the top layer of the inserts were removed by scrubbing. Subsequently, the inserts were fixed in 3% paraformaldehyde (Sigma, St. Louis, MO) in PBS for 20 min before staining with crystal violet for 30 min. Excess stain was washed off and the inserts were allowed to dry. Cells from 5 randomly selected fields were counted using photographs taken under a light microscope at 200x magnification.

4.3 Materials and methods Chapter 3

4.3.1 Reagents and antibodies

The chemicals used in our experiments were: bafilomycin A1 (Sigma, B1793), pp242 (Sigma, P0037), rapamycin (Sigma, R8781), Torin 1 (Tocris Bioscience, #4247), dimethyl sulfoxide (DMSO, Sigma, D2650), AHA (L-azidohomoalanine) reagent (Invitrogen, #C10289), tris [(1-benzyl-1H-1,2,3-triazol-4-yl)methyl] amine (TBTA, Sigma, #678937), Tris (2-carboxyethyl) phosphine (TCEP, Sigma, C4706), CuSO4(sigma, #451657), TAMRA alkyne (Invitrogen, #A10267), Dulbecco's Modified Eagle Medium (DMEM containing 4500 mg/L D-glucose, without L-glutamine, sodium pyruvate, L-methionine, and L-cystine) (Invitrogen, #21013), dialyzed fetal bovine serum (Invitrogen, # 26400044), methanol (Sigma, #34860), 4% formaldehyde in PBS, 0.5% Triton^{TM} X-100 in PBS, 3% Bovine serum albumin (BSA) in PBS (3% BSA in PBS, pH 7.4), 1% SDS in 50 mM Tris-HCl (pH 8.0), and amino acid-free medium.

The antibodies used in our experiments included: microtubule-associated protein 1 light chain 3 (LC3, Sigma, L7543), p62 (Sigma, P0067), Atg7 (ProScience, #3617), Atg5 (Nanotools, #0262), β-actin (Sigma, A5441), phospho-S6 (S235/236) (Cell Signaling Technology, #2211), S6 (Cell Signaling Technology, #2217), phospho-4E-BP1 (Thr37/46) (Cell Signaling Technology, #2855) and 4E-BP1 (Cell Signaling Technology, #9452).

4.3.2 Cell culture

Atg5 wild type (Atg5 WT) and Atg5 knockout (Atg5 KO) MEFs were kindly provided by Dr. N Mizushima (Kuma, Hatano et al. 2004; Hosokawa, Hara et al. 2006). Atg7 WT and Atg7 KO MEFs were kindly provided Dr. M Komatsu (Komatsu, Waguri et al. 2005). All cell lines were maintained in DMEM (Sigma, #D1152) containing 10% fetal bovine serum (HyClone, SV30160.03) in a 5% CO_2 atmosphere at 37℃.

4.3.3 Metabolic labeling of newly synthesized proteins with AHA

As shown in Figure 3.1A, AHA is an effective surrogate for methionine, an essential amino acid, that does not require any further manipulations to be incorporated as a substrate by the methionyl-tRNA synthetase into the proteins during *de novo* protein synthesis (Kiick, Saxon et al. 2002; Link and Tirrell 2003).

The cells with 70~80% confluency in a 6-well plate were washed with warm PBS and cultured in L-methionine-free DMEM for 30 min to deplete the intracellular methionine reserves. Following methionine depletion, the cells were labeled with AHA in 10% FBS DMEM (methionine-free) for 18 h. In this assay, dialyzed FBS was used to eliminate L-methionine from other source. After labeling, the cells were washed with PBS and cultured in regular DMEM containing 10x L-methionine (2 mM) for 2 h to chase out short-termed proteins. The cells then underwent various treatments as designated.

4.3.4 Cell fixation and permeabilization

After incubation, the medium containing AHA was removed and the cells were washed once with PBS. Following the removal of PBS, cells were treated as designated experiments. The cells were then harvested and fixed in 4% formaldehyde in PBS for 15 min at room temperature. After fixation, the cells were washed twice with 3% BSA in PBS and permeabilized with 0.5% Triton™ X-100 in PBS for 20 min at room temperature. Finally, the cells were resuspended in PBS and stored at 4℃ for the detection of corresponding

alkyne-tagged detection molecule.

4.3.5 Click AHA Detection

The amount of AHA incorporated into the protein can be detected using the "click" reaction between an azide and an alkyne (Dieterich, Link et al. 2006), and a broad range of functionally and biochemically diverse proteins that incorporated with AHA can be specifically tagged with a corresponding alkyne-containing dye or hapten, and subject to subsequent analysis by flow cytometry or standard biochemistry techniques such as gel electrophoresis (Figure 3.1B).

Before click reaction, the cells were washed by PBS and 3% BSA. For each reaction, TAMRA alkyne (10μM), Tris (2-carboxyethyl) phosphine (TCEP) (1 mM, 100x fresh stock in water), Tris[(1-benzyl-1H-1,2,3-triazol-4-yl)methyl] amine (TBTA ligand) (100 μM, 100×stock in DMSO), and $CuSO_4$ (1 mM,100x stock in water) were added into the suspended cells. The samples were incubated at room temperature for 2 h, and then the reaction cocktail was removed and the cells were washed once with 3% BSA in PBS.

4.3.6 In Gel fluorescence detection

After AHA labeling, the cells were lysed in 0.2% SDS in PBS. Equal amounts (100 μg) of proteins were tagged with the fluorescent dye and clicked proteins were precipitated by acetone and air-dried. 1× SDS loading buffer (100 μL) was added to dissolve the sample and the sample (50 μL) was separated by 10% SDS gel electrophoresis. Finally, gels were visualized using a Typhoon 9410 laser scanner (GE, health care) and images were analyzed by TotalLab software.

4.3.7 Analysis of AHA signal intensity using flow cytometry.

After fluorescence tagging, nascent protein synthesis was assessed by flow cytometry and AHA signal intensity was determined in the FITC channel. We quantified the cell's fluorescence intensity and calculated the ratio of the

treated cell's fluorescence intensity to the control cell's fluorescence intensity. This represented the rate of degradation of long-lived proteins at given time points. The average and standard deviation were calculated as follows:

Relative fluorescence intensity (%) = (treated group – negative control) / (control group – negative control) × 100

Based on the AHA labeling and click reaction as described above, we here developed a protocol for quantification of the long-lived protein degradation in autophagy, as shown in Figure 3.2.

4.3.8 Autophagy induction and inhibition

The cells were labeled with AHA as described above and cultured in common medium with 10× L-methionine (2 mM) for 2 h to chase out short-termed protein in the presence or absence of autophagy inhibitors (wortmannin and bafilomycin A1). The medium was removed by aspiration and the cells were then incubated in amino acid-free medium (plus 0.1% of bovine serum albumin and 2 mM L-methionine) or treated with mTOR inhibitors (rapamycin, pp242 or Torin 1) to induce autophagy in the presence or absence of autophagy inhibitors at indicated time points.

4.3.9 Western blotting

At the end of the designated treatments, cells were lysed in Laemmli SDS buffer (62.5 mM Tris at pH 6.8, 25% glycerol, 2% SDS, phosphatase inhibitor and proteinase inhibitor cocktail). An equal amount of protein was resolved by SDS-PAGE and transferred onto PVDF membrane. After blocking with 5% non-fat milk, the membrane was probed with designated primary and secondary antibodies, developed with the enhanced chemiluminescence method and visualized with the Kodak Image Station 4000R (Kodak).

4.3.10 Statistical Analysis

All western blot and image data presented are representatives from at least three independent experiments. The numeric data are presented as means ± SD from three independent experiments and analyzed using student's *t*-test.

Chapter 5

Concluding Remarks and future direction

In summary, we have described several proteomics approaches, including identification-based, quantitative and chemical proteomics methods. We have successfully demonstrated the potential of these methods in disease mechanism, drug target and autophagy proteolysis studies.

In the first part of this thesis, we described a novel approach combining isobaric tag for relative and absolute quantification (iTRAQ) with Clickable ABPP, named ICABPP, to specifically and comprehensively identify drug targets in live cells. This approach was applied to identify the protein targets of andrographolide (Andro), a natural product with known anti-inflammatory and anti-cancer effects, in live cancer cells. A spectrum of specific targets of Andro was identified, revealing the mechanism of action of the drug and its potential novel application as a tumor metastasis inhibitor, which was validated through cell migration and invasion assays. Moreover, the target binding mechanism of Andro was unveiled with a combination of drug analogue synthesis, protein engineering and mass spectrometry-based approaches and the drug-binding sites of two protein targets, NF-κB and actin, were determined.

Our ICABPP approach can be easily optimized and applied to various kinds of affinity chromatography or ABPP-based target identification processes. Currently, besides andrographolide, we have already designed and synthesized several other drug probes for unbiased specific targets identification, including artemisinin, curcumin, celastrol, triptolide and aspirin (figure 5.1). Using our recently developed ICABPP method, we have also identified the specific targets of these drugs.

As shown in figure 5.2, our celastrol probes can specifically label a set of proteins in comparison with DMSO control. From our LC-MS/MS data, several previously reported celastrol targets have been successfully identified (Table 5.1). Target validation experiments are in progress and will be reported

in due course in future. Our results showed that ICAPP methods can be easily used for target identification for different kinds of drugs. We anticipate it to be widely adopted in drug development and optimization.

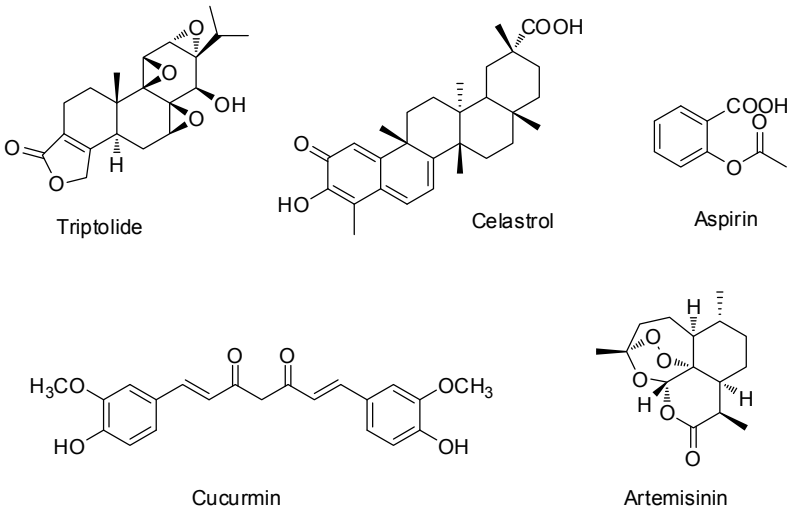

Figure 5.1 Drugs that have been successfully developed into activity based probes and used in ICAPP for targets identification in our laboratory.

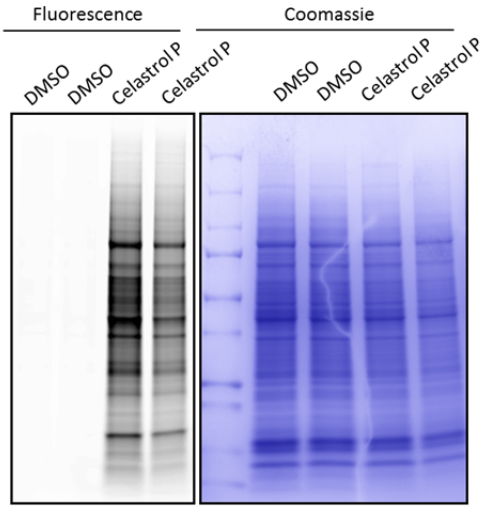

Figure 5.2 The *in situ* fluorescent labeling of HCT116 cells using celastrol probe (2 μM) together with a DMSO-treated negative control. Probe-labeled proteomes were visualized by click conjugation to the Cy3 azide tag, SDS-gel separation, and fluorescent scanning.

Score	Accession No.	Name
26.9	sp|P15121|ALDR_HUMAN	Aldose reductase
3.7	sp|O14965|AURKA_HUMAN	Aurora kinase A
9.3	sp|Q96GD4|AURKB_HUMAN	Aurora kinase B
2.7	sp|Q9HB09|B2L12_HUMAN	Bcl-2-like protein 12
20.5	sp|P10644|KAP0_HUMAN	cAMP-dependent protein kinase type I-alpha regulatory subunit
13.4	sp|P13861|KAP2_HUMAN	cAMP-dependent protein kinase type II-alpha regulatory subunit
8.8	sp|P26358|DNMT1_HUMAN	DNA (cytosine-5)-methyltransferase 1
3.3	sp|P28340|DPOD1_HUMAN	DNA polymerase delta catalytic subunit
12.7	sp|Q02750|MP2K1_HUMAN	Dual specificity mitogen-activated protein kinase kinase 1
4.7	sp|P33981|TTK_HUMAN	Dual specificity protein kinase TTK
29.1	sp|Q9HC38|GLOD4_HUMAN	Glyoxalase domain-containing protein 4

Table 5.1 Potential celastrol targets identified using ICABPP approach, which were also reported as celastrol targets in other studies.

In the second part of my thesis, we have successfully developed a novel method by using AHA labeling as a simple, sensitive, specific and quantitative tool to measure autophagic protein degradation. This assay is mainly applicable to cell culture systems *in vitro* and it could be easily adapted for high-throughput screening of autophagy modulators.

In future, we will focus on individual protein degradation rate and reveal inherent protein intracellular stability. Following AHA labeling, subcellular fractionation and affinity enrichment of protein complexes can be prepared and mass spectrometry will be performed to assess the temporal and spatial dynamics of certain subcellular compartments, organelles and protein-protein interaction networks.

Other than the proteolysis level in autophagy, we are also interested in the newly synthesized proteins during autophagy induction. Theoretically, autophagy is a process under the extreme nutrition deprivation condition,

during which the protein synthesis pathway should been shut down or kept at a very low level. To test this, we have incubated the starved cell with AHA for 4hrs to label the newly synthesized protein during autophagy induction. Our preliminary results showed there are definitely some proteins newly synthesized even under the starvation condition with amino acid free media (Figure 5.3).

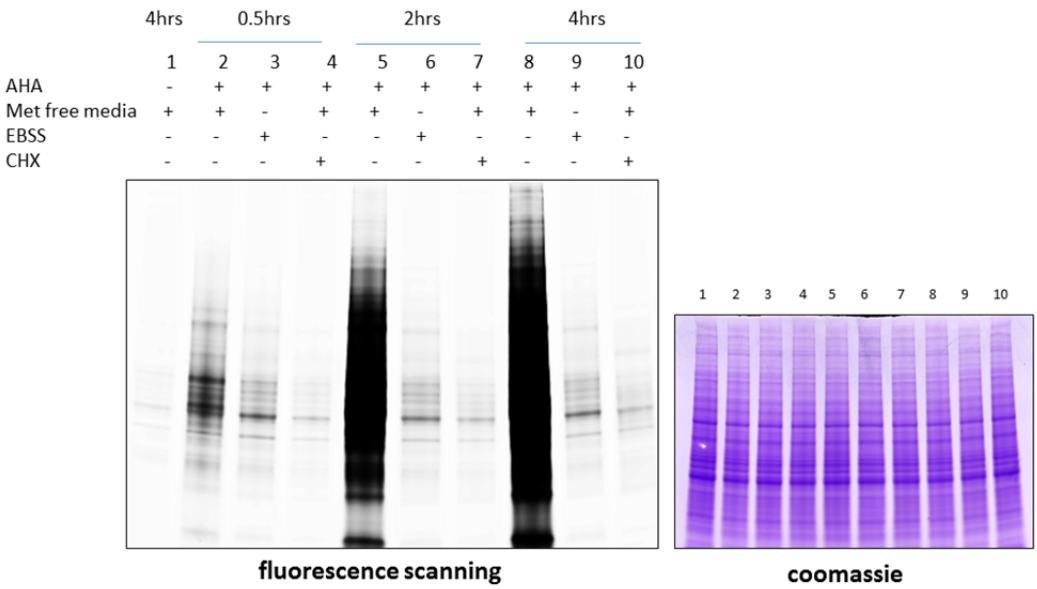

Figure 5.3 The *in situ* fluorescent labeling of newly synthesized proteins of Hela cells under normal and starvation conditions. Cells were cultured in full media or amino acid free media (EBSS) for 0.5, 2 and 4hrs. Cycloheximide (CHX) was added to inhibit the protein synthesis. AHA (50 μM) labeled proteomes were visualized by click conjugation to the Cy3 alkyne tag, SDS-gel separation, and fluorescent scanning. The coomassie staining showed the equal protein loading.

We have successfully identified some of the newly synthesized proteins during autophagy and carried out the pathway analysis. As shown in figure 5.4, the results suggested the newly synthesized proteins are closely involved in

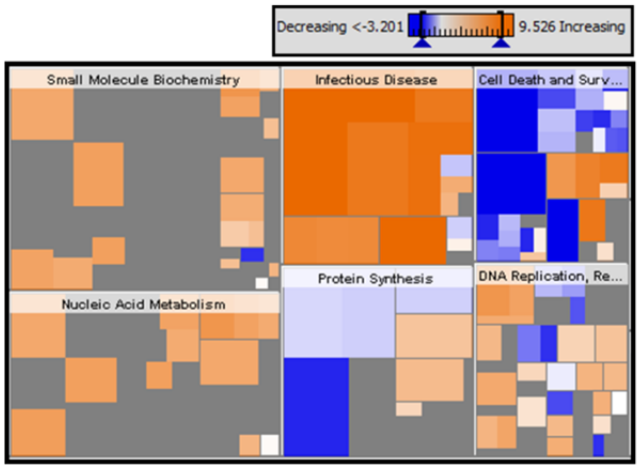

Figure 5.4 IPA pathways analysis of the newly synthesized proteins during autophagy inductions. The results suggested these newly synthesized proteins may sustain cell survival, decrease cell death and decrease protein synthesis. (Red color represents increased activity and blue color represents decreased activity)

sustaining cell survival and decreasing cell death, which is consistent with the fact that autophagy is a cell survival process. More detailed mechanistic study and validation are needed in future to clearly delineate the roles of these newly synthesized proteins during autophagy.

In summary, the quantitative chemical proteomics approaches developed and used in this thesis should be extremely useful in drug target identification and autophagy proteolysis studies.

Chapter 6

References

Aebersold, R. & Goodlett, D.R. (2001). Mass spectrometry in proteomics. *Chem. Rev.* 101,269-295.

Aldini, G. et al., (2007). 12, 14-prostaglandin J2 Target in Neuroblastoma Cells: Mass Spectrometric, Computational, and Functional Approaches To Investigate the Effect on Cytoskeletal. *Biochemistry*, 46, 2707–2718.

Andela, V.B. et al., (2000). Tumor Metastasis and the Reciprocal Regulation of Prometastatic and Antimetastatic Factors by Nuclear Factor κ B Advances in Brief Tumor Metastasis and the Reciprocal Regulation of Prometastatic and Antimetastatic Factors by Nuclear Factor B. *Cancer Res*, 6557–6562.

Bantscheff, M. et al., (2007). Quantitative chemical proteomics reveals mechanisms of action of clinical ABL kinase inhibitors. *Nat. Biotechnol.*, 25(9), 1035–1044.

Bao, Z. et al., (2009). A novel antiinflammatory role for andrographolide in asthma via inhibition of the nuclear factor-kappaB pathway. *Am. J. Respir. Crit. Care Med.*, 179(8), 657–665.

Barazi, H.O. et al., (2002). Identification of Heat Shock Protein 60 as a Molecular Mediator of α 3 β 1 Integrin Activation Identification of Heat Shock Protein 60 as a Molecular Mediator of Integrin Activation. *Cancer Res*, 1541–1548.

Best, M. D. (2009). Click chemistry and bioorthogonal reactions: unprecedented selectivity in the labeling of biological molecules. *Biochemistry* 48(28), 6571-6584.

Blagoev, B. et al., (2003). A proteomics strategy to elucidate functional protein-protein interactions applied to EGF signaling. *Nat. Biotechnol.*, 21(3), 315–8.

Böttcher, T., Pitscheider, M. & Sieber, S.A., (2010). Natural products and their biological targets: proteomic and metabolomic labeling strategies. *Angew. Chem. Int. Ed.*, 49(15), 2680–2698.

Böttcher, T. & Sieber, S.A., (2008). Beta-lactones as privileged structures for the active-site labeling of versatile bacterial enzyme classes. *Angew. Chem. Int. Ed.*, 47(24), 4600–3.

Böttcher, T. & Sieber, S.A., (2008). Beta-lactones as specific inhibitors of ClpP attenuate the production of extracellular virulence factors of Staphylococcus aureus. *J. Am. Chem. Soc.*, 130(44), 14400–14401.

Böttcher, T. & Sieber, S.A., (2010). Showdomycin as a versatile chemical tool for the detection of pathogenesis-associated enzymes in bacteria. *J. Am. Chem. Soc.*, 132(20), 6964–72.

Brown, E.J., Albers, M.W., Tae Bum Shin, Ichikawa, K., Keith, C.T., Lane, W.S., Schreiber, S.L., (1994). A mammalian protein targeted by G1-arresting rapamycin-receptor complex. *Nature*, 369(6483), 756–758.

Chen, C.-H. et al., (2012). A Novel Function of YWHAZ/β-Catenin Axis in Promoting Epithelial-Mesenchymal Transition and Lung Cancer Metastasis. *Mol. Cancer Res.*, 10(10), 1319–1331.

Chelius, D., et al.,(2003) Global Protein Identification and Quantification Technology Using Two-Dimensional Liquid Chromatography Nanospray Mass Spectrometry. *Analytical Chemistry*, 75(23), 6658-6665.

Choe, L., et al., (2007) 8-Plex quantitation of changes in cerebrospinal fluid protein expression in subjects undergoing intravenous immunoglobulin treatment for Alzheimer's disease. *Proteomics,* 7(20), 3651-3660.

Corthals, G.L., Wasinger, V.C., Hochstrasser, D.F., and Sanchez J.C., (2000) The dynamicrange of protein expression: a challenge for proteomic research. Electrophoresis 21,1104-1115

Das, B. et al., (2010). Synthesis, cytotoxicity, and structure-activity relationship (SAR) studies of andrographolide analogues as anti-cancer agent. *Bioorg. Med. Chem. Lett.*, 20(23), 6947–6950.

Dieterich, D. C., J. J. Hodas, et al. (2010). In situ visualization and dynamics of newly synthesized proteins in rat hippocampal neurons. *Nat Neurosci* 13(7), 897-905.

Dieterich, D. C., J. J. Lee, et al. (2007). Labeling, detection and identification of newly synthesized proteomes with bioorthogonal non-canonical amino-acid tagging. *Nat Protoc* 2(3), 532-540.

Dieterich, D. C., A. J. Link, et al. (2006). Selective identification of newly synthesized proteins in mammalian cells using bioorthogonal noncanonical amino acid tagging (BONCAT). *Proc Natl Acad Sci U S A* 103(25), 9482-9487.

Doherty, M. K., D. E. Hammond, et al. (2009). Turnover of the human proteome: determination of protein intracellular stability by dynamic SILAC. *J Proteome Res* 8(1), 104-112.

Eichelbaum, K., Winter, M., Berriel Diaz, M., Herzig, S., & Krijgsveld, J. (2012). Selective enrichment of newly synthesized proteins for quantitative secretome analysis. *Nature biotechnology*, 30(10), 984–90.

Eirich, J., Orth, R. & Sieber, S.A., (2011). Unraveling the protein targets of vancomycin in living S. aureus and E. faecalis cells. *J. Am. Chem. Soc.*, 133(31), 12144–53.

Evans, M.J. & Cravatt, B.F., (2006). Mechanism-based profiling of enzyme families. *Chem. Rev.*, 106(8), 3279–3301.

Fonović, M. & Bogyo, M., (2008). Activity Based Probes as a tool for Functional Proteomic Analysis of Proteases. *Expert Rev. Proteomics.*, 5(5), 721–730.

Gawecka, J.E. et al., (2010). R-Ras regulates migration through an interaction with filamin A in melanoma cells. *PloS One*, 5(6), p.e11269.

Gayarre, J. et al., (2006). Addition of electrophilic lipids to actin alters filament structure. *Biochem. Bioph. Res. Co.*, 349(4), 1387–1393.

Gersch, M., Kreuzer, J. & Sieber, S.A., (2012). Electrophilic natural products and their biological targets. *Nat. Prod. Rep.*, 29(6), 659–682.

Ghosh, D. et al., (2011). Identification of Key Players for Colorectal Cancer Metastasis by iTRAQ Quantitative Proteomics Profiling of Isogenic SW480 and SW620 Cell Lines. *J. Proteome Res.*, 10, 4373–4387.

Goshe, M.B. and R.D. (2003) Smith, Stable isotope-coded proteomic mass spectrometry. *Current Opinion in Biotechnology*, 14(1), 101-109.

Gygi, S.P., Rist, B., Gerber, S. A., Turecek, F., Gelb, M. H., Aebersold, R.(1999) Directanalysis of protein complexes using mass spectrometry *Nat. Biotechnol*. 17, 994-999.

Gygi, S.P., et al., (2000) Evaluation of two-dimensional gel electrophoresis-based proteome analysis technology. Proceedings of the National Academy of Sciences of the United States of America, 97(17), 9390-9395.

Hamdan, M. and P.G. Righetti, (2002) Modern strategies for protein quantification in proteome analysis: Advantages and limitations. *Mass Spectrometry Reviews*, 2002. 21(4), 287-302.

Hanash, S., (2001) 2-D or not 2-D--is there a future for 2-D gels in proteomics? Insights from the York proteomics meeting. *Proteomics*, 1(5),. 635-637.

Hansen, K.C., et al.,(2003) Mass spectrometric analysis of protein mixtures at low levels using cleavable 13C-isotope-coded affinity tag and multidimensional chromatography. *Molecular & cellular proteomics : MCP*., 2(5), 299-314.

Harding, M.W., Galat, A., Uehling, D.E., Schreiber, S.L., (1989). A receptor for the immunosupressant FK506 is a cis-trans peptidyl-prolyl isomerase. *Nature*, 341(6244), 758–760.

Hinz, F. I., D. C. Dieterich, et al. Non-canonical amino acid labeling *in vivo* to visualize and affinity purify newly synthesized proteins in larval zebrafish. *ACS Chem Neurosci* 3(1), 40-49.

Hosokawa, N., T. Hara, et al. (2009). Nutrient-dependent mTORC1 association with the ULK1-Atg13-FIP200 complex required for autophagy. *Mol Biol Cell* 20(7), 1981-1991.

Hosokawa, N., Y. Hara, et al. (2006). Generation of cell lines with tetracycline-regulated autophagy and a role for autophagy in controlling cell size. *FEBS Lett* 580(11), 2623-2629.

Howden, A. J. M., Geoghegan, V., Katsch, K., Efstathiou, G., Bhushan, B., Boutureira, O.,Acuto, O. (2013). QuaNCAT: quantitating proteome dynamics in primary cells. *Nature methods,* 10(4), 343–346.

Hoving, S., Voshol, H., and van Oostrum, J., (2000). Towards high performance twodimensional gel electrophoresis using ultrazoom gels. *Electrophoresis* 21, 2617-2621

Hu, E. et al., (2000). Molecular cloning and characterization of profilin-3: a novel cytoskeleton-associated gene expressed in rat kidney and testes. *Exp. Nephrol.*, 9(4), 265–274.

Huo, Y., V. Iadevaia, et al. Stable isotope-labelling analysis of the impact of inhibition of the mammalian target of rapamycin on protein synthesis. *Biochem J,* 444(1), 141-151.

Ito, T. et al., (2010). Identification of a primary target of thalidomide teratogenicity. *Science (New York, N.Y.)*, 327(5971), 1345–50.

Issaq, H.J., et al.,(2005) Multidimensional separation of peptides for effective proteomic analysis. *Journal of Chromatography B: Analytical Technologies in the Biomedical and Life Sciences*, 817(1),. 35-47.

Jada, S.R. et al., (2008). Benzylidene derivatives of andrographolide inhibit growth of breast and colon cancer cells *in vitro* by inducing G(1) arrest and apoptosis. *Brit. J. Pharmacol.*, 155(5), 641–654.

Kawai, A., S. Takano, et al. (2006). Quantitative monitoring of autophagic degradation. *Biochem Biophys Res Commun,* 351(1), 71-77.

Kiick, K. L., E. Saxon, et al. (2002). Incorporation of azides into recombinant proteins for chemoselective modification by the Staudinger ligation. *Proc Natl Acad Sci U S A,* 99(1), 19-24.

Kita, M. et al., (2011). Development of Highly Cytotoxic and Actin-Depolymerizing Biotin Derivatives of Aplyronine A. *Angew. Chem. Int. Ed.*, 50(42), 9871–9874.

Klionsky, D. J., F. C. Abdalla, et al. Guidelines for the use and interpretation of assays for monitoring autophagy. Autophagy 8(4), 445-544.

Komatsu, M., S. Waguri, et al. (2005). Impairment of starvation-induced and constitutive autophagy in Atg7-deficient mice. *J Cell Biol,*169(3), 425-434.

Kovacs, A. L., G. Rez, et al. (2000). Autophagy in the epithelial cells of murine seminal vesicle in vitro. Formation of large sheets of nascent

isolation membranes, sequestration of the nucleus and inhibition by wortmannin and 3-ethyladenine. *Cell Tissue Res,* 302(2), 253-261.

Kuma, A., M. Hatano, et al. (2004). The role of autophagy during the early neonatal starvation period. *Nature*, 432(7020), 1032-1036.

Landino, L.M., (2008). Protein thiol modification by peroxynitrite anion and nitric oxide donors. *Method. Enzymol.*, 440(07), 95–109.

Lassing, I. et al., (2007). Molecular and structural basis for redox regulation of beta-actin. *J. Mol. Biol.*, 370(2), 331–348.

Leitner, A. and W. Lindner, (2004) Current chemical tagging strategies for proteome analysis by mass spectrometry. *Journal of Chromatography B: Analytical Technologies in the Biomedical and Life Sciences*, 813(1-2), 1-26.

Lelouard, H., E. Gatti, et al. (2002). Transient aggregation of ubiquitinated proteins during dendritic cell maturation. *Nature,* 417(6885), 177-182.

Levine, B. and G. Kroemer (2008). Autophagy in the pathogenesis of disease. *Cell,* 132(1), 27-42.

Li, X. et al., (2012). Quantitative chemical proteomics approach to identify post-translational modification-mediated protein-protein interactions. *J. Am. Chem. Soc.*, 134(4), 1982–1985.

Liang, S. et al., (2011). MicroRNA let-7f inhibits tumor invasion and metastasis by targeting MYH9 in human gastric cancer. *PloS One*, 6(4), p.e18409.

Link, A. J. and D. A. Tirrell (2003). Cell surface labeling of Escherichia coli via copper(I)-catalyzed [3+2] cycloaddition. *J Am Chem Soc,* 125(37), 11164-11165.

Lindsay, M.A., (2003). Target discovery. Nature Reviews Drug Discovery 2, 831-838

Liu, C.-X. et al., (2012). Adenanthin targets peroxiredoxin I and II to induce differentiation of leukemic cells. *Nat. Chem. Biol.*, 8(5), 486–493.

Liu, H., R.G. Sadygov, and J.R. Yates Iii, (2004) A model for random sampling and estimation of relative protein abundance in shotgun proteomics. *Analytical Chemistry*, 76(14),. 4193-4201.

Liu, Y. et al., (2012). Expression of nucleophosmin/NPM1 correlates with migration and invasiveness of colon cancer cells. *J. Biomed. Sci.*, 19(1), 53.

Liu, Y., Patricelli, M. P., & Cravatt, B. F. (1999). Activity-based protein profiling: the serine hydrolases. *Proc. Natl. Acad. Sci. USA,* 96(26), 14694–14699.

Lounkine, E. et al., (2012). Large-scale prediction and testing of drug activity on side-effect targets.

Mann, M., Jensen, O. N., (2003). Proteomic analysis of post-translational modifications. Nat.Biotechnol. 21, 255-61

Martinović, S., et al., (2002) Selective incorporation of isotopically labeled amino acids for identification of intact proteins on a proteome-wide level. *Journal of Mass Spectrometry*, 37(1), 99-107.

Mizushima, N. The role of the Atg1/ULK1 complex in autophagy regulation. *Curr Opin Cell Biol,* 22(2), 132-139.

Mizushima, N. (2007). Autophagy: process and function. *Genes Dev*, 21(22), 2861-2873.

Mizushima, N. and B. Levine Autophagy in mammalian development and differentiation. *Nat Cell Biol*, 12(9), 823-830.

Morris, G.M. et al., (1998). Automated Docking Using a Lamarckian Genetic Algorithm and an Empirical Binding Free Energy Function. *J. Comput. Chem.*, 19(14), 1639–1662.

Morris, G.M. et al., (2009). Software News and Updates AutoDock4 and AutoDockTools4 : Automated Docking with Selective Receptor Flexibility. *J. Comput. Chem.*, 30, 2785–2791.

Munafo, D. B. and M. I. Colombo (2002). Induction of autophagy causes dramatic changes in the subcellular distribution of GFP-Rab24. *Traffic* ,3(7), 472-482.

Nanduri, S. et al., (2004). Synthesis and structure-activity relationships of andrographolide analogues as novel cytotoxic agents. *Bioorg. Med. Chem. Lett.*, 14(18), 4711–4717.

Nakatogawa, H., K. Suzuki, et al. (2009). Dynamics and diversity in autophagy mechanisms: lessons from yeast. *Nat Rev Mol Cell Biol*, 10(7), 458-467.

Brown, G., et al., (2003) Preoperative assessment of prognostic factors in rectal cancer using high-resolution magnetic resonance imaging. *British Journal of Surgery*, 90(3), 355-364.

Nomura, D.K., Dix, M.M. & Cravatt, B.F., (2010). Activity-based protein profiling for biochemical pathway discovery in cancer. *Nat. Rev. Cancer*, 10(9), 630–638.

Ogier-Denis, E., J. J. Houri, et al. (1996). Guanine nucleotide exchange on heterotrimeric Gi3 protein controls autophagic sequestration in HT-29 cells. *J Biol Chem*, 271(45), 28593-28600.

Ong, S. et al., (2009). Identifying the proteins to which small-molecule probes and drugs bind in cells. *Proc. Natl. Acad. Sci. USA*, 106(12), 4617–4622.

Ong, S.E., et al., (2002) Stable isotope labeling by amino acids in cell culture, SILAC, as a simple and accurate approach to expression proteomics. *Molecular & cellular proteomics*, 1(5), 376-386.

Ong, S.E., I. Kratchmarova, and M. Mann, (2003) Properties of 13C-substituted arginine in stable isotope labeling by amino acids in cell culture (SILAC). *Journal of Proteome Research,* 2(2), 173-181.

Ovaa, H. et al., (2003). Chemistry in Living Cells: Detection of Active Proteasomes by a Two-Step Labeling Strategy. *Angew. Chem. Int. Ed.*, 115(31), 3754–3757.

Paulick, M. & Bogyo, M., (2008). Application of activity-based probes to the study of enzymes involved in cancer progression. *Curr. Opin. Genet. Dev.*, 18(1), 97–106.

Quideau, S. et al., (2011). Binding of Filamentous Actin and Winding into Fibrillar Aggregates by the Polyphenolic C-Glucosidic Ellagitannin Vescalagin. *Angew. Chem.*, 123(22), 5205–5210.

Ranish, J. a et al., (2003). The study of macromolecular complexes by quantitative proteomics. *Nat. Genet.*, 33(3), 349–55.

Righetti, P.G., et al.,(2004) Critical survey of quantitative proteomics in two-dimensional electrophoretic approaches. *Journal of Chromatography A*, 1051(1-2), 3-17.

Roberts, E. A. and V. Deretic (2008). Autophagic proteolysis of long-lived proteins in nonliver cells. *Methods Mol Biol*, 445, 111-117.

Ross, P.L. et al., (2004). Multiplexed protein quantitation in Saccharomyces cerevisiae using amine-reactive isobaric tagging reagents. *Mol. Cell. Proteomics.*, 3(12), 1154–1169.

Rozycki, M. et al., (1995). Crystallographically observed conformational changes and sulfhydryl reactivity in actin. *Biophys. J.*, 68(April), 3661.

Saeed, a I. et al., (2003). TM4: a free, open-source system for microarray data management and analysis. *BioTechniques*, 34(2), 374–378.

Saeed, A.I. et al., (2006). TM4 microarray software suite. *Method. Enzymol.*, 411, 134–193.

Saghatelian, A., Jessani, N., Joseph, A., Humphrey, M., & Cravatt, B. F. (2004). Activity-based probes for the proteomic profiling of metalloproteases. *Proc. Natl. Acad. Sci. USA,* 101(27), 10000–10005.

Sletten, E. M.; Bertozzi, C. R. (2009) Bioorthogonal Chemistry: Fishing for Selectivity in a Sea of Functionality. *Angew. Chem., Int. Ed*., 48, 6974-6998.

Sharma, K. et al., (2009). Proteomics strategy for quantitative protein interaction profiling in cell extracts. *Nat. Methods*, 6(10), 741–744.

Shi, H. et al., (2012). Cell-based proteome profiling of potential dasatinib targets by use of affinity-based probes. *J. Am. Chem. Soc.*, 134(6), 3001–3014.

Shi, H. et al., (2011). Proteome profiling reveals potential cellular targets of staurosporine using a clickable cell-permeable probe. *Chem. Commun.*, 47(40), 11306–8.

Shi, M. et al., (2009). Andrographolide could inhibit human colorectal carcinoma Lovo cells migration and invasion via down-regulation of MMP-7 expression. *Chem-biol. Interact.*, 180, 344–352.

Shi, W. et al., (2011). Pyrazinamide inhibits trans-translation in Mycobacterium tuberculosis. *Science (New York, N.Y.)*, 333(6049), 1630–2.

Shi, Y., et al., (2004) The role of liquid chromatography in proteomics. *Journal of Chromatography A*, 1053(1-2 SPEC. ISS.). 27-36.

Speers, A.E., Adam, G.C. & Cravatt, B.F., (2003). Activity-based protein profiling *in vivo* using a copper(i)-catalyzed azide-alkyne [3 + 2] cycloaddition. *J. Am. Chem. Soc.*, 125(16), 4686–4687.

Statsuk, A. V et al., (2005). Actin is the primary cellular receptor of bistramide A. *Nat. Chem. Biol.*, 1(7), 383–388.

Tan, H.T. et al., (2008). Quantitative and temporal proteome analysis of butyrate-treated colorectal cancer cells. *Mol. Cell. Proteomics*, 7(6), 1174–1185.

Tang, L.A.L. et al., (2012). High-performance graphene-titania platform for detection of phosphopeptides in cancer cells. *Anal. Chem.*, 84(15), 6693–6700.

Tannert, R. et al., (2010). Synthesis and structure-activity correlation of natural-product inspired cyclodepsipeptides stabilizing F-actin. *J. Am. Chem. Soc.*, 132(9), 3063–3077.

Thoreen, C. C., S. A. Kang, et al. (2009). An ATP-competitive mammalian target of rapamycin inhibitor reveals rapamycin-resistant functions of mTORC1. *J Biol Chem*, 284(12), 8023-8032.

Tournigand, C., et al.,(2004) FOLFIRI followed by FOLFOX6 or the reverse sequence in advanced colorectal cancer: A randomized GERCOR study. *Journal of Clinical Oncology*, 22(2), 229-237.

Vabulas, R. M. and F. U. Hartl (2005). Protein synthesis upon acute nutrient restriction relies on proteasome function. *Science*, 310(5756), 1960-1963.

Wang, Y.-J. et al., (2007). Andrographolide inhibits NF-kappaBeta activation and attenuates neointimal hyperplasia in arterial restenosis. *Cell Res.*, 17(11), 933–941.

Wang, Z. et al., (2010). Design, synthesis and antibacterial activity of novel andrographolide derivatives. *Bioorg. Med. Chem.*, 18(12), 4269–4274.

Willems, L.I. et al., (2011). Bioorthogonal chemistry: applications in activity-based protein profiling. *Acc. Chem. Res.*, 44(9), 718–729.

Wu, W.W., et al., (2006) Comparative study of three proteomic quantitative methods, DIGE, cICAT, and iTRAQ, using 2D gel- or LC-MALDI TOF/TOF. *Journal of Proteome Research,* 5(3), 651-658.

Xia, Y.-F. et al., (2004). Andrographolide attenuates inflammation by inhibition of NF-kappa B activation through covalent modification of reduced cysteine 62 of p50. *J. Immunol.*, 173(6), 4207–4217.

Yamaguchi, H. & Condeelis, J., (2007). Regulation of the actin cytoskeleton in cancer cell migration and invasion. *Biochim. Biophys. Acta*, 1773(5), 642–652.

Yang, P. et al., (2010). Activity-based proteome profiling of potential cellular targets of Orlistat--an FDA-approved drug with anti-tumor activities. *J. Am. Chem. Soc.*, 132(2), 656–66.

Yang, P.-Y. et al., (2010). Activity-based proteome profiling of potential cellular targets of Orlistat--an FDA-approved drug with anti-tumor activities. *J. Am. Chem. Soc.*, 132(2), 656–666.

Yang, Y., Y. Zhao, et al. (2009). Acetylation of FoxO1 activates Bim expression to induce apoptosis in response to histone deacetylase inhibitor depsipeptide treatment. *Neoplasia*, 11(4), 313-324.

Yewdell, J. W., J. R. Lacsina, et al. Out with the old, in with the new? Comparing methods for measuring protein degradation. *Cell Biol Int*, 35(5), 457-462.

Yen HC, Xu Q, Chou DM, Zhao Z, Elledge SJ. (2008) Global protein stability profiling in mammalian cells. *Science*, 322, 918-923.

Yoshimori, T., A. Yamamoto, et al. (1991). Bafilomycin A1, a specific inhibitor of vacuolar-type H(+)-ATPase, inhibits acidification and protein

degradation in lysosomes of cultured cells. *J Biol Chem*, 266(26), 17707-17712.

Yu, L.R., et al., (2004) Evaluation of the acid-cleavable isotope-coded affinity tag reagents: Application to camptothecin-treated cortical neurons. *Journal of Proteome Research,* 3(3), 469-477.

Zhou, J. et al., (2008). Andrographolide sensitizes cancer cells to TRAIL-induced apoptosis via p53-mediated death receptor 4 up-regulation. *Mol. Cancer Ther.*, 7(7), 2170–2180.

Zhou, J. et al., (2006). Critical role of pro-apoptotic Bcl-2 family members in andrographolide-induced apoptosis in human cancer cells. *Biochem. Pharmacol.*, 72(2), 132–144.

Zhou, J. et al., (2010). Inhibition of the JAK-STAT3 pathway by andrographolide enhances chemosensitivity of cancer cells to doxorubicin. Biochem. Pharmacol., 79(9), 1242–1250.

Zhou, J., S. H. Tan, et al. Dual suppressive effect of MTORC1 on autophagy: tame the dragon by shackling both the head and the tail. *Autophagy*, 9(5), 803-805.

Zhou, J., S. H. Tan, et al. Activation of lysosomal function in the course of autophagy via mTORC1 suppression and autophagosome-lysosome fusion. *Cell Res*, 23(4), 508-523.

Ziegler, S. et al., (2013). Target Identification for Small Bioactive Molecules : Finding the Needle in the Haystack Angewandte. , 2744–2792.

Zieske, L.R.,(2006) A perspective on the use of iTRAQ™ reagent technology for protein complex and profiling studies. *Journal of Experimental Botany,* 57(7), 1501-1508.

Chapter 7

Appendix

Supplemental Table of Chapter 3

Supplemental Table Specific Andro targets identified using ICABPP approach. All the proteins listed below were identified and quantified by at least two peptides. These proteins were all enriched two times by the Andro probe compared to DMSO-treated control. (The further validated targets NF-κB and β-actin are highlighted with yellow background.

No.	Total score	% Cov	Accession #	Name	Abb. Name	Peptides (95%)	116:113	117:113	116:114	117:114	Ave. Mean	Ave. Ratio	p-value
1	35.65	37.6	IPI00414676	HSP90AB1 Heat shock protein HSP 90-beta	HSP90AB1	19	2.13	2.13	2.40	2.39	1.18	2.26	0.0002
2	32.61	60.7	IPI00021439	ACTB Actin, cytoplasmic 1	ACTB	27	2.71	2.75	2.88	2.92	1.49	2.81	1E-05
3	30.15	21.6	IPI00019502	MYH9 Isoform 1 of Myosin-9	MYH9	15	2.33	2.55	2.40	2.61	1.30	2.47	6E-05
4	29.26	24.5	IPI00939304	IPO5 Isoform 3 of Importin-5	IPO5	16	3.46	3.39	4.03	3.95	1.89	3.70	9E-05
5	28.17	44.4	IPI00479186	PKM2 Isoform M2 of Pyruvate kinase isozymes M1/M2	PKM2	14	2.05	2.02	2.21	2.19	1.08	2.11	6E-05
6	26.62	46.4	IPI01022164	TUBB Uncharacterized protein	TUBB	17	2.15	1.67	2.78	2.19	1.11	2.16	0.0051
7	24.52	38.2	IPI00784154	HSPD1 60 kDa heat shock protein, mitochondrial	HSPD1	13	1.96	2.06	2.03	2.12	1.03	2.04	3E-05
8	24.4	30.1	IPI00186290	EEF2 Elongation factor 2	EEF2	14	1.94	1.87	2.29	2.18	1.04	2.06	0.0006
9	19.94	53.9	IPI00465248	ENO1 Isoform alpha-enolase of Alpha-enolase	ENO1	11	2.12	2.09	2.27	2.23	1.12	2.17	4E-05
10	19.65	39.3	IPI00930688	TUBA1B Tubulin alpha-1B chain	TUBA1B	10	2.25	2.28	2.52	2.56	1.26	2.40	0.0001
11	16.02	46.8	IPI00947127	LDHA L-lactate dehydrogenase A chain isoform 3	LDHA	8	2.12	2.18	2.41	2.48	1.20	2.29	0.0002
12	15.33	16.8	IPI00333541	FLNA Isoform 1 of Filamin-A	FLNA	7	2.09	2.15	1.85	1.92	1.00	2.00	0.0003
13	14.14	32.9	IPI00784090	CCT8 T-complex protein 1 subunit theta	CCT8	7	2.18	2.37	2.23	2.40	1.20	2.30	5E-05
14	13.24	41.6	IPI00219217	LDHB L-lactate dehydrogenase B chain	LDHB	7	1.96	1.98	2.16	2.19	1.05	2.07	0.0001
15	12.97	29.7	IPI00472724	EEF1A1P5;EEF1A1 Putative elongation factor 1-alpha-like 3	EEF1A1	7	2.33	2.40	2.37	2.44	1.25	2.38	4E-06
16	16.74	29	IPI00304925	HSPA1B;HSPA1A Heat shock 70 kDa protein 1A/1B	HSPA1A	9	2.25	2.08	2.05	1.90	1.05	2.07	0.0002
17	12.35	19.9	IPI00008164	PREP Prolyl endopeptidase	PREP	7	2.97	3.17	3.35	3.56	1.70	3.26	8E-05
18	12.29	30	IPI00003918	RPL4 60S ribosomal protein L4	RPL4	8	2.13	2.13	2.30	2.29	1.14	2.21	4E-05
19	11.72	11	IPI00910701	AARS cDNA FLJ61339, highly similar to Alanyl-tRNA synthetase	AARS	6	2.06	2.03	2.28	2.20	1.10	2.14	0.0001
20	11.15	34.2	IPI00550021	SNORD43;RPL3 60S ribosomal protein L3	RPL3	6	1.88	2.06	2.00	2.19	1.02	2.03	0.0002
21	10.71	16.9	IPI00918003	SSFA2 Uncharacterized protein	SSFA2	5	2.45	2.04	2.20	1.84	1.08	2.12	0.0011
22	10.39	42.7	IPI00982101	YWHAZ Uncharacterized protein	YWHAZ	8	2.26	2.48	2.12	2.32	1.20	2.29	0.0001
23	10.21	26.2	IPI00549248	NPM1 Isoform 1 of Nucleophosmin	NPM1	6	2.43	2.36	2.57	2.50	1.30	2.46	2E-05
24	9.74	15.5	IPI00930205	SYNCRIP heterogeneous nuclear ribonucleoprotein Q isoform 5	SYNCRIP	6	2.15	1.86	2.38	2.04	1.07	2.10	0.0007

25	9.71	68.6	IPI00216691	PFN1 Profilin-1	PFN1	6	2.09	2.00	2.13	2.04	1.05	2.06	1E-05
26	9.12	19.9	IPI00008530	RPLP0 60S acidic ribosomal protein P0	RPLP0	5	1.88	1.85	2.34	2.29	1.05	2.08	0.0013
27	8.92	10.4	IPI01015455	CPS1 166 kDa protein	CPS1	4	2.32	2.53	2.00	2.31	1.19	2.28	0.0005
28	8.51	14.6	IPI00556541	CARS cDNA FLJ38994 fis, clone NT2RI2009259, highly similar to Cysteinyl-tRNA synthetase	CARS	4	2.54	2.76	2.80	3.04	1.47	2.78	1E-04
29	8.49	25.1	IPI00025491	EIF4A1 Eukaryotic initiation factor 4A-I	EIF4A1	4	2.10	2.16	2.02	2.07	1.06	2.09	2E-05
30	8.27	13.1	IPI00645078	UBA1 Ubiquitin-like modifier-activating enzyme 1	UBA1	4	2.14	2.35	2.41	2.63	1.25	2.38	0.0002
31	8.18	25.7	IPI01015770	HNRNPK cDNA FLJ53312, highly similar to Heterogeneous nuclear ribonucleoprotein K	HNRNPK	4	2.35	2.19	2.17	2.03	1.13	2.18	0.0001
32	8.15	31.3	IPI00797270	TPI1;TPI1P1 Isoform 1 of Triosephosphate isomerase	TPI1	4	2.00	1.98	2.70	2.65	1.21	2.31	0.0023
33	8	18.1	IPI00093057	CPOX Coproporphyrinogen-III oxidase, mitochondrial	CPOX	5	2.09	2.60	1.97	2.46	1.18	2.26	0.0011
34	7.9	56.1	IPI00640741	PRDX1 19 kDa protein	PRDX1	5	2.24	2.22	2.08	2.07	1.10	2.15	5E-05
35	7.81	28.5	IPI00007188	SLC25A5 ADP/ATP translocase 2	SLC25A5	4	1.98	2.29	1.88	2.18	1.05	2.08	0.0005
36	7.69	37.1	IPI00215777	SLC25A3 Isoform B of Phosphate carrier protein, mitochondrial	SLC25A3	4	2.58	2.76	2.11	2.26	1.27	2.42	0.0007
37	7.53	17.3	IPI00291510	IMPDH2 Inosine-5'-monophosphate dehydrogenase 2	IMPDH2	4	1.99	2.03	2.01	2.09	1.02	2.03	6E-06
38	7.52	11.3	IPI00927765	EIF4G1 Uncharacterized protein	EIF4G1	4	1.84	1.92	2.19	2.23	1.03	2.04	0.0007
39	7.41	50.3	IPI00419585	PPIA Peptidyl-prolyl cis-trans isomerase A	PPIA	5	2.24	2.16	2.38	2.32	1.19	2.27	4E-05
40	7.22	38.9	IPI00867533	RPL6 60S ribosomal protein L6	RPL6	4	1.80	1.90	2.21	2.33	1.03	2.05	0.0013
41	7.12	17.3	IPI00908896	HNRNPH1 Uncharacterized protein	HNRNPH1	4	2.16	2.16	2.90	2.82	1.31	2.48	0.0015
42	7.06	34.5	IPI01014620	NME1;NME2;NME1-NME2 Uncharacterized protein	NME1	4	2.02	1.80	2.32	2.07	1.03	2.04	0.0008
43	6.9	18.1	IPI00893179	XRCC6 X-ray repair complementing defective repair in Chinese hamster cells 6	XRCC6	3	1.88	2.66	1.74	2.44	1.10	2.14	0.005
44	6.67	19.6	IPI00299573	RPL7A;SNORD24 60S ribosomal protein L7a	RPL7A	3	2.07	2.24	1.95	2.11	1.06	2.09	0.0001
45	6.54	19.3	IPI00010796	P4HB Protein disulfide-isomerase	P4HB	4	1.90	1.77	2.50	2.32	1.07	2.10	0.0029
46	6.13	10.1	IPI00788987	NFKB1 Isoform 1 of Nuclear factor NF-kappa-B p105 subunit	NFKB1	4	2.88	3.40	2.34	2.72	1.49	2.81	0.0009
47	6	26.2	IPI00219757	GSTP1 Glutathione S-transferase P	GSTP1	3	2.06	2.28	2.11	2.35	1.14	2.20	0.0001
48	5.82	12.2	IPI00383296	HNRNPM Isoform 2 of Heterogeneous nuclear ribonucleoprotein M	HNRNPM	3	2.23	2.36	2.49	2.64	1.28	2.42	0.0002
49	5.54	5.9	IPI00646493	COPA Isoform 2 of Coatomer subunit alpha	COPA	3	2.67	2.27	2.92	2.51	1.37	2.58	0.0004
50	5.47	15.6	IPI01015591	DHX15 Uncharacterized protein	DHX15	3	1.81	2.06	2.59	2.85	1.19	2.29	0.0041
51	4.68	14.6	IPI00815732	PAICS Isoform 2 of Multifunctional protein ADE2	PAICS	3	2.22	1.74	2.59	2.08	1.10	2.14	0.0027

52	4.87	14.3	IPI00925572	ASNS asparagine synthetase [glutamine-hydrolyzing] isoform b	ASNS	2	2.51	2.24	2.52	2.22	1.24	2.37	0.0001
53	8.74	29.8	IPI00018146	YWHAQ 14-3-3 protein theta	YWHAQ	6	2.25	2.28	2.21	2.26	1.17	2.25	9E-07
54	4.64	60.3	IPI00966243	CYB5B Uncharacterized protein	CYB5B	2	3.66	3.39	3.51	3.25	1.79	3.45	2E-05
55	4.59	38.7	IPI00979595	RPS2 Uncharacterized protein	RPS2	3	1.91	1.91	2.46	2.47	1.12	2.17	0.0018
56	4.21	10.4	IPI00016610	PCBP1 Poly(rC)-binding protein 1	PCBP1	2	2.72	2.73	3.02	3.03	1.52	2.87	5E-05
57	4.11	20.1	IPI01025218	SNORD84;DDX39B Uncharacterized protein	DDX39B	2	2.26	2.00	2.52	2.22	1.16	2.24	0.0005
58	4.05	25.7	IPI00909207	PRDX2 cDNA FLJ60461, highly similar to Peroxiredoxin-2	PRDX2	2	2.44	2.22	2.58	2.33	1.26	2.39	0.0001
59	4.03	23.6	IPI00024933	RPL12 Isoform 1 of 60S ribosomal protein L12	RPL12	2	1.91	2.06	1.99	2.15	1.02	2.03	9E-05
60	4.02	15.7	IPI00465233	EIF3L Uncharacterized protein	EIF3L	3	2.01	2.34	1.90	2.23	1.08	2.11	0.0006
61	4.03	9.5	IPI00303476	ATP5B ATP synthase subunit beta, mitochondrial	ATP5B	2	1.98	2.80	1.59	2.24	1.08	2.11	0.0081
62	4	47.7	IPI00024919	PRDX3 Thioredoxin-dependent peroxide reductase, mitochondrial	PRDX3	2	2.73	1.94	2.66	1.89	1.18	2.27	0.0037
63	4	17.7	IPI00221091	RPS15A 40S ribosomal protein S15a	RPS15A	2	2.12	1.86	2.20	1.93	1.02	2.02	0.0004
64	4	8.5	IPI00642936	GSTO1 glutathione S-transferase omega-1 isoform 3	GSTO1	2	1.61	2.39	1.97	2.92	1.12	2.17	0.009
65	4	13.6	IPI00555744	RPL14 Ribosomal protein L14 variant	RPL14	2	3.20	2.89	2.64	2.38	1.47	2.76	0.0005
66	4	32.6	IPI00221093	RPS17;RPS17L 40S ribosomal protein S17	RPS17	3	1.93	1.90	2.72	2.69	1.19	2.28	0.0037
67	4	5.9	IPI00105598	PSMD11 Proteasome 26S non-ATPase subunit 11 variant (Fragment)	PSMD11	2	2.16	1.92	3.03	2.59	1.26	2.39	0.0033
68	3.9	23.9	IPI01010050	VDAC2 cDNA, FLJ78818, highly similar to Voltage-dependent anion-selective channel protein 2	VDAC2	3	2.07	2.45	2.15	2.52	1.19	2.29	0.0004
69	3.67	29.4	IPI00030179	RPL7P32;RPL7 60S ribosomal protein L7	RPL7	2	1.78	2.95	1.84	3.03	1.22	2.33	0.0101
70	3.61	14.5	IPI01012504	PGD 6-phosphogluconate dehydrogenase, decarboxylating	PGD	2	1.62	2.02	2.04	2.56	1.02	2.03	0.0048
71	3.53	10.3	IPI00947363	DDX5 cDNA FLJ53366, highly similar to Probable ATP-dependent RNA helicase DDX5	DDX5	2	2.05	1.88	2.69	2.45	1.17	2.25	0.0022
72	3.47	25.1	IPI01011282	RANP1;RAN Uncharacterized protein	RANP1	2	2.09	2.18	2.36	2.46	1.18	2.27	0.0002
73	2.97	20.9	IPI00655650	RPS26 40S ribosomal protein S26	RPS26	2	2.15	2.60	2.58	3.13	1.38	2.59	0.0011
74	2.89	6.9	IPI00926491	PTCD1 cDNA FLJ56092, highly similar to Pentatricopeptide repeat protein 1	PTCD1	2	4.34	3.97	5.29	4.86	2.20	4.59	0.0002
75	2.82	32.4	IPI01012859	RPL18A Ribosomal protein L18a-like protein	RPL18A	2	1.97	1.84	2.43	2.28	1.08	2.12	0.0014

NMR spectra of RA and Andro Probe used of Chapter 3

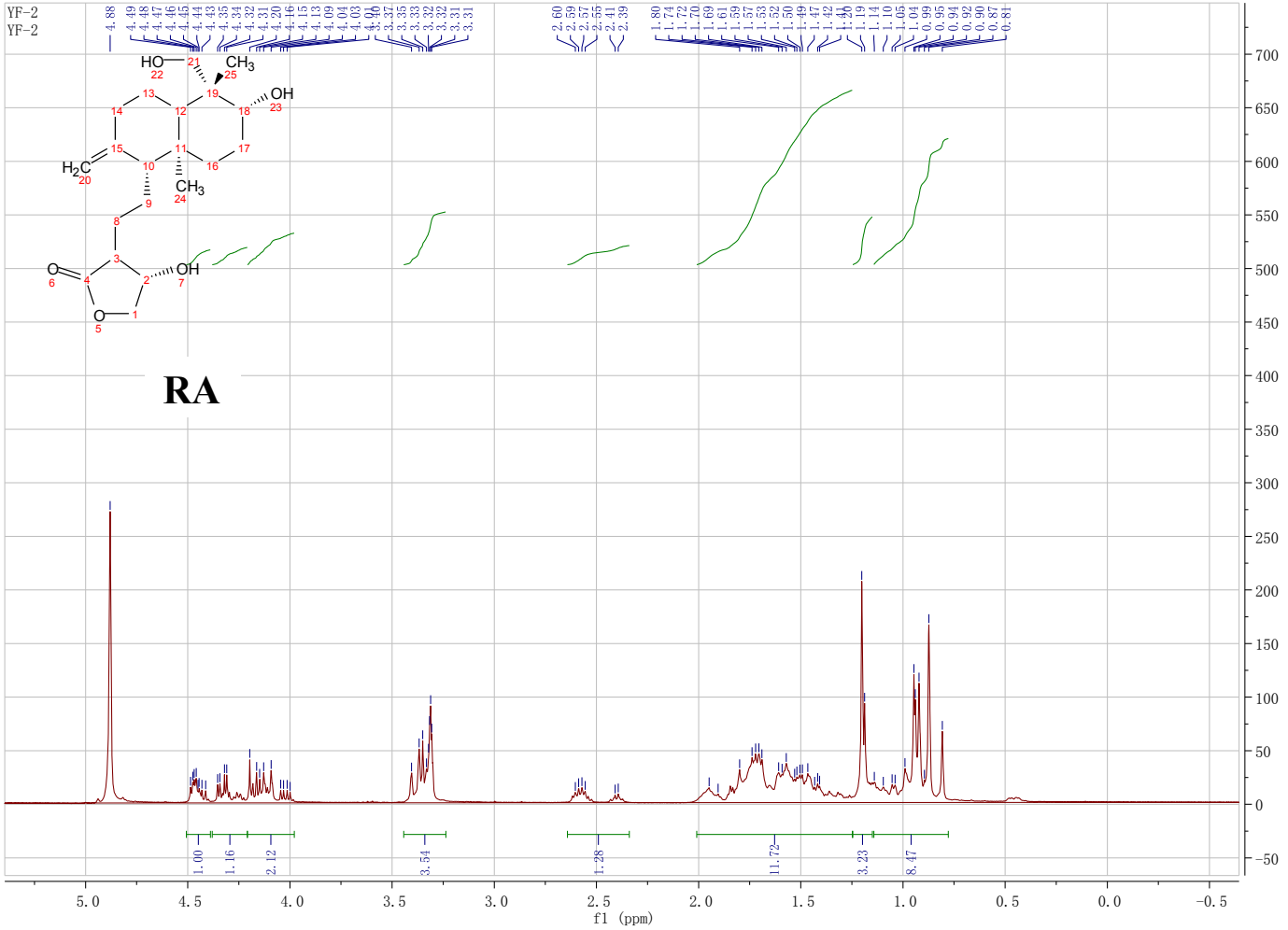

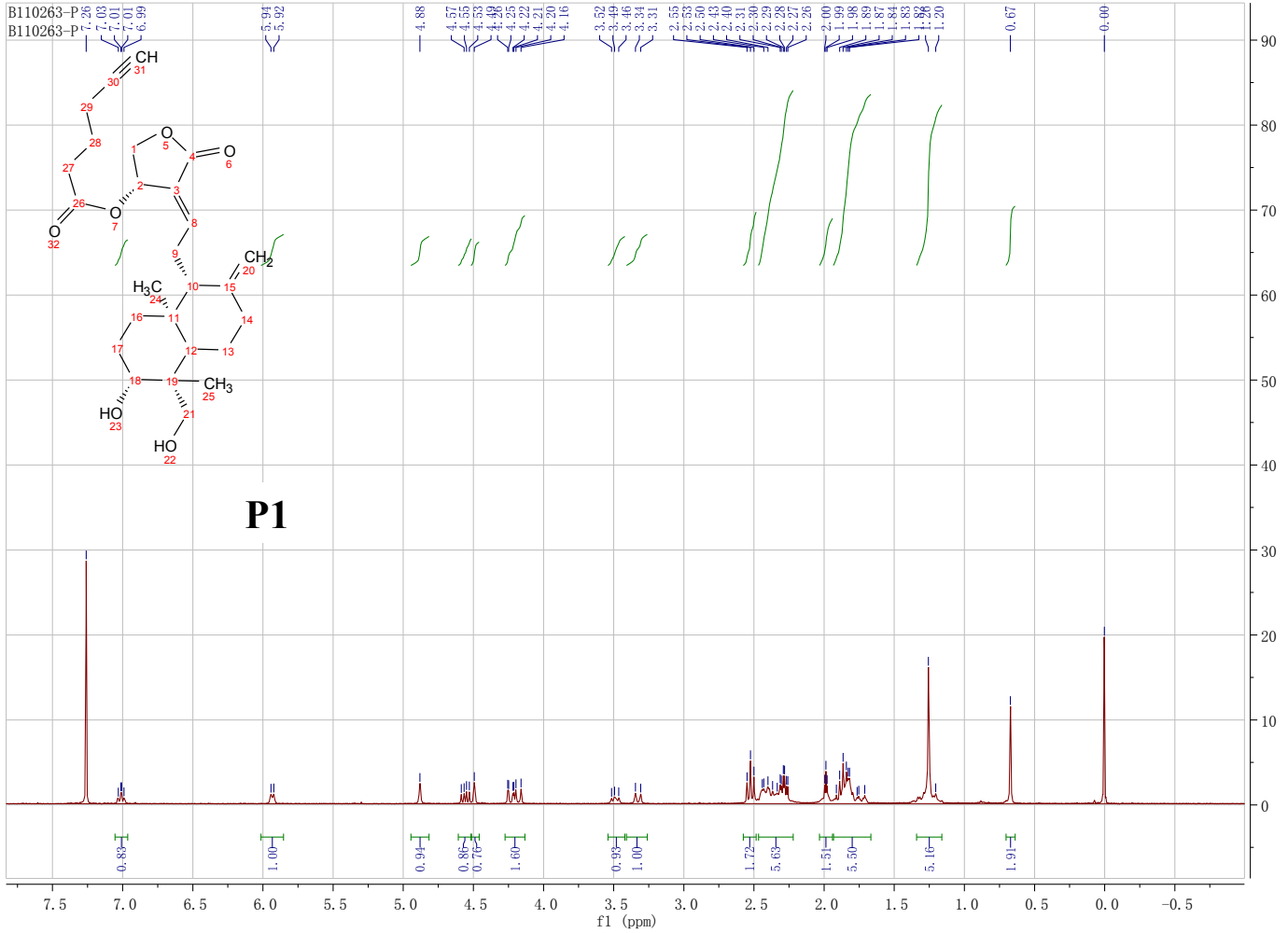
B110263-P
B110263-P
P1
f1 (ppm)

P2-^{1}H

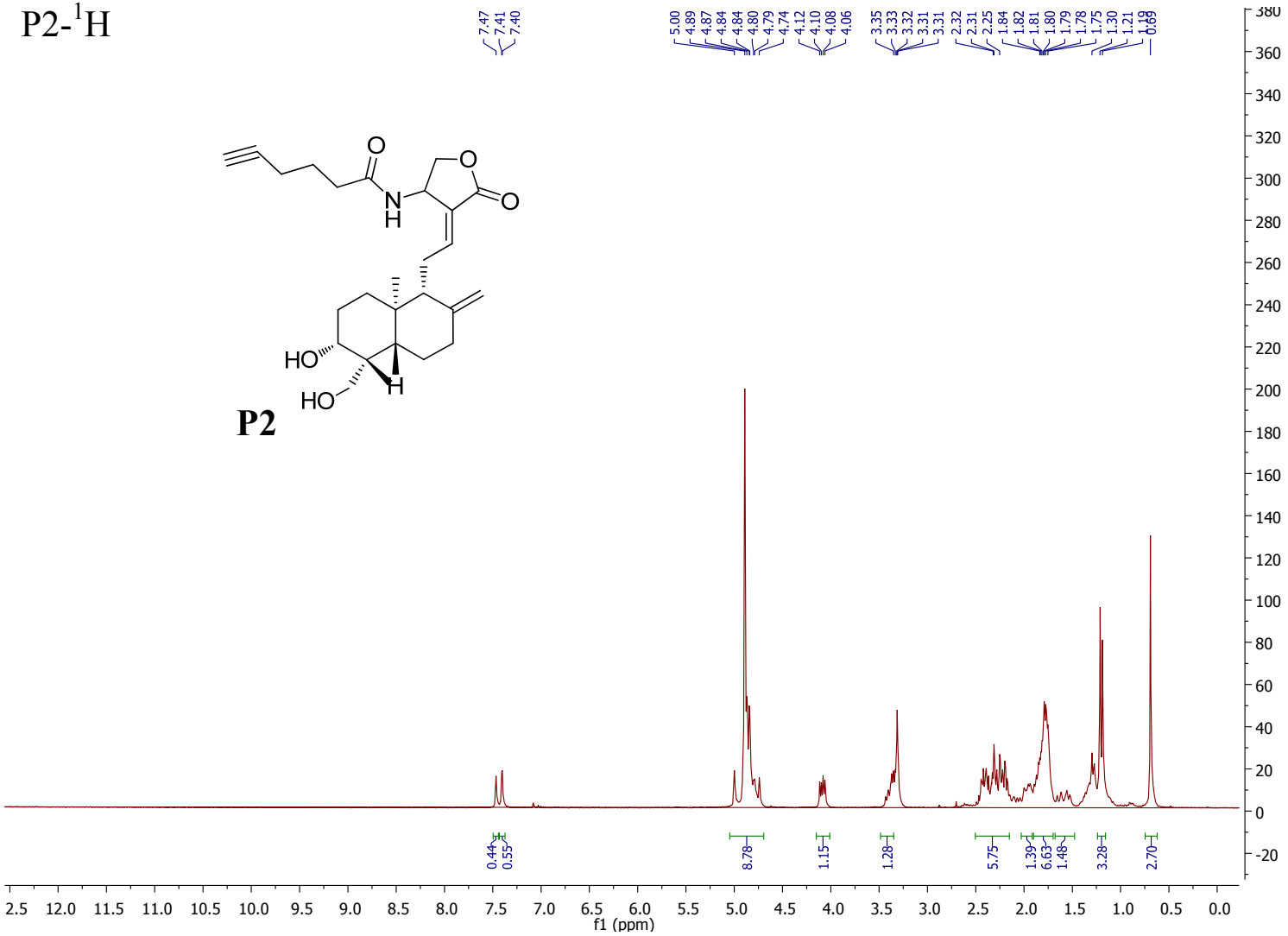
7.47
7.41
7.40
5.00
4.89
4.87
4.84
4.84
4.80
4.79
4.74
4.12
4.10
4.08
4.06
3.35
3.33
3.32
3.31
3.31
2.32
2.31
2.25
1.84
1.82
1.81
1.80
1.79
1.78
1.75
1.30
1.21
1.19
0.69
O
O
N
H
O
HO
HO
H
P2
0.44
0.55
8.78
1.15
1.28
5.75
1.39
6.63
1.48
3.28
2.70
f1 (ppm)

P2-^{13}C

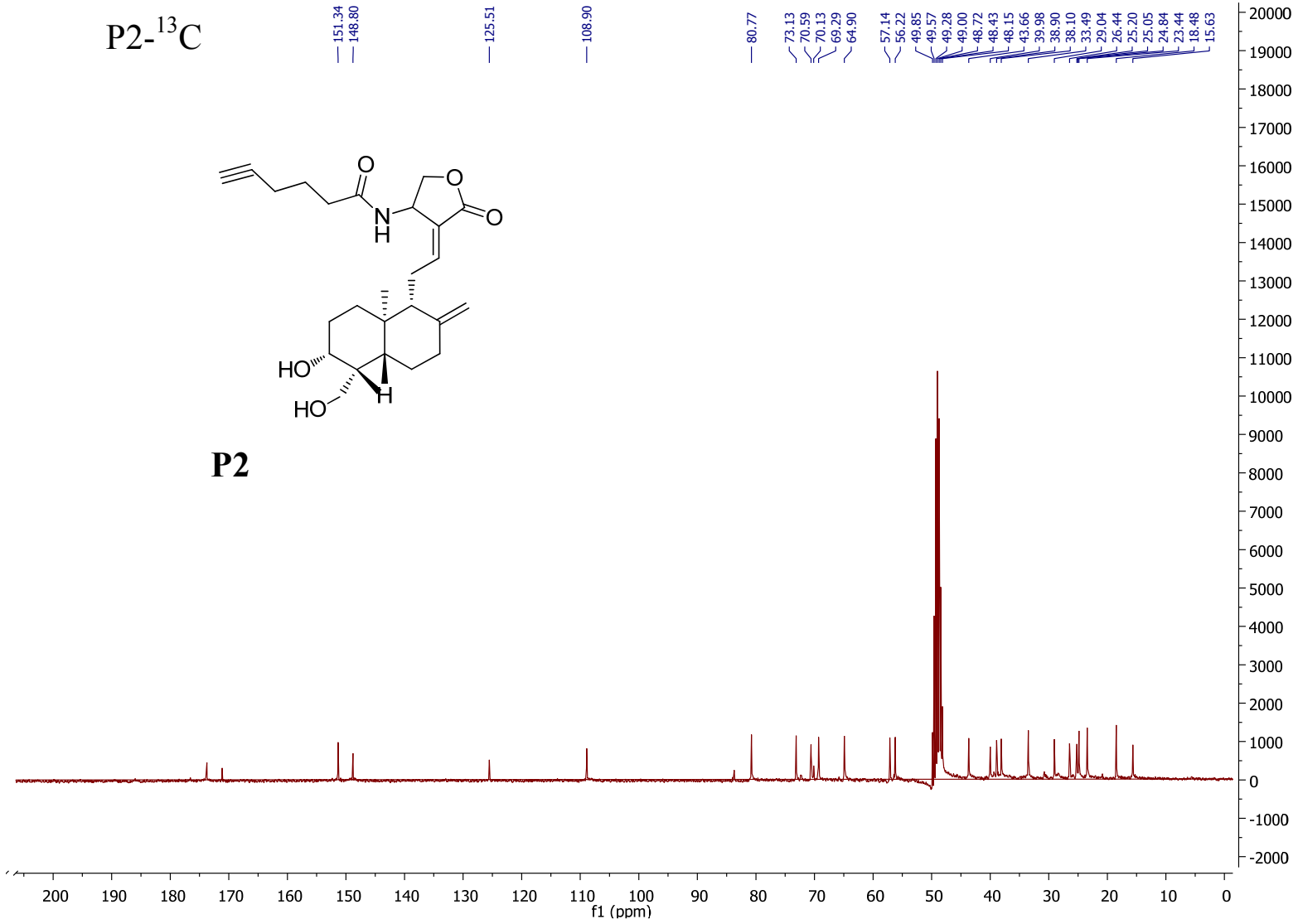
151.34
148.80
125.51
108.90
80.77
73.13
70.59
70.13
69.29
64.90
57.14
56.22
49.85
49.57
49.28
49.00
48.72
48.43
48.15
43.66
39.98
38.90
38.10
33.49
29.04
26.44
25.20
25.05
24.84
23.44
18.48
15.63
f1 (ppm)

P2